Synthesis and Characterization of Nano Tungsten Carbide from ores

A

Thesis

Submitted for the award of degree of

DOCTOR OF PHILOSOPHY

By

Harjinder Singh

(Registration No. 900912026)

Under the Supervision of

Dr. O.P. Pandey
Senior Professor

School of Physics and Materials Science
Thapar University, Patiala – 147004.
July 2013

Dedicated to My Family

Father (S. Harinder Singh) and Mother (Mrs Harbans Kaur)

Wife (Balpreet) and Sons(Agam and Mankirat)

THAPAR
UNIVERSITY
(Declared as Deemed-to-be-University u/s 3 of the UGC Act, 1956)
Thapar Technology Campus, Post Box No. 32
Patiala 147 004 Punjab India
Fax : +91-175-2364498, 2393005
URL : www.thapar.edu

CERTIFICATE

This is to certify that the thesis entitled **"Synthesis and Characterization of Nano Tungsten Carbide from ores"** which is being submitted by Mr. Harjinder Singh in fulfillment of the requirements for the award of the degree of Doctor of Philosophy in the School of Physics & Materials Science, Thapar University, Patiala, is a record of candidate's own work carried out by him under my supervision and guidance. The matter presented in this thesis has not been submitted in part or full for the award of any degree in any other University or Institute.

Date: 25.07.2013

Place: Patiala

Dr. O.P.Pandey
Senior Professor
School of Physics & Materials Science
Thapar University
Patiala-147004 (INDIA)

Index

Contents	Page No.
Certificate	i
Acknowledgement	viii
List of Publications	xi
List of Figures	xii
List of Tables	xvi
Preface	xvii
Chapter 1 Introduction	**1-15**
Overview	1
1.1 History and development	2
1.2 Tungsten carbide	2
1.2.1 Structure	3
1.2.2 Phase diagram	3
1.3 Extraction of tungsten from its ore	5
1.4 Conventional processes of WC powder synthesis	8
1.4.1 Carburization of tungsten	8
1.4.2 High temperature carburization	8
1.4.3 Direct carburization	8
1.4.4 Direct production of tungsten carbide from ore (Menstruum process)	9
1.5 Nanocrystalline materials research	9
1.6 Synthesis of nano tungsten carbide powder	10
1.6.1 Spray conversion process	11
1.6.2 Chemical vapor reaction (CVR) process	11
1.6.3 Mechanical alloying	12

1.7 Production of cemented carbides 12

1.8 Applications 13

1.9 Need for direct methods of production of nano WC from ores 14

Chapter 2 Literature Review 16-34

Overview 16

2.1 Synthesis from pure tungsten precursors 17

2.1.1 Elemental tungsten (W) 17

2.1.2 Tungsten trioxide (WO_3) 20

2.1.3 Tungsten hexacarbonyl ($W(CO)_6$) 22

2.1.4 Tungsten tetrachloride (WCl_4) 22

2.1.5 Tungsten hexachloride (WCl_6) 23

2.1.6 Tungsten hexaflouride (WF_6) 23

2.1.7 12-Tungstophosphoric Acid 23

2.1.8 Tungstic acid (H_2WO_4) 24

2.1.9 Ammonium tungstate penta hydrate ($5(NH_4)0.12WO_3.5H_2O$) 24

2.1.10 Ammonium paratungstate 24

2.2 Synthesis from Ores 24

2.2.1 Wolframite ore 24

2.2.2 Scheelite ore 25

2.3 Sintering and grain growth of nanocrystalline WC-Co 27

2.3.1 Densification 27

2.3.2 Grain Growth 27

2.4 Sintering Processes and techniques for controlling grain growth 29

2.4.1 Grain growth inhibitors 29

2.4.2 Pressure assisted sintering 29

2.4.3 Fast sintering techniques 29

Chapter 3 Experimental Procedure 35-47

Overview 35

3.1 Raw materials 36

3.2 Methodology 37

3.2.1 Synthesis by solid state reaction method 37

3.2.2 Synthesis by thermo-chemical route 39

3.2.3 Sintering of WC-Co composite 40

3.3 Materials characterization 41

3.3.1 X-ray diffraction 41

3.3.2 Rietveld analysis 42

3.3.3 Scanning electron microscopy (SEM) 44

3.3.4 Energy-dispersive X-ray spectroscopy 44

3.3.5 Transmission electron microscopy (TEM) 44

3.3.6 Selected area diffraction pattern 45

3.3.7 Lattice-plane fringes 45

3.3.8 Thermal analysis 46

3.3.9 Microhardness testing 46

3.3.10 Optical microscopy 46

Chapter 4 Results and Discussion (Scheelite ore) 48-95

Overview 48

4.1 Solid State Reaction Method 49

4.1.1 Reduction of scheelite ore to nano tungsten products 49

4.1.1.1 Characterisation of raw materials 49

4.1.1.2 Thermo gravimetric analysis 50

4.1.1.3 X- Ray diffraction analysis 52

4.1.1.4 SEM analysis 54

4.1.1.5 TEM analysis 57

4.1.2 Synthesis of single phase nanocrystalline WC powders 61

4.1.2.1 XRD and thermal analysis 61

4.1.2.2 TEM analysis of milled powders 64

4.1.2.3 Structural analysis of calcined samples 64

4.1.3 Effect of extended milling of scheelite ore 71

4.1.3.1 X-ray diffraction analysis 71

4.1.3.2 TEM and SEM analysis 73

4.2 Thermo chemical route 75

4.2.1 Single phase synthesis of nanocrystalline WC at 800°C 75

4.2.1.1 X-ray diffraction analysis 75

4.2.1.2 HRSEM and EDAX analysis 77

4.2.1.3 HRTEM analysis 81

4.2.2 Optimization of time and temperature 84

4.3 Experiments for higher yield of nano WC 92

Chapter 5 Results and Discussion (Wolframite ore) **96-111**

Overview 96

5.1 Solid state reaction method 97

5.1.1 Reduction of wolframite ore with activated charcoal 97

5.1.1.1 X-ray diffraction analysis 98

5.1.1.2 SEM studies 99

5.2 Thermo-chemical Route 101

5.2.1 Synthesis of tungsten carbide 101

5.2.1.1 X-ray diffraction analysis 102

5.2.1.2 HRTEM analysis 104

5.2.1.3 Removal of impurities 105

Chapter 6 Results and Discussion (Preparation of WC-Co Composite) 112-122

Overview 112

6.1 Preparation of WC-Co Composite 113

6.1.1 Microstructural Examination 114

6.1.1.1 WC-Co composites(WC obtained by thermo-chemical route) 114

6.1.1.2 WC-Co composites(WC obtained by solid state reaction method) 116

6.1.2 Micro hardness measurement of the composites 121

Chapter 7 Conclusions and Future Scope 123-126

Overview 123

7.1 Conclusions 124

7.2 Scope for further work 126

ACKNOWLEDGEMENTS

At this occasion of binding my thesis I would like to acknowledge the contributions of all those benevolent people, I have been blessed to associate with. Behind every student, there stand a myriad of people whose help and contribution make things successful. Since such a list can be prohibitively long, I may be excused for any omissions.

First and foremost, my utmost gratitude to my advisor and mentor **Dr. Om Prakash, Pandey**, Senior Professor, School of Physics and Materials Science, Thapar University, Patiala who has the attitude and the substance of a genius. He continually and convincingly conveyed a spirit of adventure in regard to research and scholarship. Without his guidance and persistent help this dissertation would not have been possible.

I am profound obliged to **Dr. Kulvir Singh**, (Prof. & Head) School of Physics and Materials Science for his constant encouragement, technical guidance, whole-hearted support and blessings.

I would like to thank **Dr. K.K. Raina**, Distinguish Prof. and Deputy Director, Thapar University, Patiala for his advice, encouragement and needful help.

I am also very grateful to **Dr. B. N. Chudasama** (Asstt. Prof.), School of Physics and Materials Science for his help in Rietveld Analysis and insightful technical comments and constructive suggestions at various stages of work.

I am also thankful to **Dr. Puneet Sharma** (Asstt. Prof.), **Ms Loveleen Kaur Brar** (Asstt. Prof.) and all the faculty members and staff of school of Physics and Materials Science, who never turn me down whenever I approached for any help.

I am also grateful to **Director**, Technical Education and Industrial Training, Punjab, **Mr. H. P. Singh**, Principal, Government Polytechnic College, **Mr. M. S. Bhatti**, Head, Department of Mechanical Engineerig for granting me leave for two years to complete my Ph.D. work.

Very special thanks to associate research scholars of our group; Dr. Akshay, Dr. Manoj, Dr. Vishal, Dr. Gurbinder, Dr. Jasmeet, Dr. Kamalpreet , Ms. Bhupinder, Mr. Ranvir, Mr. Suresh, Ms Samita, Ms. Mani Mahajan, Mr. Kapil Sood, Mr. Gaurav Singla, Mr. Paramjyot, Mr. Parveen Jha, Mr. Sunil Arya, Ms. Chandni, Ms Jagdeep, Ms Sakshi, Mr Satwinder, Ms Puja for their whole hearted assistance in performing experiments, characterization and constructive discussions at various stages of work. Ms Samita and Ms Mani Mahajan deserves special thanks for their help in Rietveld Analysis and finalizing the thesis.

I am also thankful to my friends and Ph.D. scholars; Mr. Ashwani, Dr. Gursewak, Mr. Sandeep, Dr. Dinesh Thakur, Dr Ravi Shukla, Mr. Rishi, Ms Parveer, Ms Samiksha , Ms Shivani, Mr. Mintu Tyagi, Dr. Raj Kumar, Ms Deepika, Ms Rajni, Ms Anupryia, Ms Rubina, and Mr Karan, Dr Dinesh Pathak, Mr. Gurmeet Singh, Mr Jaspal Singh for their help and support at all the time.

I would like to thank all those helped me in stressing time of characterization work Prof. Ajit R. Kulkarni., Mr Rajan (IIT, Mumbai), Dr. Harpreet Singh (Asso. Prof.), Mr Amit Kaushal (IIT Ropar), Mr Jagtar Singh (Punjab University, Chandigarh), Mr Sandeep (AIIMS), Dr. Gajendra Saini, Mr. Paramjyot Jha. My special thanks to Mr. Parshottam for his help in SEM analysis.

I am thankful to Mr. S.P. Verma, Ms Parveen Kumari, Mr. Indermani, Mr. Jant Singh and Mr. Lalji Verma for providing all kind of help.

I will always be indebted to Late Dr. H. B. Sharda, amid whose inspiration I joined PhD. I would express my gratitude to my parents-in-law, Mr. Devinder Singh and Mrs. Charan Kaur and other family members specially Mr. Beant, Dr Randeep, Dr. Satinder, Dr Harmeet, Dr Manjeet, Mr Tejinder for their love, care and moral support.

I must record my heartfelt appreciation for my wife, **Mrs.Balpreet Kaur**, who never complained inspite of her chronic illness and kept my spirits high. She not only managed the study of kids and family problems but also spared me with a pleasing smile from most homely chores to accomplish this project. My heart owes out naturally in appreciation of my loving sons **Agam and Mankirat** who never expressed discontent even if they felt lack of attention from me on account of Ph.D. work.

Last but not least my father **S. Harinder Singh** and my mother **Mrs. Harbans Kaur** are the two guiding pillars of my success. They deserve special mention for their inseparable support and prayers.

Above all, hidden force by **Almighty God** who gave all the strength, energy and steered me in the right direction to achieve the goal.

(Harjinder Singh)

List of Publications

Journals

1. **Harjinder Singh**, O. P. Pandey, Direct synthesis of nanocrystalline tungsten carbide from scheelite ore by solid state reaction method, **Ceramics Int.,** 39 (2013) 785–790.
2. **Harjinder Singh**, O. P. Pandey, Single step synthesis of tungsten carbide (WC) nanoparticles from scheelite ore, **Ceramics Int.,** 39 (2013) 6703–6707.
3. **Harjinder Singh**, O. P. Pandey, A New Approach to Synthesize Nano WC, **AIP Conference Proceedings** 536, 75 (2013); doi: 10.1063/1.4810107.
4. **Harjinder Singh**, O. P. Pandey, A novel approach for direct synthesis of nanocrystalline tungsten carbide from milled scheelite ore, **Met. Trans. B** (under revision)
5. **Harjinder Singh**, O. P. Pandey, Novel process for synthesis of nanocrystalline WC from wolframite ore**, Mat. Res. Bull**. (under review).

Presentations/Conferences

1. **Harjinder Singh**, O. P. Pandey, "Nano tungsten carbide production methods and energy issues", poster presentation in International Conference on Energy Efficient Materials, Manufacturing Methods & machineries for Ceramics Industries (IC2E4MCI-11) held at Agra on 19th December'11.
2. O. P. Pandey, **Harjinder Singh,** "Synthesis of WC nanoparticles from its ore", paper presentation in International Conference on Advances in Materials and Processing Challenges and opportunities (AMPCO2012) held at Indian Institute of Technology, Roorkee during 2-4th November'12.

List of Figures

		Page No.
Chapter 1		
Figure 1.1	Unit cell of WC; the small sphere represents the carbon atom in thei nterstitial site of two tungsten layers	3
Figure 1.2	Phase diagram of W-C system	4
Figure 1.3	Generalised process flow sheet for the tungsten production	6
Figure 1.4	Tungsten Hydrometallurgy – classical methods	7
Figure 1.5	Tungsten Hydrometallurgy – modern processes	7
Figure 1.6	Schematic diagram of the spray conversion process	11
Chapter 2		
Figure 2.1	Simplified flow sheet showing different steps for the synthesis of different precursors of W from the ores	18
Figure 2.2	The percent of densification of WC–Co as a function of the temperature	28
Chapter 3		
Figure 3.1	Flow chart of the procedure followed for solid state reaction method	38
Figure 3.2	Flow chart of the procedure followed for thermo-chemical route	39
Figure 3.3	Geometric derivation of Bragg's law	41
Chapter 4		
Figure 4.1	(a) TG and DTA traces for the raw scheelite (b) TG traces for the powders of activated charcoal and milled mixture (c) DTA traces for the powders of activated charcoal and milled mixture	51
Figure 4.2	X-ray diffraction patterns of the (a) raw scheelite (b) milled and 4 h calcined sample (c) milled and 10 h calcined sample (d) leached sample obtained in (c)	53
Figure 4.3(a & b)	Scanning electron micrograph of 10 h calcined milled mixture of scheelite and activated charcoal at 1100°C	55
Figure 4.4	HRSEM of calcined (10h) and leached sample	56
Figure 4.5	Transmission electron micrographs (a & b)of 10 h calcined sample after leaching showing nucleation and growth mechanism for WC (c) showing rods of tungstic	58-60

	acid (d) showing single WC nano rod (e) selected area electron diffraction (SAED) pattern showing presence of WC, W and H_2WO_4	
Figure 4.6	Scanning electron micrograph of (a) raw scheelite (b) raw scheelite milled for 40h	61
Figure 4.7	X-ray diffraction pattern of (a) raw scheelite (b) raw scheelite milled for 40 h (c) 50h milled sample (d) 100h milled sample (e) Sample (c) calcined (1025 °C for 4h) and leached (f) sample (d) calcined (1025 °C for 4h) and leached	62
Figure 4.8	DTA/TG curves of 100h milled powder calcined at 1025 °C for 4h (without leaching)	63
Figure 4.9	Transmission electron micrograph of (a) 50h milled sample (b, c and d) 100h milled sample showing nano sized capsule and sphere shaped $CaWO_4$ particles produced in 100h milled sample	65
Figure 4.10	(a & b) HRSEM of 100h milled sample calcined (1025 °C for 4h) subsequently acid and base leached	66
Figure 4.11	(a) HRTEM of 100h milled sample calcined (1025 °C for 4h) subsequently acid and base leached (b) single nanocrystalline WC particle (c) diffraction pattern of single nanocrystalline WC particle	67-68
Figure 4.12	X-ray diffraction patterns of 50 h milled sample calcined at 800, 900, 1000, and 1100 °C	69
Figure 4.13	X-ray diffraction patterns of 50 h milled sample calcined at (a) 950°C (b) 1025°C (c); 100 h milled sample calcined at (c) 950°C (d) 1025°C	70
Figure 4.14	X-ray diffraction pattern of (a) raw scheelite, (b) 150 h milled sample of scheelite and activated charcoal (c) 150 h milled, calcined (1025° C for 4 h) and leached	72
Figure 4.15	Rietveld refinement plot of observed, calculated and difference profile of nanocrystalline WC	73
Figure 4.16	TEM of 150 h milled sample	74
Figure 4.17	SEM of 150 h milled sample calcined at 1025°C (after leaching)	74
Figure 4.18	TEM of 150 h milled sample calcined at 1025°C (after leaching)	74
Figure 4.19	X-ray diffraction pattern of (a) raw scheelite (b) scheelite	76

	milled for 50 h (c) sample A showing presence of WC and minor SiO_2 phase (d) sample B showing single phase nanocrystalline WC	
Figure 4.20	Rietveld refinement plot of observed, calculated and difference profile of single phase nanocrystalline WC (sample B)	77
Figure 4.21(a & b)	HRSEM of sample B showing WC nanoparticles and activated charcoal	78
Figure 4.22	EDX of sample B on white particles (WC) nanoparticles	79
Figure 4.23	EDX of sample B showing on black particles (activated charcoal)	80
Figure 4.24	HRTEM of acid and base washed sample S5 (a) and (b) nanocrystalline WC (d) and (e) lattice fringes of nanocrystalline WC	81
Figure 4.25	X-ray diffraction patterns of acid washed samples (a) S1 (b) S2 (c) S3 (d) S4 and (e) S5	83
Figure 4.26	X-ray diffraction pattern of (a) milled scheelite; acid and base washed powders obtained after heating at (b) 650 °C (4 h) (c) 700 °C (4 h) (d) 800 °C (10 S) (e) 800 °C (4 h) (f) 800 °C (10 h) (g) 650 °C (20 h)	86
Figure 4.27	Schematic illustration of direct conversion of scheelite ore to nano tungsten carbide	87
Figure 4.28	Rietveld refinement plot of observed, calculated and difference profile of nanocrystalline WC (acid and base washed) obtained at (a) 700 °C (4h) (b) 800 °C (4h) (c) 800 °C (10h) (d) 650 °C (20h)	88
Figure 4.29	(a and b) HRTEM of WC nanoparticles obtained at 650 °C	89-90
Figure 4.30	Lattice fringes of WC nano particle	90
Figure 4.31	X-ray diffraction pattern of (a) sample S1 showing single phase nano WC (b) sample S2 showing single phase nano WC (c) sample S8 (W and H_2WO_4)	93

Chapter 5

Figure 5.1	Scanning electron micrograph of the (a) wolframite and (b) activated charcoal	98
Figure 5.2	X- ray diffractogram of wolframite showing presence of $FeWO_4$ and SiO_2	98
Figure 5.3	X-ray diffraction pattern of the milled powders calcined at 1000 °C and 1100°C	99

Figure 5.4	SEM micrograph of the milled powders calcined at 1000°C (a and b) and 1100°C (c and d)	100
Figure 5.5	Schematic illustration of synthesis and purification of Nano WC from wolframite ore	101
Figure 5.6	X-ray diffraction pattern of (a) raw wolframite (b) nanocrystalline WC synthesized from wolframite (c) Rietveld refinement plot of observed, calculated and difference profile of nanocrytalline WC	103
Figure 5.7	HRTEM of WC nanoparticles obtained after complete removal of impurities	104
Figure 5.8	X-ray diffraction patterns after leaching with concentrated HF (a) zero time (without HF leaching) (b) 5 min leaching (c) 10 min leaching (d) 20 min leaching (e) 30 min leaching (f) 37 min leaching	105
Figure 5.9	Effect of leaching time on the concentration of SiO_2	107
Figure 5.10	X- Ray Diffraction Patterns of (a) raw wolframite and acid washed samples heated at (b) 650°C(4h) (c) 700°C(4h) (d) 800°C(4h) (e) 800°C(20h)	108
Figure 5.11	X- Ray Diffraction Patterns of S3 heated at 800 °C (4h)	109
Figure 5.12	HRTEM of WC nano particles, after complete removal of impurities of sample S3	110

Chapter 6

Figure 6.1	SEM of tungsten carbide-cobalt (WC- 10wt.%Co) composite (WTC1) sintered at 1100°C (in argon).	114
Figure 6.2	SEM of tungsten carbide-cobalt (WC- 10wt.%Co) composite (WTC2) sintered at 1350°C (in argon).	114
Figure 6.3	SEM micrographs of tungsten carbide (WC- 10Co) composite sintered at 1100°C (in air).	115
Figure 6.4	SEM micrographs of tungsten carbide Co (WC-10Co) composite sintered at 1350°C (in air).	116
Figure 6.5	Optical micrograph of WC-10% Co composites sintered at (a) 1100°C(200X) WSS1 (b) 1100°C(500X), WSS1 (c) 1100°C (1500X),WSS1 (d) 1200°C(1500X), WSS2 (e) 1300°C(1500X) WSS3 at (f) 1400°C(1500X) WSS4.	117
Figure 6.6	SEM of WC-10 % wt Co composite (WSS2) sintered at 1200°C	118
Figure 6.7	SEM of WC-10 % wt Co composite sintered at 1400°C	119
Figure 6.8	Optical micrograph of WC-15% Co composite sintered at (a) 1200°C, WSS5 (b) 1300°C, WSS6 (c) 400°C,WSS7	120

List of Tables

Chapter 3

Page No.

Table 3.1 Chemical composition of wolframite ore 36

Table 3.2 Chemical composition of scheelite concentarate 37

Chapter 4

Table 4.1 Details of phase analysis along with their percentage 54

Table 4.2 Summary of different reactants, reaction conditions and Products obtained 82

Table 4.3 Variation in WC crystallite size with temperature and time 91

Table 4.4 WC lattice parameters obtained by Rietveld refinement. 91

Table 4.5 Summary of the optimization experiments conducted for higher yield of WC 92

Chapter 5

Table 5.1 Experimental conditions 107

Chapter 6

Table 6.1 Sample labels with sintering time, temperature and composition 113

Table 6.2 Sample labels, their composition, sintering temperature and hardness of the developed WC-Co composite 121

Preface

Development of new materials with improved properties is the basic theme of materials science research. In order to do so new techniques are explored which include modification in processing route. Currently more emphasis is being given on development of new processes for the synthesis of nano materials. In order to make the processes economical, more emphasis is given on direct synthesis of high purity nano materials from the raw materials itself. This will enable to make use of these nano materials on large scale. The same is the case with nano WC where its production from pure tungsten precursors makes it costly product. It is well established fact that the use of nano WC gives rise to increased hardness and toughness as compared with the micro-crystalline counterpart having the same composition. The science behind increased physical properties is that nanocrystalline materials posses high density of core defects like grain boundaries, inter phase boundaries, dislocations etc. Moreover, nano WC finds new area of application like catalysis in many energy devices.

Literature review indicates that all efforts on direct synthesis of pure single phase nanocrystalline WC from the ore has led to impure/mix phase formation. Keeping in view this technological challenge, direct synthesis of pure nano carbide (WC) from its ores (Scheelite and Wolframite) is taken up in the present work. Nano WC is synthesized from the ores of W where the impure phases are removed after the synthesis process. This is a reverse process when compared to currently used hydrometallurgical practice where prior removal of impurities is done. These unconventional routes have distinct advantages like, decrease in number of steps involved in synthesis, lesser use of acids/bases for removal of impurities (no digestion of the ore is required) and subsequently reducing the amount of effluent generation. Above all the overall process is economical and eco-friendly too. The as synthesized nano WC powders were consolidated in the matrix of Co. The composite powders showed grain growth with increase in sintering temperature. However, controlled sintering process leads to retention in nano phase WC with slight coarsening effect. The hardness of these composites are well above the acceptable limit as has been reported in the literature.

The present work deals with the synthesis and characterization of nano WC directly from the Scheelite and Wolframite ores. The entire work of the thesis is divided into seven chapters.

In **Chapter 1,** the brief history and development of tungsten carbide (WC), its crystal structure, properties and phase diagram is discussed. The hydro-metallurgical processes for the extraction of pure tungsten precursor from the ores, scheelite and wolframite are given in brief. Further, the conventional methods of production of WC and nano WC from pure tungsten precursors and ores are described. Study reveals that there is no route available for synthesis of nano WC directly from the ores. Also the diverse applications of nano tungsten carbide are discussed.

Chapter 2 presents the detailed literature review of synthesis of monolithic WC and WC/Co nano powders. The literature review indicated that only solid state reaction was attempted for the synthesis of nano WC directly from ores that resulted in micron sized and/or mixed/impure phase formation. After reviewing all the segments of literature, the need for further development of solid state reaction method for direct synthesis of single phase nano WC from the ores was felt. The reported solid state reaction method requires the reduction temperature in the range of 1000 to 1100°C. However, for the production of still smaller size WC particles (< 50 nm), the synthesis temperature has to be lowered to retain the nano size of WC. Based on these gaps, the aims and objectives of the thesis work was decided.

Chapter 3 describes about the experimental procedures followed in the present work. On the basis of literature survey solid state reaction method was used for the synthesis of nano WC from the Scheelite and Wolframite ore. For low temperature method several experiments were planned, which include "Dry-autocalving" and was successfully used for the synthesis of single phase nano WC. For the reactions a specially designed autoclave was used. The details of synthesis and characterization techniques are described in this chapter.

Chapter 4, deals with results and discussion part of the present work of experiments conducted from scheelite ore. All the experiments were conducted without any **purification** of scheelite ore. Removal of impurities was done after the synthesis of nanocrystalline WC. This chapter is divided into three sections; first one describes the results of solid state reaction method. The second one describes the results of thermo-chemical route. The third

section gives the details of scaling experiments conducted by thermo-chemical route. In the first section, the details of systematic experiments conducted from the milled mixture scheelite ore with activated charcoal for different time periods are described. Reduction of 10h milled mixture of scheelite and activated charcoal was studied. The scheelite ore got converted into nano W and WC. The unreacted scheelite got converted into nano rods of 5 to 7 nm upon HCl leaching. Further experiments were carried out with the aim to synthesize single phase nano WC. The scheelite and activated charcoal was milled for 50h and 100h. The 100h milled sample showed complete reduction/carburization of scheelite at 1025°C. After removal of impurities single phase nano WC was obtained. Further experiments were carried out on 150h milled sample, which resulted into smaller nano WC (10 to 25 nm) particles with some unreacted scheelite.

The second part presents the results of synthesis by dry autoclaving. The nano WC was synthesized by heating the mixture of Scheelite, Mg and activated charcoal at 800°C for 20h in an autoclave. After removal of reaction by products and impurities, single phase nano WC particles were obtained. Further, experiments were conducted for optimising temperature and time for synthesis of single phase nano WC. Single phase nano WC (14.1±0.1 nm average crystallite size) was obtained at low temperature (650°C). The third section gives the details of scaling experiments conducted to get higher amount of nano WC. The lattice parameters of synthesized WC were calculated from refined crystal structure by Rietveld Method.

In **chapter 5,** the results obtained from the Wolframite ore are discussed. This chapter is divided into two parts; first one describes the results by solid state reaction method. The second part describes the experiments conducted by thermo-chemical route. By solid state reaction method, nano W_2C and Fe_2W_2C were obtained from the 50h milled mixture of wolframite and activated charcoal calcined at 1100°C in argon atmosphere. In the second part, the results of synthesis of single phase nanocrystalline WC directly from the wolframite ore (containing nearly 50% impurity in as received ore) by thermo-chemical route are described. The mixture of wolframite, Mg and activated charcoal was heated at 800°C for 20h in an autoclave. The resultant powders were washed by dilute HCl (1:1). The acid leached powders contained nano WC and SiO_2 impurity which was leached out by HF. Furthermore, experiments were conducted at 800, 700 and 650°C with holding time of 4 h. The sample heated at 800°C for 4h, showed complete transition to product WC phase. After

removal of all the impurities, sample contained single phase nano WC particles of 5 to 7 nm. The powders were characterized by X-ray diffraction and high resolution transmission electron microscopy (HRTEM). The lattice parameters were calculated from Rietveld analysis using Fullprof program.

The **chapter 6** deals with discussion on the results obtained from the composite (10 and 15 wt.% Co) synthesized using WC nano particles obtained by solid state reaction method from scheelite ore. The sintering behaviour of these composites at different temperatures (1200, 1300 and 1400°C) in argon atmosphere is discussed in detail.

In **chapter 7**, the entire work of present study is summarised and concluded. The present work shows that single phase nano WC particles of different sizes can be synthesized directly from the ore concentrates; scheelite and wolframite. We have exploited acid resistant property of WC for our work over the conventional routes. Since WC is resistant to HCl attack, the major impurities can be leached out from the mixture of nanocrystalline WC and ore impurities. Impurities present in the ore do not interfere in the synthesis of nanocrystalline WC. Impurities also act as grain growth inhibitor thus facilitating in synthesis of WC nanoparticles, which are leached out after synthesis.

Future scope of work

The synthesized WC nanoparticles can be tested for catalytical properties for use in fuel cell to reduce the cost as a substitute for Pt. The sintering kinetics of composite from as synthesized nano WC with grain growth inhibitors can be studied. Direct synthesis of other carbides of other transition elements or other nano materials directly from their ores or impure compounds is another area of experimentation.

Chapter 1

INTRODUCTION

Overview

This chapter reviews the brief history and development of tungsten carbide (WC). The details of WC crystal structure, properties and phase diagram are also presented. The different methods of extraction of tungsten from its ores are also described. Further, conventional methods of tungsten carbide production are presented. Different methods for the synthesis of nano tungsten carbide is also given in brief. The diverse application of cemented carbides in cutting tools, mining tools, wear parts, military, nuclear, sports, surgical instruments, drawing applications and as catalyst are discussed. This chapter emphasizes the need to have direct methods for the production of nano tungsten carbide from the ores.

1.1 History and development

Tungsten monocarbide (WC) was discovered by P. Williams in 1898 [1]. The hardness of WC was comparable to that of diamond, but brittleness rendered it useless commercially. In 1923, K Schröter invented hard-metal (combining WC and cobalt by liquid-phase sintering) and got patent in 1926. Hard-metal (cemented carbide) is now the main application for tungsten [2-4].

Although more than 30 tungsten-bearing minerals are known, only two of them are important for extraction: wolframite (Fe, $MnWO_4$) and scheelite ($CaWO_4$). Wolframite is a general term for iron and manganese tungstates where the iron/manganese ratio can vary. A mineral with more than 80% $FeWO_4$ is called Ferberite and a mineral with more than 80% $MnWO_4$ is called Hübnerite. During cooling of the magma, differential crystallisation occurs, and scheelite and wolframite are often found in veins where the magma has penetrated cracks in the earth's crust. Most of the tungsten deposits are in younger mountain belts, for example the Alps, Himalayas and the Pacific rim. World tungsten resources have been estimated at 7 Mt W, including deposits that have so far not been proven to be economically workable [1]. It is suggested that 30% of the resources are wolframite and 70% are scheelite ores. The former mineral contains 76.5% WO_3, while the latter contains 80.5% WO_3. There are major deposits of these minerals in China (with about 57% of the world total), Russia, Austria and Portugal. The most of the tungsten produced is used for making tungsten carbide.

1.2 Tungsten carbide

Tungsten carbide (WC) is an interstitial compound of C atoms filling into W crystal having high melting point (2600 to 2850°C) and high hardness (16-22 GPa, 500g load Vickers test), combined with a high fracture toughness (28M Pa). WC is hardest binary carbide at elevated temperatures (1000 kg mm^{-2} at 1000°C) [5]. In addition to these properties, it has a very high compressive strength (5 GPa at 20°C) and exhibits a high resistance to both oxidation and corrosion.

1.2.1 Structure

WC crystallizes in the hexagonal structure in P-6m2 symmetry (space group 187) with one formula unit per unit cell. The cell dimensions are a = 2.906 Å and c = 2.837 Å with c/a = 0.976. The atoms are in the following special positions: W in 1 a: 0, 0, 0; C in 1 d: 1/3, 2/3, 1/2 [6]. From a structural viewpoint, the W atoms form a hexagonal lattice in which the metal atoms are situated at the corners of the trigonal prisms. The centre of each second prism in a layer of such trigonal prisms is occupied by a carbon atom as shown in Fig. 1.1.

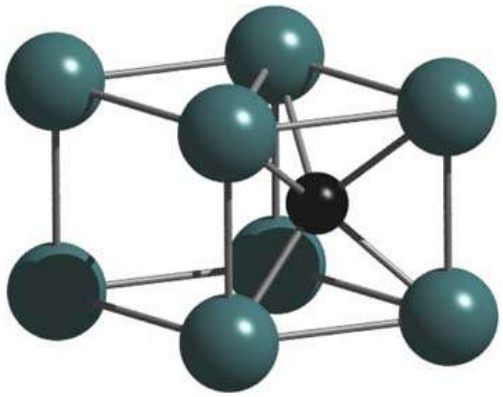

Figure 1.1: Unit cell of WC; the small sphere represents the carbon atom in the interstitial site of two tungsten layers [6].

1.2.2 Phase diagram

The phase WC, also called δ-WC, is a line compound with insignificant deviation from stoichiometric composition (Fig.1.2) [7]. Tungsten also forms two other carbides: $WC_{0.5}$ (normally named β-W_2C) with a hexagonal compact (hcp) structure and cubic γ-WC_{1-x}, (where x≈0.4) phase [8, 9]. β-W_2C phase is stable in a rather small temperature range at high temperatures and crystallizes in three structure types: PbO_2, Fe_2N and CdI_2 types, denoted by β, β′ and β″, respectively. These polymorphs are stable at different temperatures and compositional ranges.

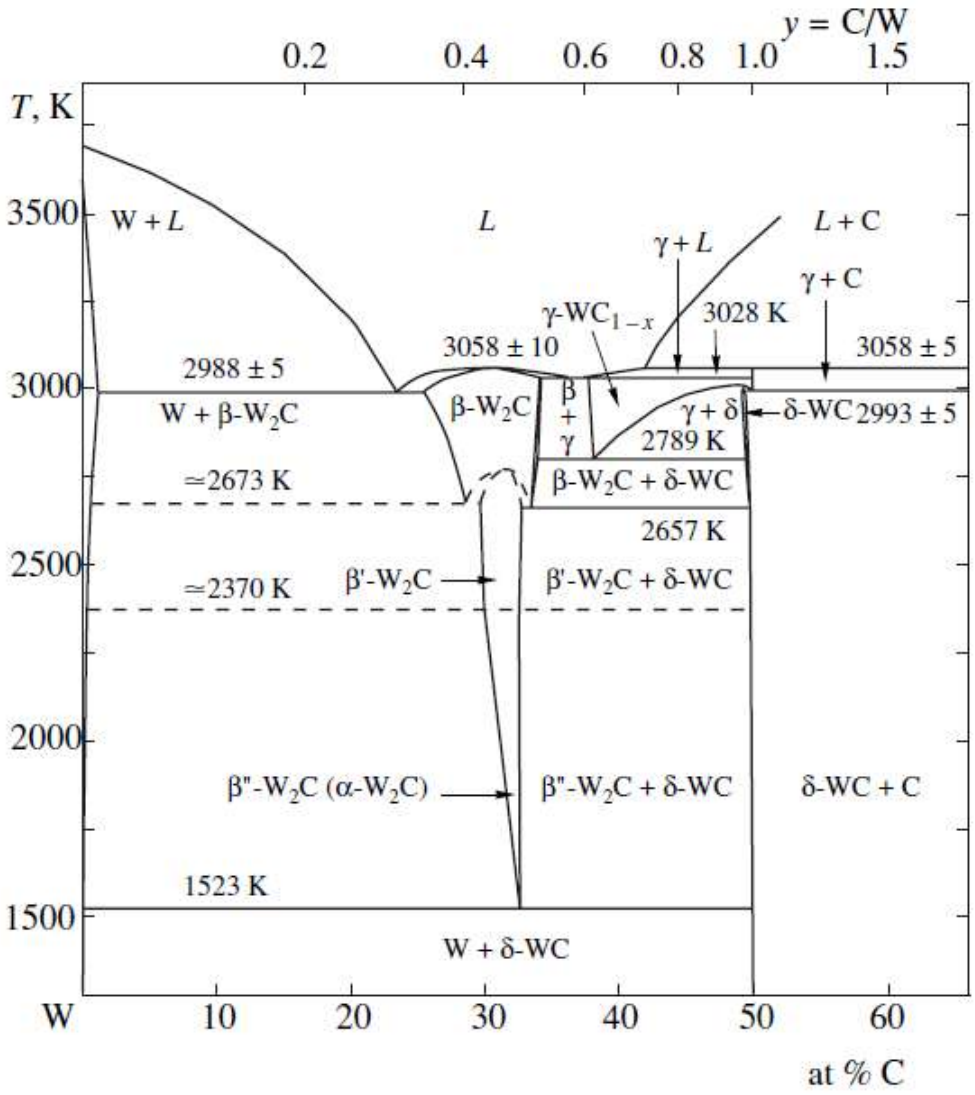

Figure 1.2: Phase diagram of W-C system [8].

The W_2C phase is originated from a eutectoidal reaction between elemental W and δ-WC at 1250 °C, melts congruently at approximately 2758 °C and forms eutectic melts with the W solid solution at 2215 °C and with γ-WC_{1-x} at near 2715±5 °C [9,10]. The γ-phase results from a eutectoidal reaction between β and δ at 2516 °C and melts at approximately 2785 °C. δ-WC is the only binary phase stable at room temperature and has almost no compositional change up to 2384 °C but may become slightly carbon deficient between this temperature and its incongruent melting point.

1.3 Extraction of tungsten from its ore

The primary source of tungsten are the minerals, Scheelite ($CaWO_4$) and Wolframite (Fe, Mn)WO_4. Due to the extremely high melting point of tungsten, its extraction is carried out by hydro, rather than pyro-metallurgical processes [3]. In last 100 years many processes have been developed for extraction of tungsten form the ore. The generalised process flow sheet is shown in Fig. 1.3 [11]. The ore processing routes further can be classified as **classical methods** and **modern methods** [2].

In the **classical** procedure, scheelite was mainly processed by acid digestion while wolframite was dissolved by an alkaline digestion. Fig. 1.4 shows simplified flow sheet of classical procedure. The important solid, pure intermediate in both cases is tungstic acid, derived either directly or after several precipitation steps. Tungstic acid is formed by a precipitation, which is a more or less instantaneous process. Foreign ions present in solution during the precipitation are partly entrapped or co-precipitated and contaminate the tungstic acid. In the **modern process**, APT is the intermediate which, in contrast to tungstic acid, is gained by crystallization (Fig. 1.5). Crystallization compared to precipitation is a much slower process; consequently less of the impurities present in the mother liquor is contained in the crystallized product. The second important difference between classical and modern technology is the method used to separate the large amount of sodium ions. The old method used a calcium tungstate precipitation and subsequent hydrochloric acid treatment for that purpose, while in the modern process solvent extraction or ion exchange converts sodium into ammonium isopolytungstate solution. Although recycling of chemicals is performed in many cases, such as sulfide recycling in molybdenum precipitation, ammonia recycling in APT crystallization, and solvent circulation in solvent extraction, still a certain waste of chemicals and also of energy exists which add to the high cost and to environmental pollution.

The main example is the sodium carbonate pressure leaching process to digest scheelite. Here, at least a threefold stoichiometric excess of sodium carbonate is used. In addition, the corresponding amount of sulfuric acid to neutralize it in the subsequent process is required [4].

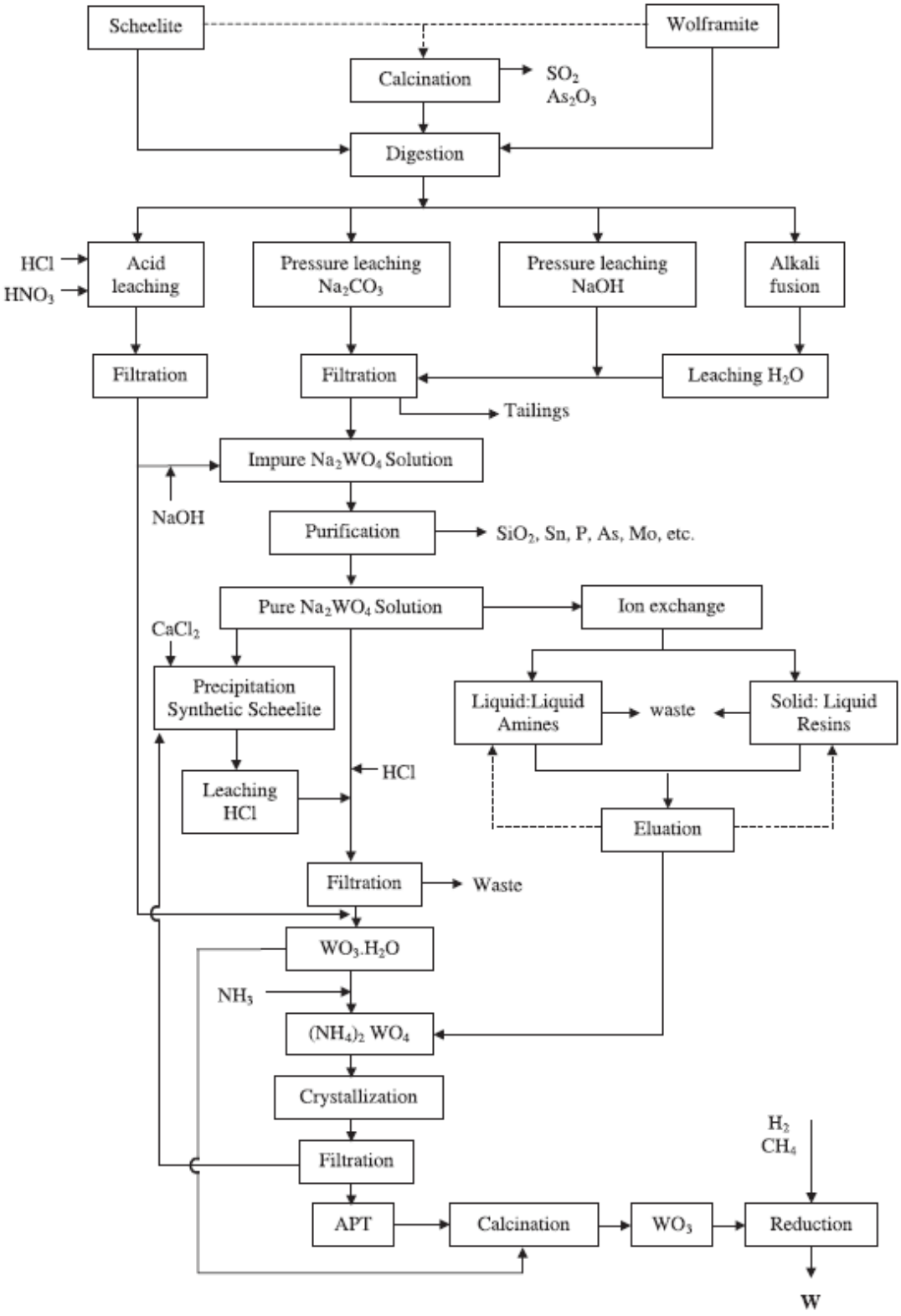

Figure 1.3: Generalised process flow sheet for the tungsten production [10].

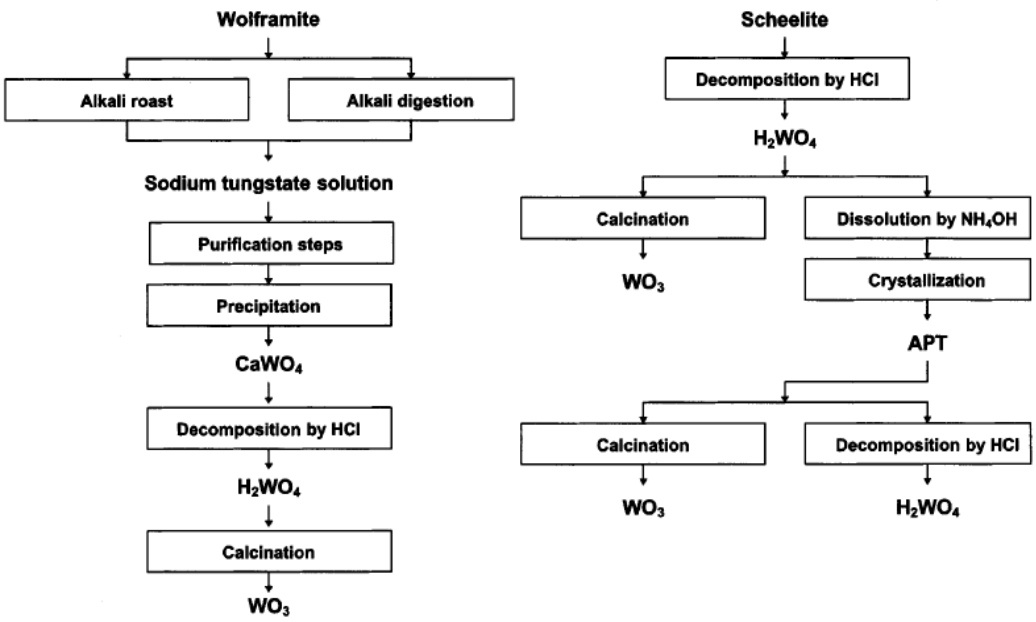

Figure 1.4: Tungsten hydrometallurgy – classical methods [4].

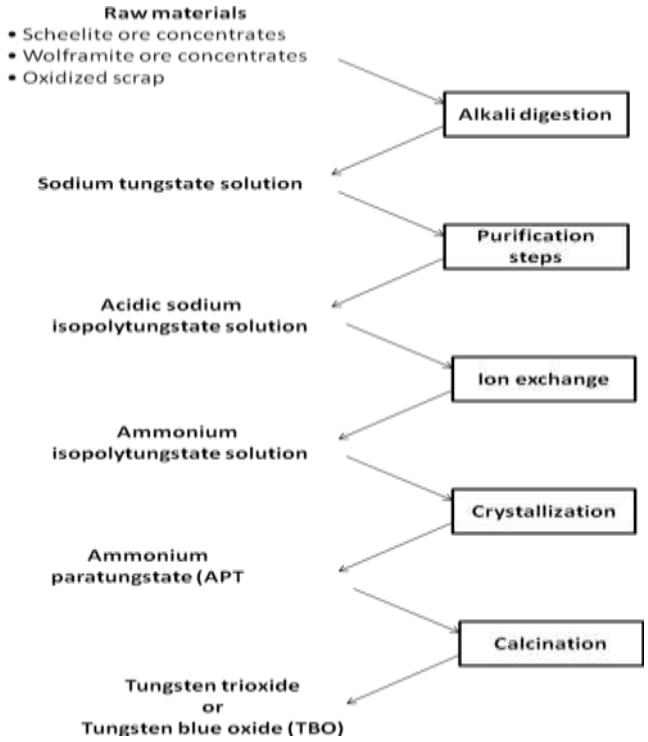

Figure 1.5: Tungsten hydrometallurgy – modern processes [4].

Finally, the equivalent tonnage of sodium sulfate leaves the plant in the solvent extraction raffinate.

1.4 Conventional synthesis processes of WC

Conventionally elemental tungsten (W) and tungsten trioxide (WO_3) have been used as raw material for WC powder production. There exists one direct method, "Manstruum" which can produce WC coarse particles from the ore concentrates [4].

1.4.1 Carburization of tungsten

Tungsten powder is reacted with carbon at temperatures between 1300 and 1700 °C in hydrogen atmosphere. The average particle size WC produced is comparable to particle size of the tungsten powder. Only a slight increase in size occurs due to the change in density from 19.3 g/cm^3(W) to 15.7 g/cm^3 (WC) [4]. In addition a certain agglomeration is observed at higher temperatures. High purity carbon black is usually preferred as carbon source in comparison to graphite, due to its higher reactivity and lower price.

1.4.2 High temperature carburization

The carburization of the W+C blend is done at temperatures ranging between 1800 and 2200 °C. High-temperature carburized powders are usually coarse (10-50 μm) [4]. At temperatures greater than 1900 °C, extensive grain (crystallite) coarsening takes place, most likely by coalescence, yielding in WC crystallite sizes up to 50 μm. Smaller, average-sized powder (5-10 μm) can partly consist of single-crystal particles.

1.4.3 Direct carburization

An alternative for producing WC powders on an industrial scale is the *direct* carburization of WO_3, which was patented in Japan [4]. It has been exclusively used there for several years to produce submicron and ultrafine WC powders of high quality. The carburization is carried out in two stages, reduction in nitrogen atmosphere at 1350 °C and carburization in hydrogen atmosphere at 1650 °C.

$$WO_3 \rightarrow (WO_{2.9}) \rightarrow WO_{2.72} \rightarrow WO_2 \rightarrow W \rightarrow W_2C \rightarrow WC \qquad (1.1)$$

During reduction needle like $WO_{2.72}$ decomposes to ultrafine WO_2 nuclei, which are further transformed to WC of approximately the same size.

1.4.4 Direct production of tungsten carbide from ore (Menstruum process)

The process is also called "macro process" and is unique in way that it produces WC directly from ore concentrates scheelite, ferberite, or wolframite [4]. A mixture of ore concentrate with Fe_3O_4, Al, CaC_2, and/or C reacts exothermally after initiation (by using a starter) to form WC, Fe, CaO, and Al_2O_3. The metallic components gather in the bottom part of the melt and the oxidic in the less dense slag at the top. The process represents an aluminothermic reduction of iron and tungsten oxides. The tungsten metal formed intermediately in the molten iron is carburized and, due to the limited solubility of WC in Fe, it crystallizes. The reactants are proportioned to develop a self-sustained exothermic reaction at about 2500 °C. The following chemical reactions proceed (Me can be Fe or Mn)

$$3Fe_3O_4 + 8Al \longrightarrow 9Fe + 4Al_2O_3 \quad (1.2)$$

$$MeWO_4 + 2Al + CaC_2 \longrightarrow Me + WC + CaO + Al_2O_3 \quad (1.3)$$

$$6CaWO_4 + 3CaC_2 + 10Al \longrightarrow 6WC + 9CaO + 5Al_2O_3 \quad (1.4)$$

A severe disadvantage of the process is the generation of heavy metal salts, mainly $FeCl_3$ (produced by acidic dissolution of Fe), the disposal of which is an environmental problem. Another disadvantage is that no grain size steering is possible, besides milling of the final WC. Further processing of milled Menstruum WC affords special skill, because a milled 5 µm powder behaves differently from a conventionally prepared grade. Menstruum WC is used in hard facing as well as in high-impact non machining applications.

1.5 Nanocrystalline materials research

The materials with nano sized (< 100 nm) grains are known as nanocrystalline materials. It is now well established fact that mechanical properties of the materials are significantly

altered by just reducing the grain size to nanometric range in bulk materials. The nanocrystalline materials are a new class of disordered solids having high density of defect cores (grain boundaries, interphase boundaries, dislocations etc.) [11]. Even half or more number of atoms is situated in the core of these defects. The unique properties of nanoscale particles and nano grain bulk materials can be attributed to two basic phenomenon:

1. The first is that the number of atoms at the surface and/ or grain boundaries in these materials are comparable to that of the atoms located in the crystal lattice, thus the chemical or physical properties are increasingly dominated by the atoms at these locations. As the grain size is reduced, large fraction of atoms may lie at the grain boundaries which may contribute to enhancement in toughness of the materials.
2. The second phenomenon is the "quantum size effect" or quantum confinement effect. When particles approach the nanometric size range, their electronic and photonic properties can be significantly modified as a result of the absence of a few atoms in the lattice structure.

Nanocrystalline materials can be synthesized either by consolidating small clusters or breaking down the polycrystalline bulk material into crystalline units with dimensions of nanometers [12]. These approaches have been classified into **bottom-up** and **top-down**. In the **bottom-up** approach the nanostructure are arranged atom- by-atom, layer -by layer. In the **top- down** approach we start with the bulk material is broken down to the lower size till the microstructure exhibit nanostructure.

1.6 Synthesis of nano tungsten carbide powder

Tool makers realised the use of fine grain particles as early as 1929 [13]. But in last two decades, advancement in the nano technology area (especially SEM/TEM/HRTEM) made it possible to characterize particles less than 100nm. The use of WC as catalyst is still keeping research alive in this area. Nano tungsten carbide powders have been synthesized from various tungsten precursors and adopting different methods.

1.6.1 The spray conversion process

This is versatile technique used for production of not only nano WC powders, but also composite powders WC-Co with addition of grain growth inhibitors at level of powder formation. The schematic presentation of the process is shown in Fig. 1.6 [14,15].

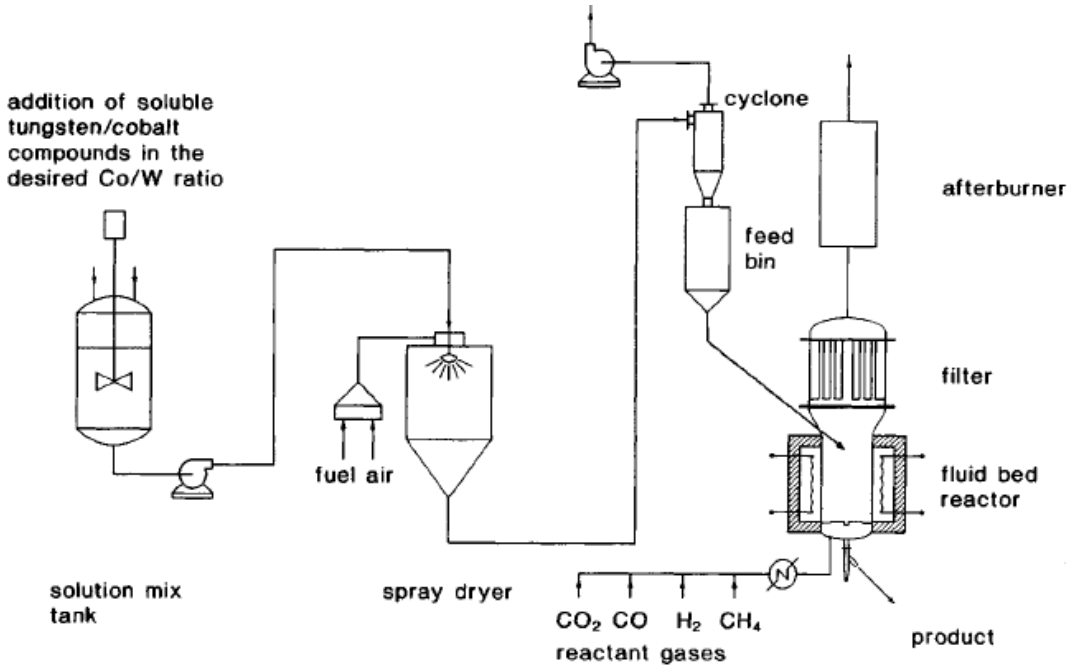

Figure 1.6: Schematic diagram of the spray conversion process [13,14].

This is a simple three step process involves formation of aqueous solution of soluble salts of tungsten, spray drying to form an amorphous powder and carburizing with carbon containing gases to form nano WC [13].

1.6.2 The chemical vapor reaction (CVR) process

In general, the chemical vapor synthesis of WC–Co materials involves the reduction of a tungsten salt precursor with hydrogen and carburization with a hydrocarbon gas [13]. If tungsten chloride is used as the precursor and the methane and hydrogen gases are used as the reducing agent as well as carbon source, the reaction equation will proceed as follows:

$$WCL_6\,(g) + H_2(g) + CH_4(g) \longrightarrow WC(s) + 6HCl(g) \qquad (1.5)$$

The free energy of the above reaction in the temperature range 800–1200°C is -469 to -630 kJ. In general, vapor phase reactions create a supersaturated vapour which is thermodynamically less stable than the formation of the solid material in nanopowder form. It includes chemical supersaturation in which it is thermodynamically favorable for the vapour phase molecules to react chemically to form a condensed phase rather than stay in the vapor form [16]. Different precursors like tungsten hexacarbonyl ($W(CO_6)$) [17], tungsten hexafluoride (WF_6) [18], or tungsten hexachloride (WCl_6) [19] having low volatilization temperatures have been used for synthesis of nano tungsten carbide.

1.6.3 Mechanical alloying

Mechanical alloying (MA) is a solid-state powder processing technique involving repeated welding, fracturing, and rewelding of powder particles in a high-energy ball mill [20]. MA has now been shown to be capable of synthesizing a variety of equilibrium and non-equilibrium alloy phases starting from blended elemental or pre-alloyed powders. The non-equilibrium phases synthesized include supersaturated solid solutions, metastable crystalline and quasicrystalline phases, nanostructures, and amorphous alloys. Li et al. [21] have also proposed a model for the refinement of grain size during ball milling and noted that the grain size in the early stages of milling follows the relation:

$$d = Kt^{-2/3} \qquad (1.6)$$

where d is the grain size, t is the time and K is a constant. The minimum grain size achievable by milling is determined by the competition between the plastic deformation via dislocation motion and the recovery and recrystallization behavior of the material [22].

1.7 Production of cemented carbides

Cemented carbides represent a group of hard and wear-resistant refractory composites in which hard carbide particles are bound together or are "cemented" by a ductile and tough binder matrix. Although the term "cemented carbide" is still widely used, mainly in english-speaking countries, and well describes the nature of the composite, they are even

better known internationally as "hardmetals." Hardmetals combine the high hardness and strength of the covalent carbide(s) (WC, TiC, TaC) with the toughness and plasticity of the metallic binder (Co, Ni, Fe). This unique combination of hardness and toughness makes them outstanding as tool materials in the manufacturing industry. Tungsten carbide (WC) is the basic and most widely used hard component. Cobalt was found to be the best binder metal.

1.8 Applications

Cemented carbides posses high hardness even up to 1000°C, which makes it ideal for usage in cutting tools for machining, mining and rock drilling applications [10]. Cemented tungsten carbide is also used for manufacturing standard pellets for wire, tube and bar drawing applications. These applications demand crucial combination of properties like wear resistance, surface finishing, hardness, compressive strength etc. WC-Co hard metal wear parts are used in large numbers in arduous service conditions where abrasion, erosion, and attrition are the main wear mechanisms resulting in premature failure of the component. These wear parts include nozzles, guides, plungers, balls, and many other shapes. Tungsten carbide is often used in armor-piercing ammunition, especially where depleted uranium is not available or is politically unacceptable. W_2C projectiles were first used by German Luftwaffe tank-hunter squadrons in World War II. Tungsten carbide is also an effective neutron reflector and as such was used during early investigations into nuclear chain reactions, particularly for weapons.

Hard carbides, especially tungsten carbide, are used by athletes, generally on poles that strike hard surfaces. Trekking poles, used by many hikers for balance and to reduce pressure on leg joints, generally use carbide tips in order to gain traction when placed on hard surfaces (like rock). It is also used for making surgical instruments meant for open surgery (scissors, forceps, hemostats, blade-handles, etc.) and laparoscopic surgery (graspers, scissors/cutter, needle holder, cautery, etc.).

Fuel cell is current hot topic of research for future energy requirements. The nano WC/Carbon is being used as catalyst in place of costly platinum in Polymer Membrane

Exchange Fuel Cell (PEMFC). The tungsten carbide has been used in other catalytic applications like hydronitrogenation, hydrosulfurization, alkane isomerisation, and other hydrocarbon conversion reactions. The catalytic properties become prominent with reduced particle size especially in the nanometric range.

1. 9 Need for direct methods of production of nano WC from ores

The use of nanosized WC particles in cemented carbides improves its tribomechanical properties dramatically. Also the catalytical properties are improved with the use of WC in nanometric range. The production process of WC from the ores covers in two parts. First one is the production of pure precursor(s) like WO_3, W, $W(CO)_6$, WCl_6,WCl_4 and APT; and second is production of nano WC from these precursor(s). The precursor(s) like W(CO)6, WCl_6 and WCl_4 are obtained by further processing of elemental tungsten. If we analyze whole process starting from ore, its digestion in acids/bases, purification and conversion into pure tungsten compound, it takes multiple high temperature treatments along with the use of excess amount (stoichiometry) of chemicals which makes the nano WC production costly, lengthy and energy intensive. For the large scale industrial use of nano WC, The process should be economical simple with minimum usage of chemicals. Keeping these things in mind, this research project was taken up.

Refernces

[1] Mining Journal special publication, Tungsten, June 2008.

[2] Zhengui Yao, Jacob J. Stiglich and T. S. Sudarshan, Materials Modification, Inc., VA 22031.

[3] G.S. Upadhyaya, Cemented tungsten carbides: production, properties and testing.Westwood, New Jersey, USA: Noyes publications; 1998.

[4] E. Lassner, W.D. Schubert, Tungsten Properties, Chemistry, Technology of the Element, Alloys, and Chemical Compounds. Kluwer Academic/Plenum Publishers, New York, 1999.

[5] Z. Wu, Y. Yang, D. Gu, Q. Li, D. Feng, Z. Chen, B. Tu, P.A. Webley, D. Zhao, Small, 5(23) (2009) 2738- 2749.

[6] R.P Herber, W.D.Schubert, B. Lux, Int. J. Ref. Metals Hard Mat., 24 (2006) 360–364.

[7] H.O. Pierson, Handbook of Refractory carbides and nitrides, Noyes Publications, Westwood, New jersey, USA, 1996.

[8] A.S. kurlov, A.I. Gusev, Inorg. Mat., 42(2), (2006) 121-127.

[9] C.M. Fernandes, A.M.R. Senos, Int. J. Ref. Metals Hard Mat. 29 (2011) 405–418.

[10] J.I. Martinsa, A. Moreiraa, S.C. Costa, Hydrometall. 70 (2003) 131–141.

[11] M.A. Meyers, A. Mishra, D.J. Benson, Prog. Mater. Sci. (2006) 427–556.

[12] G. Cao, Nanostructures & nanomaterials Synthesis, properties and applications, Imperial College Press, (2003).

[13] Z. Z. Fang, X. Wang, T. Ryu, K. S. Hwang, H.Y Sohn, Int. J Refract. Met. Hard Mater. 27 (2009) 288-299.

[14] L. E. McCandlish, B. H. Kear, and S. J. Bhatia, US Patent 5,352,269 (1994).

[15] L. E. McCandlish and P. Seegopaul, *Proc. European Conf. on Advances in* Hard Materials Production, Stockholm, pp. 93-100, EPMA, Shrewsbury, UK (1996).

[16] M.T. Swihart, Curr. Opin. Colloid. Interf. Sci., 8(1), (2003) 127–33.

[17] J.C. Kim, B.K. Kim, Scripta. Mater. 50(7) (2004) 969–972.

[18] M. Fitzsimmons, V.K. Sarin, Surf. Coat. Technol. 76(1-3) (1995) 250–255.

[19] J. Hojo, T. Oku, A. Kato, J. Less-Comm. Metal, 59(1) (1978) 85–95.

[20] C. Suryanarayana, Progress in Materials Science 46 (2001) 1-184.

[21] S. Li, K. Wang, L. Sun, Z. Wang, Scripta Metall. Mater., 27 (1992) 437-442.

[22] J. Eckert, J.C. Holzer, C.E. Krill III, W.L. Johnson, J. Mater. Res, 7 (1992) 1751-1761.

Chapter 2

Literature Review

Overview

This chapter reviews the different methods and procedures used for synthesis of monolithic WC and WC/Co nano powders. The entire literature is categorized into three parts; first one describes the details of the synthesis of WC and WC/Co nano powders from the pure tungsten precursors. The second part deals with synthesis from the ores (Wolframite/Scheelite). Literature review indicates that all efforts on direct synthesis of pure single phase nanocrystalline WC from the ore has led to impure/mix phase formation. Keeping in view this technological challenge, this research work has been undertaken. The third part deals with literature on sintering and consolidation of nanocrystalline WC powders, where the retention of nano size (<100 nm) of WC in sintering is scientific challenge.

The cemented tungsten carbides with nanocrystalline grain structure have significantly improved the mechanical properties over the conventional grade powders. These improvements in mechanical properties have led to longer life of the tools with better performance. Direct industrial applications and the associated advantages with nanocrystalline cemented carbides, is the motivation behind intensive research efforts in this area. However, its production is difficult task and has many challenges. Among these the major one is to have economical and eco-friendly production of nanocrystalline WC. The second one is retention of nanocrystalline WC grains in the cemented carbides.

Many different process technologies have been introduced to produce nanostructured tungsten carbide and tungsten carbide–cobalt composite powders. This include improvements in the conventional solid state synthesis route leading to more radical techniques such as spray conversion and chemical vapor reaction and deposition methods [1]. The synthesis of nano WC requires a wide range of pure tungsten precursors like tungstic acid (H_2WO_4), $(NH_4)_2WO_4$, ammonium para tungstate (APT), WO_3, W, WCl_6,WCl_4, WF_6 and 12- phosphotungstic acid as a base material in different methods. However, the synthesis of the pure precursors is via complicated processes. The simplified extraction sequence of these pure tungsten precursors from the ores is shown in Fig. 2.1. Even the first step in extraction of tungsten i.e digestion of the ore is complicated one. Research efforts are still going on to improve digestion of the ore [2-6]. Each step adds to cost, energy, time and environment hazard. There have been a few research efforts to synthesize WC directly from the ore, but none could result in pure single phase nanocrystalline WC. These research efforts from pure precursors and ores are summarized below.

2.1 Synthesis from pure tungsten precursors

2.1.1 Elemental tungsten (W)

Razavi et al. [7] synthesized single phase nano WC by mechanical alloying tungsten (W) and amorphous carbon (C). The materials were milled in stoichiometric ratio (W+C = WC) in a planetary ball mill. In order to prevent oxidation and undesired reaction during milling, milling cups were filled with 99.00% purity argon gas at a pressure of 250 kPa. The milling cups and balls used were of high chrome stainless steel.

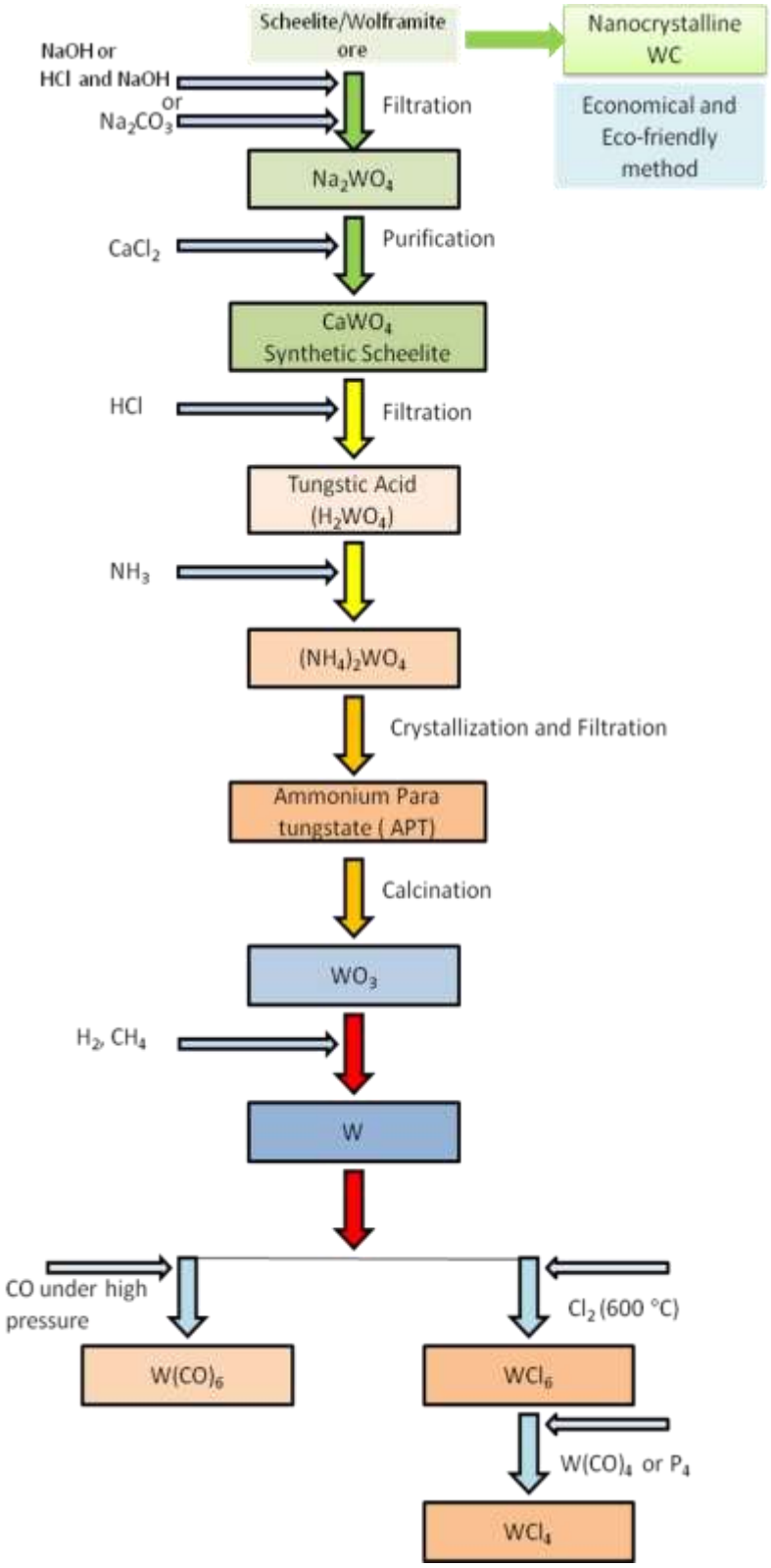

Figure 2.1: Simplified flow sheet showing different steps for the synthesis of different precursors of W from the ores.

They have observed that the formation of WC from W and C proceeds through three stages: first nucleation, second growth of these nucleated sites and finally in the third stage grains reach towards each other and then stops growth.

Vallance et al. [8] synthesized tungsten carbide on subminute timescales by solid state reaction of elemental tungsten and graphite in a microwave heating cavity experimental arrangement. The experiments were performed in two reactors for comparison. The first one being unmodified domestic microwave oven (DMO) (800 W, 2.45 GHz) and the second consisted of variable-power (1–15 kW, 2.45 GHz) microwave generator connected through an automatic *E–h* tuner (for impedance matching, where *E* is the electric field and *h* the magnetic field) to a TE_{10n} single-mode cavity. The optimum conditions for producing single-phase WC were 40 s at 3 kW (variable microwave generator) compared to 20 min (1200 s) in a DMO and up to 10 h (36000 s) conventionally. The synthesis time was reduced by nearly three orders of magnitude.

Zhu et al. [9] studied the combined effect of ball milling and dielectric barrier discharge plasma (DBDP) on treatment of pure metals Al, Fe and W and synthesized WC. Owing to synergism of ball milling and DBDP, the fabricated powders have unique features such as lump like morphology with very fine primitive particles and high specific surface area.

Lin et al. [10] synthesized tungsten carbide nano powders by electric discharge machining followed by annealing under a nitrogen atmosphere. The tungsten work pieces were initially melted and evaporated on the working surface during the electric discharge machining process, and then the tungsten powders were reacted with the carbon electrode in the working medium of kerosene to form the nanocrystalline WC_{1-x} powders. While annealing the powders under N_2 atmosphere, the cubic phases of WC_{1-x} gradually changed to hexagonal W_2C and then were transformed fully to nano crystalline hexagonal WC at 1200°C.

2.1.2 Tungsten trioxide (WO_3)

Kirakosyan et al. [11] synthesized WC-C and W_2C-C materials by self propagating combustion reaction. The tungsten oxide was deposited on a surface of fine grained carbon black by two methods. In the first case $(NH_4)WO_4$ was used as source of tungsten. For this purpose 20 g of ammonium tungstate was dissolved in 500 ml of deionized water and solution was added in parts to 16 g of carbon black. The produced pulp was dried in a drier fitted with magnetic stirrer for 1 h at 120°C. For making WO_3 the dried powders were heated for 4 h at 350°C. The combustion reaction was carried out by using stoichiometric quantity of magnesium which produced WC. In the second case tungsten oxide was made by dissolving WC in 50% hydrogen peroxide. The combustion reaction of this powder produced $\propto$-W_2C carbide.

Ma et al. [12] synthesized tungsten carbide nanoparticles from mechanically activated tungsten oxide and graphite. Mechanical activation was carried out for 10 h in a QM-1SPU planetary ball mill under argon atmosphere. The ball to powder weight ratio was 10:1. The calcination of powders was carried out under vacuum at 741°C and 1215°C respectively for 1 h. The mechanically activated sample produced nano WC at 1215°C with small quantity of W. The WC was formed via intermediates including mangeli phases ($WO_{2.72}$ and WO_2) and metallic tungsten. Milling of 10 h was sufficient for full conversion of WO_3 to WC.

Guo et al. [13] synthesized tungsten carbide nanocrystals by simple reaction of WO_3, Mg and anhydrous CH_3CH_2OH. The reaction precursors were heated in an autocalve at 600°C. In this process two types of WC crystals were produced; one was pure WC, and other wrapped by carbon. The diameter of WC nanocrystals ranged from 100 to 200 nm.

Akshay et al. [14,15] used thermo-chemical reaction route to synthesize WC-nanoparticles from WO_3. Two different carbon sources were used to study the effect of these sources on synthesis. During experimentation the reaction parameters were varied to optimize the processing variables for the formation of tungsten carbide (WC) nanoparticles. Maximum yield of WC was obtained with reaction time of 20 h.

Lytle et al. [16] **c**arried out pseudomorphic carburizations of three-dimensionally ordered macroporous (3DOM or inverse opal) WO_3 with morphological retention on a sub-100 nm length scale without catalyst. Superior structural replication was achieved by directly carburizing WCl_6-PMMA preform composites. The extent of carburization was thermodynamically controlled, whereas morphological deterioration via sintering was kinetically governed.

Won et al. [17] synthesized nano-sized tungsten carbide powder using WO_3,Mg and C in the presence of sodium halides and carbonate. Sodium fluoride, which has the highest melting temperature, was the most effective halide for decreasing the size and phase transformations of tungsten carbide. The addition of a small amount of ammonium carbonate accelerated the carburization of tungsten carbide and enabled the formation of pure-phase tungsten carbide. Won et al.[18] also synthesized nano sized refractory metal carbides (W_2C, Mo_2C, TaC, NbC, ZrC, and TiC) by combustion reactions of transition metal oxides (WO_3, MoO_3, Ta_2O_5, Nb_2O_5, ZrO_2, and TiO_2), magnesium, carbon, and sodium fluoride. The average particle size of carbides prepared in this study was below 100nm.

Reddy et al. [19] studied the influence of the precursor structure on nanostructured W–C phase evolution during reduction and carburization of WO_3 under hydrogen environment. Nanostructured WC was obtained from a chemically synthesized precursor consisting of hexagonal, monoclinic and partially amorphous WO_3 and amorphous C by heat treatment at 1000°C. The phase analysis of the heat treated product also revealed a small fraction of amorphous WC. No trace of W_2C, W or WC_{1-x} was detected.

Aravinth et al. [20] synthesized tungsten carbide nano particles by carburizing tungsten/tungsten oxide/non-stoichiometric tungsten oxide particles obtained from a wire explosion process with multi walled carbon nano tubes (MWCNT). TEM study showed that the tungsten carbide particles were spherical in shape with mean size of 19nm.

Lei et al. [21] synthesized nano NbC, TaC, VC, hexagonal WC and MoC at relatively low temperatures using an organic reagent melamine and transition metal oxides as reaction precursors.

Li et al. [22] synthesized WC, NbC and TaC nanoparticles by solid state reaction process using graphite like phase of C_3N_4 (g-C_3N_4) as the carbonizing reagent at a relatively low temperature (1150°C). The results showed that g-C_3N_4 was a highly efficient carbonizing reagent and the oxides WO_3, Nb_2O_5 and Ta_2O_5 were completely converted into corresponding carbides at 1150°C.

2.1.3 Tungsten Hexacarbonyl ($W(CO)_6$)

Kim et al. [23] synthesized WC_{1-x} carbide by chemical vapour condensation process using tungsten hexacarbonyl $W(CO)_6$ precursor. The precursor was decomposed into W and CO at 120°C**.** The carburization of W was done in the range of 600 to 800°C. With the increase in reaction temperature the grain size was found to decrease from 53 to 28 nm. The grain size was drastically reduced under vacuum atmosphere because of the reduced residence time of vapour molecules in the reaction chamber.

Pol et al. [24] synthesized WC nanotubes by low temperature (900°C) thermal decomposition of $W(CO)_6$ in the presence of Mg powder. The reaction was carried out in closed Swagelok cell at autogenic pressure. The dia of WC nanotubes ranged from 30 to 70 nm and length varied from 1 to 10 µm.

2.1.4 Tungsten tetrachloride (WCl_4)

Giordano et al. [25] synthesized metal nitrides and carbides (such as Mo_2N, Mo_2C, W_2N and WC) nanoparticles from $MoCl_5$ and WCl_4 using urea as the carbon-source. $MoCl_5$ and WCl_4 are in first step contacted with alcohols and an appropriate amount of urea to form a polymer-like, glassy phase, which acted as the starting product for further conversions. Just by heating this phase it was possible to prepare either molybdenum and tungsten nitrides or carbides simply by changing the metal precursor/urea molar ratio. Sizes estimated by WAXS range 4 to 20 nm in diameter for Mo and W nitrides or carbides. The specific surface area was found in between 10 and 80 m^2/g.

Nartowski et al. [26] synthesized transition metal carbides by solid-state metathesis reactions via a fast (10 s), single-step reaction. Thermal initiation of a mixture of calcium carbide with anhydrous metal chloride inside an evacuated ampoule around 450 °C produced a transient red melt which on cooling, formed a black solid with some calcium chloride layered on the surface (within 2 to 10 s).

2.1.5 Tungsten hexachloride (WCl_6)

Hojo et al. [27] prepared tungsten carbides (WC, W_2C) powders of 0.04–0.05 μm by vapour phase reaction of the WCl_6-CH_4-H_2 system at 1000–1400 °C. Won et al. [28] synthesised ultrafine tungsten carbide powder from WCl_6-C_2H_2-H_2 mixtures. Under the claimed experimental conditions, a mixture of α-WC and β-W_2C was produced. Taeyong et al. [29, 30] prepared WC and WC-Co composite powders by chemical vapour synthesis using tungsten hexachloride WCl_6 as the precursor. Ma et al. [31] synthesized nanocrystalline hexagonal WC via co-reduction of WCl_6 and sodium carbonate with metallic magnesium.

2.1.6 Tungsten hexaflouride (WF_6)

Fitzsimmons and Sarin [32] performed thermodynamic equilibrium calculations using SOLGASMIX-PV at varying partial pressure of WCl_6-CH_4-H_2 and WF_6-CH_4-H_2. Chemical vapour deposition (CVD) phase diagrams were constructed from these calculations. These phase diagram were used to determine process parameters for the deposition of Monolithic hexagonal WC. It was observed that coatings grown low temperatures contained phases other than those predicted in CVD phase diagrams.

2.1.7 12-Tungstophosphoric acid

Shanmugam et al. [33] synthesized tungsten carbide nanorods and nanoplatelets by direct pyrolysis of a hybrid composite material of 12-tungstophosphoric acid and exadecyl-trimethylammonium bromide in a closed Swagelok cell at 1000°C. The diameter of the nanorods was 30-50 nm, and the length varied from 200 to 500 nm. The size of the platelets was around 55 nm. The WC exhibits an interesting structural surface with kinks, steps, and terraces.

2.1.8 Tungstic acid (H_2WO_4)

Thakur et al [34] synthsized WC-Co nanoclusters in situ reduction of tungstic acid and cobalt chloride in the nanoporous silica gel matrix by heat treating at 1623 K for 0.5 h. Average particle sizes of WC and Co in the nanoclusters were around 30 and 25 nm.

2.1.9 Ammonium tungstate penta hydrate ($5(NH_4)0.12WO_3.5H_2O$)

Morishita et al. [35] synthesized WC involving the nano metal cobalt by a gas-solid reaction between the cobalt non equilibrium supersaturated-tungsten powder and carbon mono-oxide gas (CO). The metal Co domains formed in the WC were found to be spherical with a diameter of approximately 60 nm. A nano-scale fine structure composed of the WC with average diameter, d_{Av}, of approximately 500 nm was obtained.

2.1.10 Ammonium paratungstate

Ryu et al. [36] synthesized nanosized tungsten carbide powder with ammonium paratungstate (APT) as the precursor by thermal plasma process. The reduction and carburization of vaporized APT produced nanosized tungsten carbide (WC_{1-x}) powder, which sometimes contained a small amount of W_2C phase. The produced tungsten carbide (WC_{1-x}) powder was 20 nm in particle size. The synthesized powders were also subjected to a hydrogen heat treatment to fully carburize the WC_{1-x} and W_2C phases to the WC phase as well as to remove excess carbon.

The literature work described above indicates that lot of work has been done to synthesise nano WC powders from pure precursors [7-36]. But these precursor(s) are obtained by lengthy processing, as shown in Fig. 2.1. For the minimal processing, synthesis should be done from ore itself.

2.2 Synthesis from ores

2.2.1 Wolframite ore

Jadmbaa et al. [37] synthesized nano WC from wolframite ore, $FeWO_4$ (WO_3: 71.85, Fe_2O_3: 20.36, MnO_2: 5.46, and SiO_2: 1.1 wt.%), containing low amount of silica. They used active charcoal of average particle size of 35 nm and having surface area of 68 m^2/g. The ore was ball milled before formulating the mixture in order to reduce the particle size

to 10-μm regime. The composition of the mixture (Wolframite and active carbon) was set equal to the stoichiometry of the reaction. Powders were loaded in air in a planetary ball mill. A 250-mL jar and zirconium balls were used for grinding. The balls to powder weight ratio was kept at 50:1. Milled powders were uniaxially compressed into pellets at 50 MPa. The pellets were calcined in a tube furnace by heating at a constant rate of 20°C/min up to 900°C or 1100°C under flowing argon gas. The final product contained nano WC along with Fe_3W_3C, Fe_7W_6, W, Fe_3C and Fe as impurities.

MacKenzie et al. [38] studied the mechano-chemical activation of mixtures of wolframite ($FeWO_4$) with carbon, by ^{57}Fe Mossbauer spectroscopy. They took activated carbon of average particle size of 35 nm having surface area of $68m^2/g$ and graphite which was pre-milled to tabular particles of 50μm size. The results indicated that mechanochemically induced reactions were essentially independent of nature of carbon used.

Akshay et al. [39] synthesized nano WC from wolframite ore, $FeWO_4$ (WO_3: 50.7, Fe_2O_3: 34.227, SiO_2: 9.579, Al_2O_3: 3.155, MnO: 1.785, TiO_2: 0.270, SnO_2: 0.156 and K_2O: 0.128 wt. %) supplied by Wolfram Bergbau, Austria. The ore was leached by hydrochloric acid (1:1) to get WO_3. To break silica a few drops of HF were added in HCl (1:1) solution before leaching. Silica was leached easily by converting it into hexafluoro silicic acid. The reactions were carried out in a sealed autocalve at 800°C for 20 h with different liquid carbon sources. The WC phase was formed by using acetone as carbon source out of the three methanol, ethanol and acetone.

2.2.2 Scheelite ore

Johnston et al. [40] studied the direct reduction carburization of reagent grade calcium tungstate ($CaWO_4$) with solid carbon at 1227°C. The $CaWO_4$ and activated carbon were mixed in twice the stoichiometry ratio required to obtain final tungsten carbide. The scheelite ore was completely reduced to WC, W and CaO reaction products. They concluded that tricalcium tungstate (Ca_3WO_6) was produced at first step of reduction as an intermediate product.

Welham [41,42] synthesized micron sized tungsten carbide from the scheelite ($CaWO_4$) ore by solid state reaction method. The mixture of scheelite and graphite (in stoichiometric ratio) was milled for 40 h for mixture activation. The milled powders were annealed at 1000°C, which led to direct production of WC, W_2C and with small amount of unreacted scheelite. The calcined powders were easily leached to get highly porous micron sized tungsten carbide particles. **Welham** [43] studied the effect of milling of scheelite + magnesium with graphite and in nitrogen atmosphere. When mixture was milled with graphite nanocrystalline W_2C was formed. In N_2 atmosphere milled powders on subsequent annealing at 1000°C produced 10nm crystallites of elemental tungsten.

Lee et al. [44] prepared tungsten powder by a self-propagating high-temperature synthesis (SHS) process of a $CaWO_4$-Mg mixture. They used $CaWO_4$ of 98.5 to 99.5% purity. Mg vapor was discovered to affect such combustion parameters e.g. combustion temperature (T_c), the combustion velocity (U), the relative mass change (Δm) and the relative elongation (Ah) of the sample significantly. These effects could be reduced by decreasing the internal argon pressure, sample density and the reducing agent content.

Butukhanov et al. [45] studied the possibility of reduction of calcium tungstate in an inert medium (in vacuum and argon). The natural materials, namely scheelite and datolite concentrates having components WO_3 and B_2O_3 were used. The main products of reduction were W_2B_5, WC, W_5Si_3, and SiC. The apparent activation energy of carbon diffusion in the carbide phase was evaluated, and it was shown that the reduction of scheelite concentrate could be carried out during electroslag remelting (ESR).

Literature survey indicates that none of the reported investigations from ore(s) could lead to the synthesis of single phase pure nanocrystalline WC [37, 40, 41-43, 45]. Moreover, only solid state reaction method was attempted to synthesize nanocrystalline WC. Furthermore, if the synthesis is to be done without purification of the ore, then the process to remove impurities after synthesis is not given. This issue is not addressed properly in these studies**.**

2.3 Sintering and grain growth of nanocrystalline WC-Co

There has been a significant technological development with respect to sintering. However, nanocrystalline WC–Co powders lose their nanoscale characteristics upon sintering due to extremely rapid grain growth during sintering. Although commercial processes are now available for producing sintered WC–Co with ultrafine grain sizes (<200 nm), controlling grain growth during sintering and producing bulk nanocrystalline hard materials remains a critical technology challenge [1]. The consolidation of nano sized WC-Co powders have been approached with different techniques with the objective to retain WC nano structure. Apart from standard methods, liquid phase sintering LPS [46-51], hot isostatic pressing HIP [52] unconventional processes such as microwave sintering [48-50] and spark plasma sintering (SPS) [56–61], high frequency induction-heated sintering (HFIHS) [62], rapid omni compaction (ROC) [63], and ultrahigh pressure rapid hot consolidation (UPRC) [64], pulse electric current sintering [65] and high pressure spark plasma sintering (HPSP) [66] have been used.

2.3.1 Densification

The first benefit of using nanocrystalline particles is the reduction in sintering temperature and the same behaviour was observed for WC-Co powders [67].

Maheshwari et al. [68] studied the sintering of WC–10Co powders with different initial particle sizes. Fig. 2.2 shows the percent of densification as a function of the continuous heating temperature for various initial particle sizes. Clearly, the entire temperature range of sintering decreases steadily as the initial average particle size decreased from 30 μm to 10 nm.

2.3.2 Grain growth

The key challenge in the use of nanocrystalline WC in cemented carbides is the retention of its nanocrystalline size during sintering. Excessive grain growth occurs during heating. So the understanding of grain growth mechanism is essential. There have been numerous suggestions that the rapid grain growth occurs by coalescence of grains. Coalescence. describes a unique way of grain growth, which can be accomplished through mass transport

mechanisms. Possible mechanisms for coalescence include various diffusion process, or even grain rotations. Direct evidence of coalescence is, however, very difficult to identify.

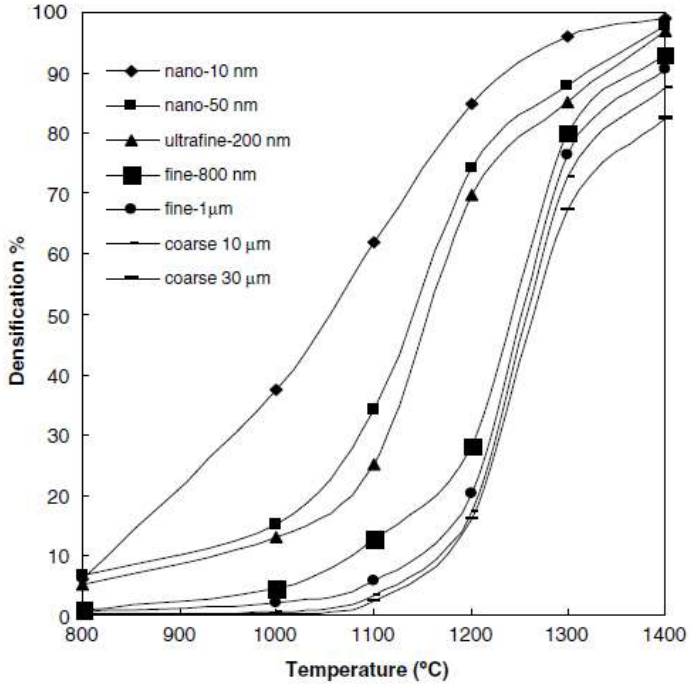

Figure 2.2: The percent of densification of WC–Co as a function of the temperature [65].

Wang et al. [69] studied grain growth and densification behaviour during heating up of nanocrystalline WC–Co powder. The powders were heated in a vacuum furnace with a heating rate of 10°C/min. The samples were then furnace cooled immediately after reaching the preset temperature with no holding time. The original 10 nm grain size was increased almost 90-fold to 900 nm by 1400°C. This ‘‘explosive” grain growth occured almost instantly during heat-up, with no holding time [70-73]. It appears that a critical temperature exists above which the grain growth accelerates dramatically as a function of temperature.

Fang et al. [74] studied the grain growth of nano WC during heat-up, and found the growth of nanosized tungsten carbide via coalescence of preferred-oriented attached and faceted particles within aggregates. The shape change and faceting of the surface of nano WC particles are indicative of rapid mass transport even at low temperature. It has been

speculated that when nanoscales are approached, mass transportation mechanisms become more dominant.

2.4 Sintering processes and techniques for controlling grain growth

2.4.1 Grain growth inhibitors

Grain growth inhibitors have been used to retard grain growth during sintering. It was found that 100–150 nm grain sizes at full density could be obtained via standard LPS with the addition of 1.5 wt.%VC [47, 75]. The use of grain growth inhibitors is widely practiced for sintering fine grain and ultrafine grain WC– Co materials in the industry. Commonly used inhibitors include chromium carbide, tantalum carbide, and vanadium carbide. Their relative effectiveness can be ranked in the order VC > Cr_3C_2 > NbC > TaC, although other considerations such as corrosion resistance and hot hardness may affect the choice of grain growth inhibitors. Other than carbides, doping of ceria and yattria nano particles also retards the grain growth [76, 77].

2.4.2 Pressure assisted sintering

A fundamental reason for using external pressure during sintering is to promote densification by adding a driving force. It is a particularly important factor for sintering nanostructured powder because it does not directly contribute to the driving force for grain growth. The effects of pressure are constrained by the pores and any gases in the pores. Higher pressures are capable of collapsing pore structures and inducing plastic flow and rapid bonding in powder compacts at elevated temperatures. This eliminates the need for long holding times at high temperatures and hence prevents grain growth [51, 78].

2.4.3 Fast sintering techniques

Compared to conventional sintering techniques, fast sintering techniques are characterized by shorter densification time at lower temperature, resulting from external field coupled with applying pressure such as SPS, HFIHS, etc. [79, 80]. SPS, for example, the application of electrical fields, can generate rapid and simultaneous heating within samples due to the pulse electrical current through the graphite die and/or samples.

In summary very few attempts have been made to synthesize WC from ore(s) itself. These studies could not lead to single phase WC. Moreover, synthesized WC particle size was more than nano range. No procedure was developed for removal of impurities after synthesis, particularly SiO_2. Only solid state reaction method was used for these studies, which involves reaction temperature more than 1000°C. No report is available on consolidation of nanocrystalline WC synthesized from the ore in the matrix of Co. If we analyze the whole process of extraction of pure precursor(s) from ore and further synthesis of nanocrystalline WC, the total process is multistep involving use of chemicals at most of the stages with or without use of temperature/pressure. Clearly the direct synthesis from ore will reduce the number of steps and minimal usage of chemicals. Considering the fact that no method is available for synthesis of nanocrystalline WC from ore(s), present investigations have been undertaken to synthesize pure WC nano particles involving lesser number of steps from the ore(s) itself.

References

[1] Z. Z. Fang, X. Wang, T. Ryu, K. S. Hwang, H.Y. Sohn, Int. J. Ref. Metals Hard Mat., 27 (2009) 288–299.

[2] J. F. Paulinoa, J. C. Afonso, J. L. Mantovano, C. A. Vianna, J. W. S. D. Cunha, Hydrometal., 127-128 (2012) 121–124.

[3] Z. Zhao, J. Li, S. Wang, H. Li, M. Liu, P. Sun, Y. Li, Hydrometal., 108 (2011) 152–156.

[4] J.I. Martins, A. Moreira, S.C. Costa, Hydrometal. 70 (2003) 131–141.

[5] Z. Zhao, Y. Liang, H. Li, Int. J. Ref. Metals Hard Mat., 29 (2011) 289–292.

[6] R.P.S Gaur, The J. The Min. Metals and Mater. Soc., 58 (9) (2006) 45-49.

[7] M. Razavi, R.M. Rahimipour, and R. Yazdani-Rad, J. All. Compds., 509 (2011) 6683-6688.

[8] S. R. Vallance, S Kingman, D H. Gregory, Adv. Mater., 19 (2007) 138–142.

[9] M. Zhua, L.Y. Dai, N.S. Gu, B. Cao, L.Z. Ouyang, J. All. Comp., 478 (2009) 624–629.

[10] M.-H. Lin, Cera. Inter., 31 (2005) 1109–1115.

[11] Kh.G. Kirakosyan, Kh.G. Manukyan, S.L. Kharatyan, and R.A. Mnatsakanyan, Mat. Chem. Phys., 110 (2008) 454-456.
[12] J. Ma, S.G. Zhu, Int. J. Ref. Metals Hard Mat. 28 (2010) 623–627.
[13] C. Guo, Y. Liu, X. Ma, Y. Qian, L. Xu, Chem. Lett., 35(11) (2006) 1210-1211.
[14] A. Kumar, K. Singh, and O.P. Pandey, Phys. E., 41 (2009) 677-684.
[15] A. Kumar, K. Singh, and O.P. Pandey, Phys. E., 42 (2010) 2477-2483.
[16] J. C. Lytle, N.R. Denny, R.T. Turgeon, A. Stein, Adv. Mater., 19 (2007) 3682–3686.
[17] H. I. Won, H. H. Nersisyan, C. W. Won, J. Nanopart. Res., 12 (2010) 493–500.
[18] H.I Won, N. Hayk, C. W. Won, H. H. Lee, J. Mater. Sci., 46 (2011) 6000–6006.
[19] K. Madhav Reddy, T. N. Rao, J. Joardar, J. All. Compds., 494 (2010) 404-409.
[20] S. Aravinth, B. Sankar, M. kamraj, S.R. Chakravarthy, R. Sarathi, Int. J. Ref. Metals Hard Mat., 33 (2012) 53-57.
[21] M. Lei, H.Z. Zha, H. Yang, B. Song, W.H. Tang, J. the Euro.Cera. Soc. 28 (2008) 1671–1677.
[22] P.G. Li, M. Lei, Z.B. Sun, L.Z. Cao, Y.F. Guo, X. Guo, W.H. Tang, J. All. Compds., 430 (2007) 237–240.
[23] J.C. Kim, B.K. Kim, Scri. Mate., 50 (2004) 969–972.
[24] S. V. Pol, V. G. Pol, A. Gedanken, Adv. Mater., 18 (2006) 2023–2027.
[25] C. Giordano, C. Erpen, W. Yao, M. Antonietti, Nano Letts., 8(12) (2008) 4659-4663.
[26] A. M. Nartowski, I. P. Parkin, A. J. Craven, M. MacKenzie, Adv. Mater., 10(10) (1998) 805-808.
[27] J. Hojo, T. Oku, A. Kato, J. Less-Common Met., 59 (1978) 85-95.
[28] C.W. Won, B. Chun, H. Y. Sohn, J. Mater. Res., 8 (1993) 2702-2708.
[29] T. Ryu, H. Y. Sohn, G. Han, Y.-U. Kim, K.S. Hwang, M. Mena, Z.Z. Fang, Metall. Mater. Trans. B., 39B (2008) 1-6.
[30] T. Ryu, H. Y. Sohn, K.S. Hwang, Z.Z. Fang, J. Mater. Sci., 43 (2008) 5185-5192.
[31] Jianhua Maa, Yihong Du, J. All. Compds., 448 (2008) 215–218.
[32] M. Fitzsimmons, V. K. Sarin, Sur. Coat. Tech. 76-77 (1995) 250-255

[33] S. Shanmugam, D.S. Jacob, A. Gedanken, The J Phys. B Chem. Letts. 109 (2005) 19056-19059.

[34] A. D. Thakur, M. G. Chaudhuri, G. C. Das, Into. J Appl. Cera. Tech., (2013) 1-8. DOI:10.1111/ijac.12048.

[35] M. Morishita, H. Yamamoto, T. Okahira, M. Yoshika, N. Fukumuro, H. Matsuda, M. Ikebe, H. Yanagita. H. Nishimaki, J. Am. Ceram. Soc. 95(12) (2012) 3797-3801.

[36] T. Ryu, H. Y. Sohn, K. S. Hwang, Z. Z. Fang, J. Am. Ceram. Soc. 92(3) (2009) 655-660.

[37] J. Temuujin, M. Senna, T. Jadambaa and D. Byambasuren, J. Am. Ceram. Soc., 88 (4) (2005) 983–985.

[38] K.J.D. MacKenzie, J. Temuujin, C. McCammon, M. Senna, J. the Euro. Cera. Soc. 26 (2006) 2581–2585.

[39] A. Kumar, K. Singh, O.P. Pandey, Int. J. Ref. Metals Hard Mat., 29 (2011) 555–558.

[40] R.F. Johnston, H.T. Nguyen, Miner. Eng., 9(7) (1996) 765-773.

[41] N.J. Welham, Mat. Sci. Eng. A, 248 (1998) 230–237 .

[42] N.J. Welham, AIChE J., 46(1) (2000) 68–71.

[43] N.J. Welham, Room temperature reduction of scheelite (CaWO4), J. Mater. Res., 14(02) 1999 619-627.

[44] J. H. Lee, J. C. Jung, I. P. Borovinskaya, V. I. Vershinnikov, C. W. Won, Metals and Mat., 6(1) (2000) 73-80.

[45] V. L. Butukhanov, T. B. Ershova, E. V. Khromtsova, ISSN 0040-5795, Theo. Found. Chem. Eng., 42(5) (2008) 699–702.

[46] D.F. Carroll, Int. J. Refract. Metal. Hard Mater., 17(1-3) (1999) 123–132.

[47] Z.Z. Fang, J.W. Eason, Int. J. Refract. Metal Hard Mater., 13(5) (1995) 297–303.

[48] L.E. McCandlish, B.H. Kear, B.K. Kim, Nanostruct. Mater., 119 (1992) 119.

[49] L.E. McCandlish, P. Seegopaul, R.K. Sadangi, Adv. Powder Metall. Particulate Mater., 3 (1995) 313–317.

[50] L. Zhang, T.E. Madey, Nanostruct. Mater., 2(5) (1993) 487–493.

[51] E. Soares, L.F. Malheiros, J. Sacramento, M. A. Valente, F.J. Oliveira, J. Am. Ceram. Soc., 95 (6) (2012)1822–1831.

[52] I. Azcona, A. Ordonez, J.M. Sanchez, F. Castro, J. Mater. Sci., 37(19) (2002) 4189–4195.

[53] D. Agrawal, J.P. Cheng, P. Seegopaul, L. Gao, Powder Metall., 43(1) (2000) 15–26.

[54] E. Breval, J.P. Cheng, D.K. Agrawal, P. Gigl, M. Dennis, R. Roy, Mater. Sci. A, 391(1-2) (2005) 285–295.

[55] R. Bao, J. Yi, H. Zhang, Y. Peng, Int. J. Refract. Metal. Hard Mater., 32 (2012) 16-20.

[56] D. Sivaprahasam, S.B. Chandrasekar, R. Sundaresan, Int. J. Refract. Metal. Hard Mater., 25(2) (2007) 144–152.

[57] G. Maizza, S. Grasso, Y. Sakka, T. Noda, O. Ohashi, Sci. Technol. Adv. Mater. 8(7–8) (2007) 644–654.

[58] S.I. Cha, S.H. Hong, B.K. Kim, Mater. Sci. A, 351(1-2) (2003)31–38.

[59] C.C. Jia, H. Tang, X.Z. Mei, F.Z. Yin, X.H. Qu, Mater. Lett., 59(19-20) (2005)2566–2569.

[60] A.K. Nanda Kumar, M. Watabe, K. Kurokawa, Vacuum, 88(2013) 88-92.

[61] V. Bonache, M.D. Salvador, A. Fernandez, A. Borrell, Int. J. Refract. Metal. Hard Mater., 29 (2011) 202-208.

[62] H.C. Kim, I.K. Jeong, I.J. Shon, I.Y. Ko, J.M. Doh, Int. J. Refract. Metal. Hard. Mater., 25(4) (2007) 336–340.

[63] E. M. Dubensky, R.T. Nilsson, Dense fine grained mono tungsten carbide transition metal cemented carbide body and preparation thereof. US patent 5773735; 1996.

[64] X. Wang, Z. Fang, H.Y. Sohn. In: Engquist J, editor. Proceedings of the 2007 international conference on powder metallurgy & particulate materials, Denver, US; 2007. p. 08-1.

[65] B. Wang, K. Matsumaru, J. Yang, Z. Fu, K. Ishizaki, J. Am. Ceram. Soc., 95 (8) (2012) 2499–2503.

[66] S. Grasso, J. Poetschke, V. Richter, G. Maizza, Y. Sakka, M.J. Reece, J. Am. Ceram. Soc., 96 (6) (2013) 1702–1705.

[67] Schubert WD. In: 2000 International conference on tungsten hard metals and refractory alloys, Annapolis, MD, USA; 2000.

[68] P. Maheshwari, Z.G.Z. Fang, H.Y. Sohn, Int. J. Powder Metall., 43(2) (2007) 41–47.

[69] X. Wang, Z.Z. Fang, H.Y. Sohn, Int. J. Refract. Metal. Hard. Mater., 26(3) (2008) 232–241.

[70] F. Zhou, J. Lee, E.J. Lavernia, Scripta. Mater., 44(8-9) (2001) 2013–2017.

[71] Z.J. Shen, H. Peng, J. Liu, M. Nygren, J. Eur. Ceram. Soc., 24(12) (2004) 3447–3452.

[72] R. Klemm, E. Thiele, C. Holste, J. Eckert, N. Schell, Scripta. Mater., 2002;46(9):685–90.

[73] G. Hibbard, K.T. Aust, G. Palumbo, U. Erb, Scripta. Mater.,44(3) (2001)513–518.

[74] Z. Fang, P. Maheshwari, X. Wang, H.Y. Sohn, A. Griffo, R. Riley, Int. J. Refract. Metal. Hard. Mater., 23(4-6) (2005) 249–257.

[75] G. Gille, B. Szesny, K. Dreyer, H. H. Vanden Berg, J. Schmidt, T. Gestrich, Int. J. Refract. Metal. Hard. Mater., 20(1) (2002) 3–22.

[76] X. Sun, Y. Wang, D.Y. Li, Wear 301 (2013) 406–414.

[77] O.A.M. El-Kady, Materials and Design 52 (2013) 481–486.

[78] L. Bartha, P. Atato, A.L. Toth, R. Porat, S. Berger, A. Rosen, J. Adv. Mater., 32(3) (2000) 23–26.

[79] A. Michalski, D. Siemiaszko, Int. J. Refract. Metal. Hard. Mater., 25(2) (2007) 153–158.

[80] L. Sun, C.C. Ha, M. Xian, Int. J. Refract. Metal. Hard. Mater., 25(2) (2007) 121–124.

Chapter 3

Experimental Procedure

Overview

The experimental procedures followed for the synthesis of nano WC from the ores (Scheelite and Wolframite) by solid state reaction method and thermo-chemical route in a self designed high temperature autoclave are described in this chapter. The characterization procedures along with instruments details to generate and analyze the data have also been given. The synthesized nano WC is further used to develop (WC-Co) under different experimental conditions.

The present chapter describes details of the experimental procedures for the synthesis of WC nano powders from ores and their characterization. The details of these are presented below.

3.1 Raw materials

The two commercially important ores of the tungsten; scheelite (North American Tungsten Corporation, Canada) and wolframite (Wolfram Bergbau Austria) have been used in the present work. The other chemicals used were ethanol (99%, Merck, Germany), acetone (99%, Merck, Germany), Mg turnings (99%, S.D. Fine Chemicals), activated charcoal (99%, S.D. Fine Chemicals), HCl (S.D. Fine Chemicals) and HF (S.D. Fine Chemicals). All the materials including ore and ore concentrates were used without any purification. Table 3.1 gives the details of constituents present in Wolframite ore. All the constituents were in oxide form. The concentration of WO_3 (source of W) in wolframite ore was around 50% and rest were impurities.

Table 3.1

Chemical composition of wolframite ore.

S. No.	Compound	(Wt. %)
1	WO_3	50.70
2	Fe_2O_3	34.23
3	SiO_2	9.58
4	Al_2O_3	3.15
5	MnO	1.78
6	TiO_2	0.27
7	SnO_2	0.16
8	K_2O	0.13

Similarly the chemical composition of scheelite ore which was a concentrated ore is given in Table 3.2. It is important to note that concentration of W as WO_3 in scheelite was between 60 to 70%, which was higher than wolframite ore. Also the concentration of SiO_2 impurity in scheelite was around 1% which is much less as compared to wolframite (9.6%). Since scheelite procured was in form of ore concentrate so this variation is understandable.

Table 3.2 Chemical composition of scheelite concentarate (in wt. %).

		Unit	Assay Range			Unit	Assay Range
Aluminum	Al	%	0.1 - 0.2	Niobium	Nb	ppm	2
Antimony	Sb	ppm	1 - 2	Nickel	Ni	ppm	5
Arsenic	As	ppm	40 - 60	Phosphorus	P	%	0.05 - 0.25
Barium	Ba	ppm	40 - 60	Potassium	K	%	0.02 - 0.04
Beryllium	Be	ppm	2	Rhenium	Re	ppm	<1
Bismuth	Bi	%	0.1 - 0.6	Rubidium	Rb	ppm	<1
Calcuim	Ca	%	12 - 15	Selenium	Se	ppm	10 - 20
Cadmium	Cd	ppm	1	Silica	SiO_2	%	0.7 - 1.2
Cerium	Ce	ppm	400	Silver	Ag	ppm	<1
Cobalt	Co	ppm	2 - 4	Sodium	Na	%	0.5
Chromium	Cr	ppm	200 - 300	Strontium	Sr	ppm	50 - 100
Cesium	Cs	ppm	<1	Sulphur	S	%	0.2 - 1.0
Copper	Cu	ppm	100 - 200	Tantalum	Ta	ppm	<1
Gallium	Ga	ppm	5	Tellurium	Te	ppm	<1
Germanium	Ge	ppm	1	Thorium	Th	ppm	1 - 2
Gold	Au	ppm	<1	Titanium	Ti	ppm	100 - 200
Hafnium	Hf	ppm	<1	Thallium	Tl	ppm	2
Indium	In	ppm	<1	Tin	Sn	ppm	5 - 10
Iron	Fe	%	1.5 - 3.5	Tungsten	W	%	56.9 - 58.5
Lanthanum	La	ppm	40 - 50		as WO_3	%	60 - 74
Lead	Pb	ppm	20 - 50	Uranium	U	ppm	20
Lithium	Li	ppm	15 - 30	Vanadium	V	ppm	5 - 10
Magnesium	Mg	%	0.15 - 0.30	Yttrium	Y	ppm	200 - 300
Manganese	Mn	%	0.15 - 0.30	Zinc	Zn	ppm	100
Mercury	Hg	ppm	< 1	Zirconium	Zr	ppm	3 - 5
Molybdenum	Mo	ppm	300				

3.2 Methodology

3.2.1 Synthesis by solid state reaction method

The methodology of the experimentation for the solid state reaction method is shown in the form of flow chart in Fig. 3.1. The particle size of scheelite ore ($CaWO_4$) was in the range of 100 to 400 µm whereas wolframite ore was in the range of 0.5 to 4µm. The procured ores were milled for different time periods to reduce the particle size. The milling of powders was done in Fritsch (Puloerisette) and Retsch (PM 100) to reduce the particle size. The powders were milled in tungsten carbide jar (250 ml) using tungsten carbide balls (10mm). The initial experiments could not lead to complete transformation of $CaWO_4$ to fully carburized WC. In order to get latter phase, a variation in experimental conditions like milling time, rpm and ball to powder weight ratio was done which are described at appropriate places in **results and discussion sections**.

The milled scheelite/wolframite were mixed with activated charcoal in appropriate ratios and milled for activation of the mixture. The milled mixture powders were loaded in a die of 15 mm diameter and a pressure of 115kg/cm^2 was applied on the plunger of the die. The pressure was maintained for one minute and after that pressure was released. These pellets were taken out and calcined in a tubular furnace at different temperatures under flowing argon gas. The calcined pellets were taken out and dissolved in dilute HCl (1:1). The powders containing acid solution was kept for 1h to facilitate the dissolution of CaO, MgO and other impurities of the ores. The acid washed powders were further base treated by 0.25M NaOH (1 h holding time) to remove traces of silica and other oxides in the calcined powders.

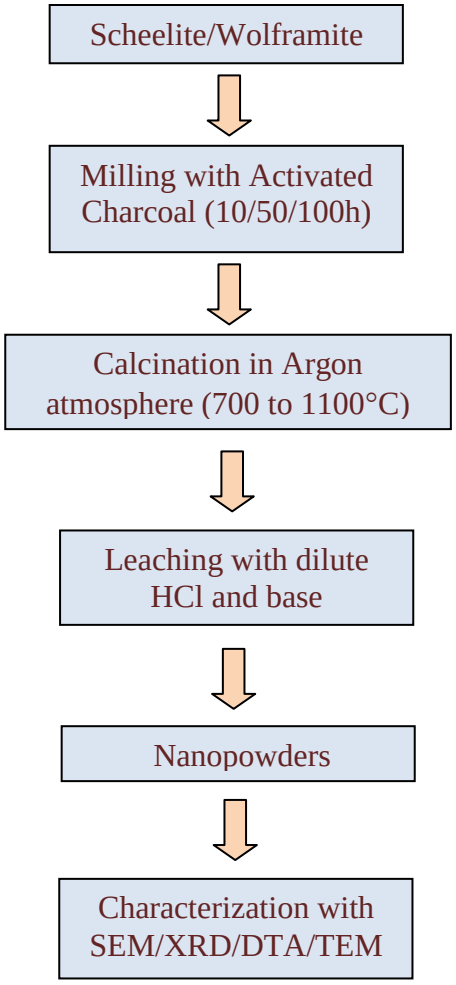

Figure 3.1: Flow chart of the procedure followed for solid state reaction method.

3.2.2 Synthesis by thermo-chemical route

The synthesis of nano carbide was also done at high temperature and high pressure. In this method vapors and gases are generated which are essential to carry out complete reactions. So, we have used thick walled autoclave (65ml) of SS 304 material in the experiments. Based on our earlier work, an autoclave of higher capacity was designed to perform the experiments at higher temperatures [1]. Since the provision of pressure sensor which could work at such a high temperature was not available so pressure could not be measured.

Magnesium (Mg) turnings have been used as reducing agent whereas activated charcoal and acetone as carbon source in different experiments. Initial experiments were carried out by heating the scheelite and Mg with liquid carbon sources at 800°C by filling more than 50% of the autoclave volume [2-3]. However, autoclave was unable to withstand high pressure and leaking was observed. Moreover, when the amount of liquid carbon source was reduced to less than 50% of the autoclave, mixed phase formation was observed (details are described in results and discussion section).

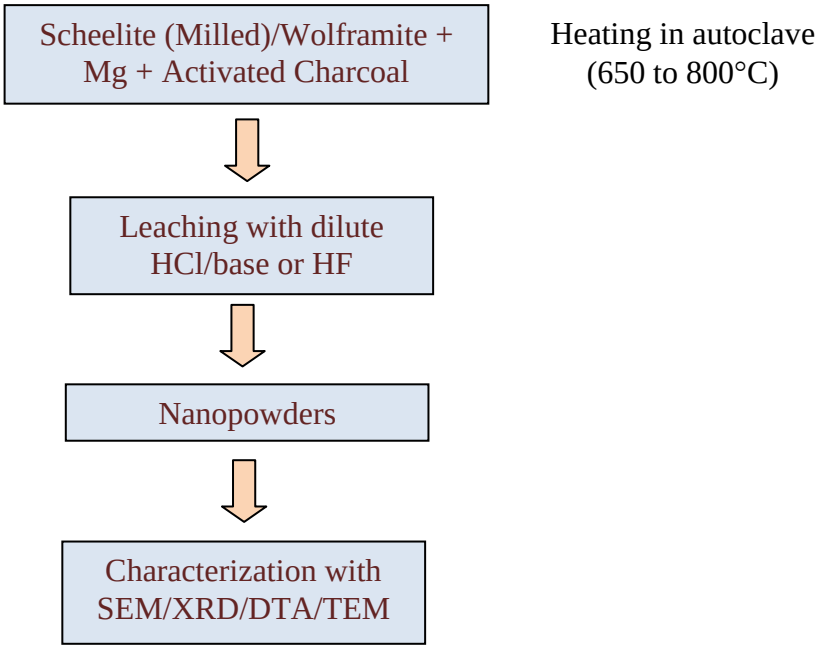

Figure 3.2: Flow chart of the procedure followed for thermo-chemical route.

Considering these facts, some of the experiments were also performed in "dry autoclaving" condition at a relatively lower temperature (<800°C) where activated charcoal was used as carbon source. The dry autoclaving is a process in which chemical reactions are carried out without solvents above the dissociation temperature of chemical precursors [4]. This process is comparatively much safer than solvothermal method. Experiments were performed using known quantities of scheelite/wolframite, Mg and activated charcoal to optimize the conditions.

To get the product phase from the ores of W, the sealed autoclave containing the ingredients was kept in a furnace at different temperatures for varied time periods (details given in next sections). The furnace was heated at the rate of 5°C/min. After the experiment, autoclave was allowed to cool in the furnace. The powders were taken out and washed with dilute HCl (1:1) to remove CaO, MgO and other impurities followed by base treatment (0.25M NaOH) to remove traces of silica in case of scheelite ore. However, the wolframite ore contained nearly 9.5% silica (SiO_2) as impurity. SiO_2 was successfully removed by HF leaching (details mentioned in section 5.2**)**

3.2.3 Sintering of WC-Co composite

The as synthesized WC nano particles from scheelite ore, obtained by solid state reaction method and thermo-chemical route were used for the preparation of WC-Co composites where cobalt was used as binder. Since nano sized Co powders were getting oxidized and were burning so the experiments were performed with ultrafine (micron sized) Co powders (Electronica Tough Carb Ltd., India). The amount of cobalt (Co) was varied from 10 to 15 % of WC weight. For the preparation of composites WC and cobalt powders were mixed in pestle mortar for 2 h. To this mixture few drops of 2 wt% of polyvinyl alcohol was mixed. Known weight of dried powders was transferred in 15 mm die. The powders were pressed in hydraulic press (Polyhedron, India; Model 5010) at a compaction pressure of 503 MPa. After holding for one minute the pressure was released and pellets was taken out from the die. These pellets were sintered at 1200, 1300 and 1400°C in argon atmosphere.

3.3 Materials characterization

The characterization of WC nano particles was done with help of X-ray diffraction (XRD), thermal gravimetric/differential thermal analysis (TG/DTA), scanning electron microscope (SEM), FESEM, transmission electron microscope (TEM), HRTEM while the sintered WC-Co composite were characterized using optical and scanning electron microscope (SEM). The details of these techniques are given below:

3.3.1 X-Ray diffraction

X-ray diffraction (XRD) is a versatile, non-destructive technique that reveals detailed information about the chemical composition and crystallographic structure of natural and manufactured materials [5-6]. X-ray powder diffractrogram was recorded at room temperature by Xpert Pro PANalytical diffractometer using monochromatic CuK_{α} radiation (λ = 1.5418 Å) with Ni filter at a scan speed of 5^{o}/minutes. Powders were exposed to X-ray where grains are randomly orientated which ensures all crystallographic directions that are sampled by the beam. When X-rays are scattered from a crystal lattice (Fig. 3.3), peaks of scattered intensity are observed which correspond to the following conditions:

1. The angle of incidence = angle of scattering.
2. The path length difference is equal to an integer number of wavelengths.

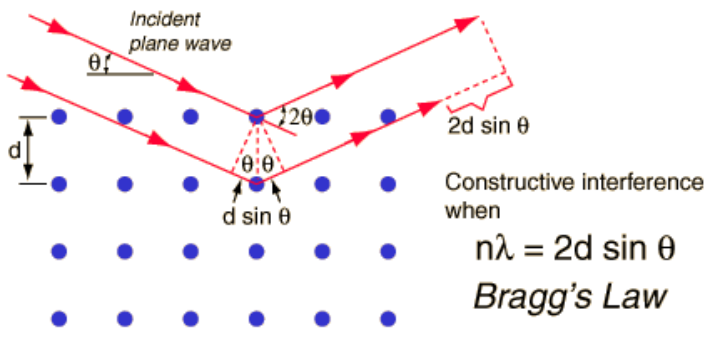

Figure 3.3: Geometric derivation of Bragg's law

From the Bragg's law, the inter planner spacing and crystal structure is obtained using formula

$$2dSin\theta = n\lambda$$

where d = interplanar spacing, λ = wavelength of incident x-ray, θ = diffraction angle, n = integer. The data obtained from XRD is indexed by standard powder diffraction files provided by International Centre for Diffraction Data -ICDD (formerly known as JCPDS).

3.2.2 Rietveld analysis

X-ray diffraction patterns of single phase nano WC were refined by Rietveld method for calculating precise lattice parameters [6-8]. In Rietveld method, the XRD patterns are decomposed by using Pawley and/or Le Bail algorithms. Rietveld refinement is computationally intense and employs the nonlinear least squares method, which requires a reasonable initial approximation of many free variables. These usually include peak-shape parameters, unit cell dimensions and coordinates of all atoms in the model of the crystal structure. Other unknowns (e.g., constant background, scale factor, overall atomic displacement parameter, etc.) may be simply guessed at the beginning and then effectively refined as the least squares fit converges to a global minimum. The Rietveld refinement uses a least squares approach to refine a theoretical line profile until it matches the measured profile. The minimized function, Φ, is therefore, given by:

$$\Phi = \sum_{i=1}^{n} W_i \left\{ Y_i^{obs} - Y_i^{calc} \right\}^2$$

Where, w_i is the weight assigned to the i^{th} data point. The summation is carried over all measured data points, *n*. In Rietveld refinement, both the pattern *i.e.* Y_i^{obs} *and* Y_i^{calc} are plotted in same window. To see the difference between Y_i^{obs} *and* Y_i^{calc}, the fitting quality of the diffraction pattern is presumed. For the good fitting both pattern should completely overlap to each other i.e. $Y_i^{obs} - Y_i^{calc} = 0$. Visual examination of the difference usually

provides important clues about which additional parameter(s) must be adjusted (refined). The following numerical factors are normally used to characterize Rietveld refinement quality. The profile residual (or reliability) factor, Rp:

$$R_p = \frac{\sum_{i=1}^{n} \left| Y_i^{obs} - Y_i^{calc} \right|}{\sum_{i=1}^{n} Y_i^{obs}} \times 100\%$$

The weighted profile residual, R_{wp}:

$$R_{wp} = \left[\frac{\sum_{i=1}^{n} W_i \left\{ Y_i^{obs} - Y_i^{calc} \right\}^2}{\sum_{i=1}^{n} W_i \left(Y_i^{obs} \right)^2} \right]^{1/2} \times 100\%$$

The expected profile residual, R_{exp}:

$$R_{exp} = \left[\frac{n - p}{\sum_{i=1}^{n} W_i \left(Y_i^{obs} \right)^2} \right]^2 \times 100\%$$

Where *p* is the number of free least squares parameters.

And the goodness of fit, χ^2:

$$\chi^2 = \frac{\sum_{i=1}^{n} W_i \left\{ Y_i^{obs} - Y_i^{calc} \right\}^2}{n - p} = \left[\frac{R_{wp}}{R_{exp}} \right]^2$$

For the best fitted data χ^2 should be minimum.

3.2.3 Scanning electron microscopy (SEM)

The scanning electron microscope (SEM) is a type of electron microscope that images the sample surface by scanning it with a high-energy beam of electrons. The electrons interact with the atoms that make up the sample producing signals that contain information about the sample's surface topography, composition and other properties such as electrical conductivity. The types of signals produced by the SEM include secondary electrons (SE), back scattered electrons (BSE), characteristic X-rays, light (cathodoluminescence), specimen current and transmitted electrons. The morphology of the powders were studied with scanning electron microscope (Jeol JSM 6510V) and FESEM (Jeol 7600F). Before SEM analysis, the samples were ground, polished and gold plated to enhance conductivity if required.

3.2.4 Energy-dispersive X-ray spectroscopy

Energy-dispersive X-ray spectroscopy (EDS or EDX) is an analytical technique used for the elemental analysis or chemical characterization of sample. It is one of the varients of X-ray fluorescence spectroscopy which relies on the investigation of a sample through interactions between electromagnetic radiation and matter, analyzing X-ray emitted by the matter in response to being hit with charged particles. Its characterization capabilities are based on the fundamental principal that each element has a unique atomic structure allowing X-rays that are characteristic of an element’s atomic structure to be identified uniquely from one another. The system is attached with the scanning electron microscope and this technique is used for the elemental analysis of the materials. For EDS analysis Oxford INCA model no 51-ADD0076 (Inca) spectrometer is used.

3.2.5 Transmission electron microscopy (TEM)

Transmission electron microscopy (TEM) is a microscopy technique in which a beam of electron is transmitted through an ultra thin specimen. It interacts with the specimen as it passes through. An image is formed from the interaction of the electrons transmitted through the specimen; the image is magnified and focused onto the imaging device, such as fluorescent screen, on a layer of photographic film, or to be detected by a sensor such

as CCD camera. TEMs are capable of imaging at a significantly high resolution than light microscopes, owing to the small de Broglie wavelength of electrons. This enables the instrument's user to examine fine details even as small as a single column of atoms, which is tens of thousands times smaller than the smallest resolvable object in a light microscope. At smaller magnifications TEM image contrast is due to absorption of electrons in the materials, due to thickness and composition of the materials. At higher magnifications complex wave interactions modulate the intensity of the image , requiring expert analysis of observed images. Alternate modes of use allow for the TEM to observe modulations in chemical identity, crystal orientation, electronic structure and sample induced electron phase shift as well as the regular absorption based imaging. The TEM examinations were performed using TEM Models, PHILIPS CM200 and HRTEM JEOL-JM 2100F at different magnifications. For TEM study the synthesized powder was suspended in ethanol. One drop of the suspension was dropped on carbon coated copper grid and alcohol was allowed to evaporate.

3.2.6 Selected area diffraction pattern

By adjusting the magnetic lenses such that the back focal plane of the lens rather than the imaging plane is placed on the imaging apparatus in TEM, a diffraction pattern can be generated. For thin crystalline samples, this produces an image that consists of a pattern of dots in the case of single crystal, or a series of rings in case of a polycrystalline or amorphous solid materials. For the single crystal case the diffraction pattern is dependent upon the orientation of the specimen and the structure of the sample illuminated by the electron beam. This image provides the investigator with information about the space group symmetry in the crystal and the crystal's orientation to the beam path.

3.2.7 Lattice-plane fringes

The crystal-lattice planes can be imaged and resolved, provided that the information about the lattice structure – that is, the primary and the Bragg reflected beam – can pass through the objective diaphragm and that the contrast is not destroyed by insufficient spatial and temporal coherence [9]. The primary beam and Bragg reflection are inclined at an angle $\theta g = 2\theta_B$ ($2d \sin \theta_B = \lambda$). The plane waves interfere in the image plane with

smaller angular separation $\theta g/M$ (M: magnification) between the primary and reflected waves. The distance between the maxima of the resulting two-beam interference fringes is Md. Today it is possible to resolve lattice-plane fringes with *d equal to approx.* 0.1 nm.

3.2.8 Thermal analysis

Thermal analysis of the samples was done by differential thermal analysis (DTA) and thermo gravimetric (TG) techniques. For thermal analysis the material under study and an inert reference are heated (or cooled) under identical conditions, while recording any temperature difference between sample and reference. This differential temperature is then plotted against time (TG), or against temperature (DTA curve). Changes in the sample, either exothermic or endothermic, can be detected relative to the inert reference. Thus, a DTA curve provides data on the transformations that have occurred, such as oxidation, reduction, crystallization and melting. Similarly TG data provides the weight loss. In the present work thermal analysis was done by Diamond TG/DTA, Perkin Elmer.

3.2.9 Microhardness testing

Micro hardness of the composite was measured using Vickers micro hardness tester, Mitutoyo, Japan at 100g load.

3.2.10 Optical microscopy

Optical micrographs of sintered WC-Co composites were recorded using optical microscope (Model Eclipse MA-100, Nikon). The samples under study were first mechanically polished using standard procedures then examined under the microscope.

References

[1] Akshay Kumar, Preparation and Characterization of Tungsten Carbide Micro/Nano Composites, Ph.D. Thesis, 2011.

[2] A. Kumar, K. Singh, O.P. Pandey, Phys. E., 42 (2010) 2477-2483.

[3] A. Kumar, K. Singh, and O.P. Pandey, Int. J. Refract. Met. Hard Mater., 29 (2011) 555-558.

[4] V.G. Pol, S.V. Pol, A. Gedanken, Adva. Mater., 23 (2011) 1179-1190.

[5] B.D. Cullity, Elements of X-ray diffraction. Addison-Wesley Publishing, London.1977.

[6] J. Rodriguez-Carvajal, *Program Fullprof.2k* Version 5.0, 2011 (LLB, CEA-CNRS).

[7] V.K. Pecharsky, P.Y. Zavalij, Fundamentals of powder diffraction and structural characterization of materials. Springer, USA, 2005, pp. 342-343.

[8] Georg Will Powder Diffraction; The Rietveld Method and the Two Stage Method to Determine and Refine Crystal Structures from Powder Diffraction Data Springer Berlin Heidelberg New York, 2006.

[9] L. Reimer H. Kohl, Transmission Electron Microscopy; Physics of Image Formation, Springer 2008. ISBN 978-0-387-40093-8.

[10] G. Cao, Nanostructures & nanomaterials Synthesis, properties and applications, Imperial College Press, (2003).

Chapter 4

Results and Discussion (Scheelite Ore)

Overview

In this chapter the results obtained from scheelite ore for the synthesis of single phase nanocrystalline tungsten carbide at 1025°C (solid state reaction method) and 800, 700 and 650°C (thermo-chemical route) are presented. In order to get pure WC nano phase, the processing parameters were optimized. The results of these are also described in detail. This chapter is divided into three sections; first one presents results of experiments done by solid state reaction method. The second one describes the results obtained by thermo-chemical route. The third section gives the details of some scaling experiments conducted by thermo-chemical route. The powders were characterized by XRD, TG/DTA, SEM, FESEM, TEM and HRTEM. The lattice parameters of synthesized WC were calculated from refined crystal structure by Rietveld Method. All the experiments were conducted without any purification of scheelite ore. Removal of impurities was done after the synthesis to get nanocrystalline WC.

In this chapter the results of experiments carried out from the scheelite ore without any purification to get nano WC are described. Generally ore contains different impurities, and to remove the impurities different processes are adopted which make the whole metal extraction process energy intensive and costly. After synthesis of WC the impurities are washed out with dilute acid and base where lesser amount of acid/ base are used compared to conventional processes [1-3]. Another major advantage is that it will generate lesser effluents than conventional process. Moreover, the digestion of the ore in conventional routes itself is a complicated process which requires high temperature and pressure treatments [4-7].

4.1 Solid state reaction method

4.1.1 Reduction of scheelite ore to nano tungsten products

For the reduction of scheelite ore activated charcoal was chosen as carbon source over graphite because it is more reactive than graphite. A mixture of as obtained scheelite and activated charcoal was prepared in a ratio of 1:1 by weight. Powders were loaded in 250 ml capacity tungsten carbide jar and milled in air with WC balls. The ball to charge weight ratio was kept at 50: 1. The mixture was milled for 10 h at 290 rpm in a ball mill (Fritsch, Germany). After milling the powders were taken out. Pellets of 15 mm diameter of the mixed powder were made by applying pressure of 115kg/cm^2. These pellets were taken out and calcined in a tubular furnace at 1100 °C for 4 h and 10 h under flowing argon gas. The samples were acid and base leached to remove CaO and unwanted phases. TEM analysis was done for powders leached first in HCl (1:1) followed by base leaching (10% NaOH) to remove unreacted CaO and minor phases.

4.1.1.1 Characterisation of raw materials

As described in experimental section charcoal and scheelite ore were taken as blend to reduce the ore. In order to see their stability and volatile character these were further analysed which is presented in following sections.

4.1.1.2 Thermo gravimetric analysis

The TG/DTA analysis of scheelite ore and charcoal was done at a heating rate of 10°/min and crystalline Al_2O_3 as reference material which is shown in Fig. 4.1(a). TG curve of raw scheelite shows around one percent weight loss. This is probably because of evaporation of some trace impurities. DTA curve is not showing any endothermic or exothermic peak, indicating stability of the scheelite up to 1030°C. TG and DTA curves of activated charcoal and milled mixture are shown in Fig. 4.1(b) and (c) respectively. TG curve of activated charcoal depicts steep weight loss around 500°C and there is a corresponding exothermic peak in DTA, indicating burning of carbon. The weight loss of activated charcoal is around 98% showing impurities level up to approximately 2%. The TG curve of the milled mixture shows that the weight loss has shifted towards lower temperature around 400°C with a corresponding higher exothermic peak in DTA. The weight loss temperature got lowered because of reduction in size of activated charcoal during milling.

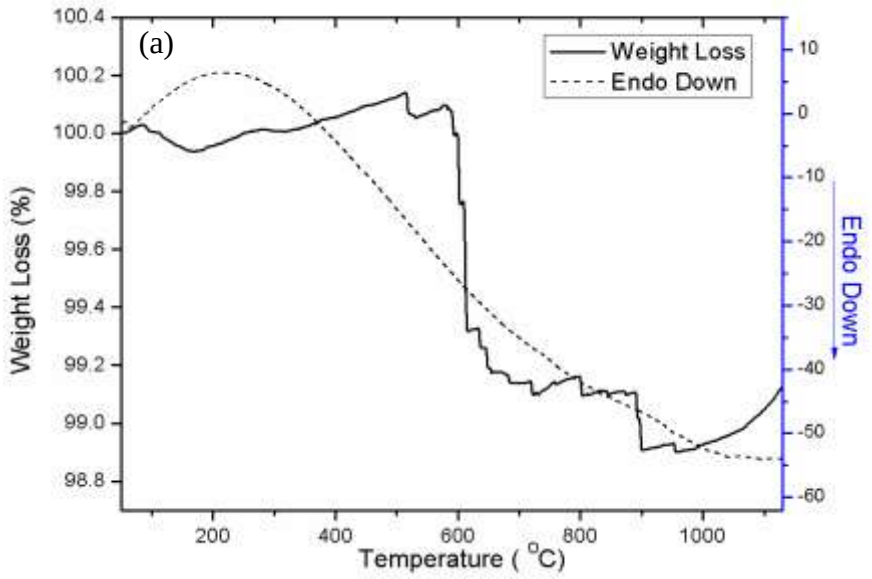

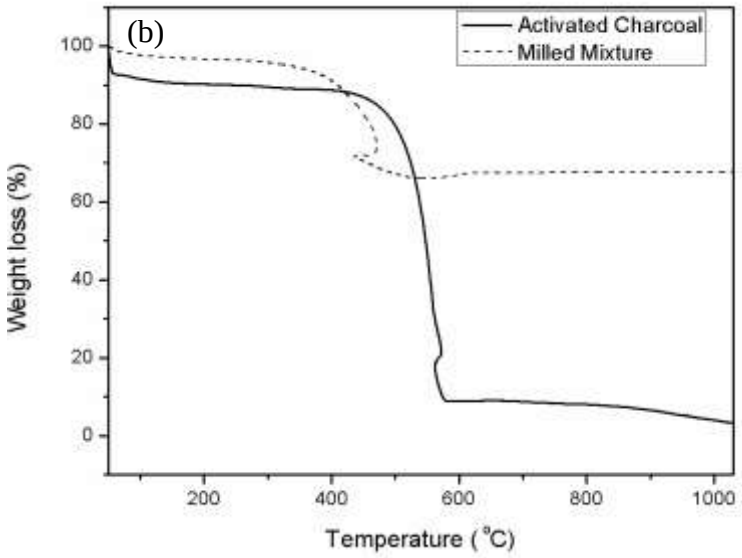

.

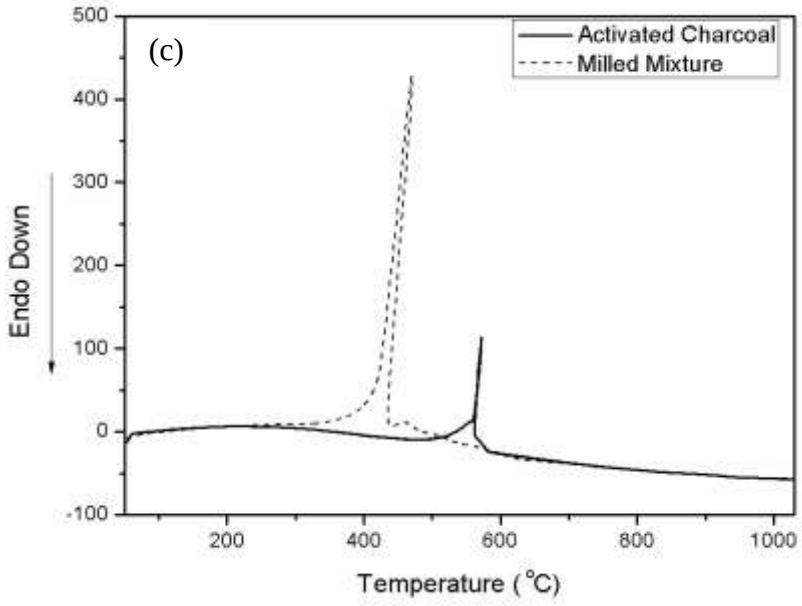

Figure 4.1: (a) TG and DTA traces for the raw scheelite.
(b) TG traces for the powders of activated charcoal and milled mixture.
(c) DTA traces for the powders of activated charcoal and milled mixture.

In DTA, exothermic peak intensity was increased because of burning of charcoal having highly reactive surfaces due to reduced size. During milling operation large amount of impact energy is transferred to the softer phase charcoal as compared to scheelite causing

major reduction in particle size of activated charcoal which provides highly reactive surfaces [8-10].

4.1.1.3 X- Ray diffraction analysis

Fig. 4.2(a) shows X-ray diffraction pattern of raw scheelite, confirming the presence of single phase $CaWO_4$ (ICDD card no. 01-072-1624). The X- ray diffraction pattern of milled (scheelite and activated charcoal) and calcined (1100°C for 4 h) sample is shown in Fig. 4.2(b). High intensity peaks corresponding to WC phase are observed in this X-ray diffraction pattern (ICDD card no. 01-073-9874). Highest intensity peak matches with elemental tungsten (ICDD card no. 01-089-2767). Also some low intensity peaks of $CaWO_4$ phase are present. It indicates that $CaWO_4$ phase has not undergone complete reduction. The calcination at 1100°C for 4 h has produced WC and W with residual scheelite.

The X- ray diffraction pattern of milled (scheelite and activated charcoal) and calcined sample (10 h at 1100°C) taken from pellet is shown in Fig. 4.2(c). Medium intensity peaks corresponding to the WC phase were observed in this X-ray diffraction pattern (ICDD card no. 03-065-4539). Highest intensity peak matches with elemental tungsten (ICDD card no. 01-089-490). Also medium intensity peaks of $CaWO_4$ phase were present, showing presence of residual scheelite after the reaction. This 10 h calcination has produced similar results in terms of phases formed as that of 4 h calcination. However, there is change in their volume fraction as calculated by X'Pert HighScore Plus (Table 1); which shows more residual $CaWO_4$ and lesser WC in comparison to 4 h calcined sample. The reason for this variation is that XRD pattern of 4h calcined sample was recorded by crushing the pellet into powder form whereas in case of 10h calcined sample XRD pattern was taken in pellet form. The XRD pattern of 10h calcined sample gives the pellets surface condition only. Further, when XRD pattern of acid and base leached 10 h calcined sample were taken in powder form the amount of WC and other fractions were almost same (Fig. 4.2(d)). Moreover, the semi quantity gives the approximate fractions of the constituent powders.

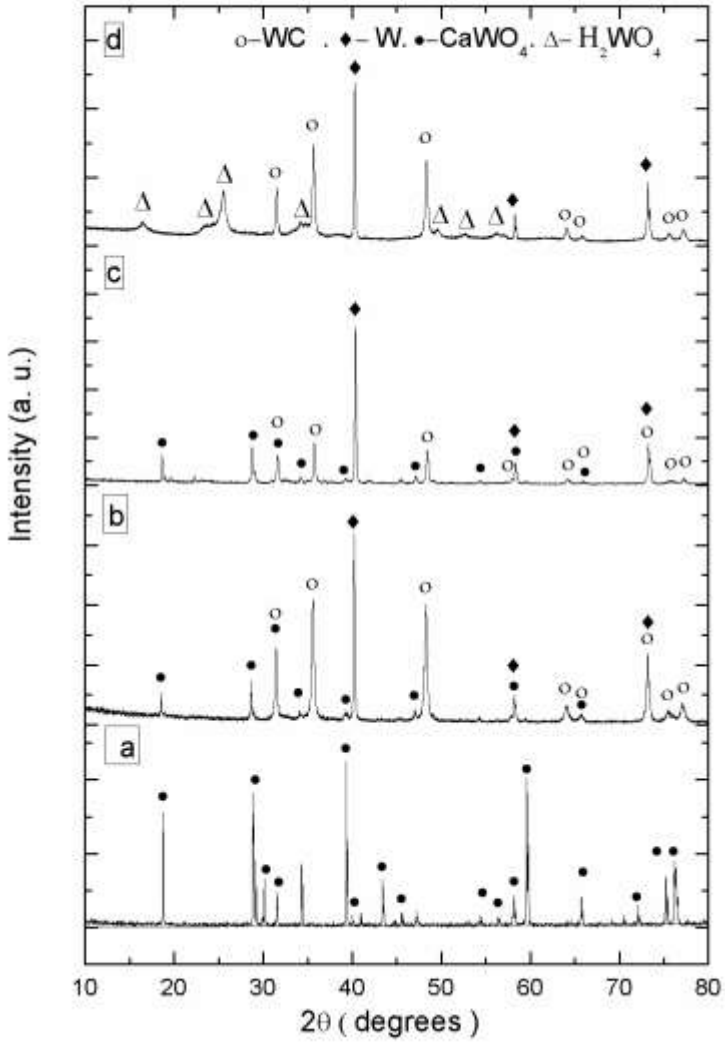

Figure 4.2: X-ray diffraction patterns of the (a) raw scheelite (b) milled and 4 h calcined sample (c) milled and 10 h calcined sample (d) leached sample obtained in (c)

This reveals that increase in calcination time from 4 h to 10 h did not improve the yield of tungsten carbide. So, 4 h calcination time is sufficient for reduction/carburization. The diffraction pattern of leached sample also shows the diffraction peaks corresponding to the tungstic acid phase, which got converted from $CaWO_4$ during leaching.

Table 4.1 Details of phase analysis along with their percentage.

Product	Phase	Card Match	Semi Quantity(%)
Raw Scheelite	$CaWO_4$	01-072-1624	100
4 h calcined sample	WC	01-073-9874	43
	W	01-089-2767	38
	$CaWO_4$	01-072-1624	19
10 h calcined sample	WC	03-065-4539	40
	W	01-089-4900	31
	$CaWO_4$	01-072-1624	30
10 h calcined sample	WC	03-065-8828	44
After acid and base leaching	W	01-075-6145	37
	H_2WO_4	01-084-0886	19

4.1.1.4 SEM analysis

Fig. 4.3(a & b) shows scanning electron micrographs of the milled (scheelite and activated charcoal), compacted and calcined sample (10 h at 1100°C). Here two different types of morphological features along with voids are visible. The unreacted $CaWO_4$ grains which exhibit flowery features depict breaking up morphology, evenly distributed on the whole pellet surface. The other phase visualizes grains of elemental tungsten and WC showing faceted morphology. During calcination, all the particles of scheelite in pellet have gone through the reaction simultaneously producing WC, and W with residual $CaWO_4$. It is possible that smaller particles got completely reduced to WC, medium sized particles to WC and W, and larger ones to WC and W along with residual $CaWO_4$, because, reduction usually starts from surface and then it proceeds to core. It seems that larger scheelite particles have undergone reduction in two steps. In first step surface scheelite particles in contact with carbon are reduced to WC, exhausting some of the carbon in immediate contact. In second step lesser carbon atoms have reduced next layer of scheelite atoms to W only, exhausting all the carbon in immediate contact, leaving behind some residual scheelite in the core. The foremost condition for the solid state

reaction to occur is that reactants should be in intimate contact with each other. Fig. 4.3(b) shows scheelite particles with breaking up morphology having empty space around it. It confirms that the residual scheelite is obtained only from larger scheelite particles which do not have any more carbon in intimate contact.

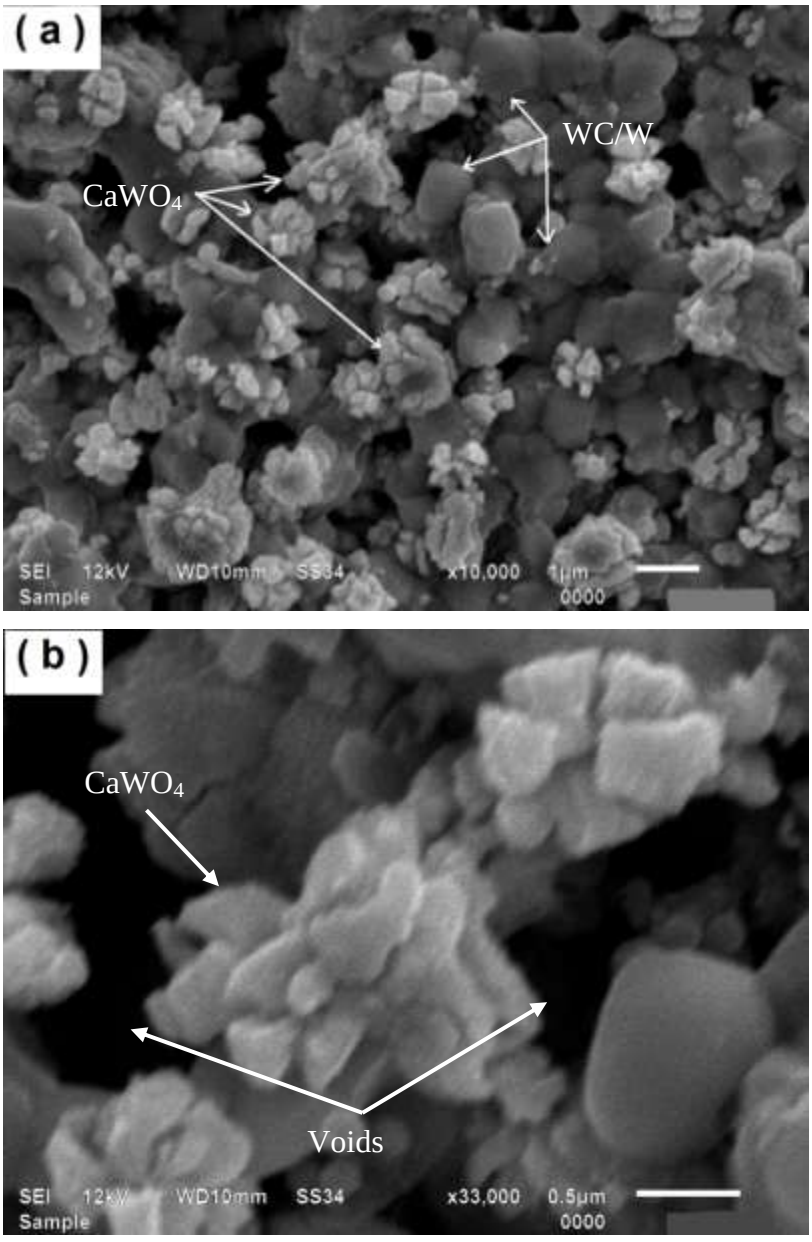

Figure 4.3: Scanning electron micrograph of 10 h calcined milled mixture of scheelite and activated charcoal at 1100°C (a) showing presence of different phases (b) high magnification micrograph showing voids near scheelite particles .

The possible reaction mechanism is given below:

Smaller Particles

$$CaWO_4 + 4C \longrightarrow WC + CaO + 3CO \quad (1)$$

Medium size Particles

$$CaWO_4 + \frac{7}{2}C \longrightarrow \frac{1}{2}WC + \frac{1}{2}W + CaO + 3CO \quad (2)$$

Larger Particles

$$CaWO_4 + \frac{7}{3}C \longrightarrow \frac{1}{3}CaWO_4 + \frac{1}{3}WC + \frac{1}{3}W + \frac{2}{3}CaO + 2CO \quad (3)$$

Reaction mechanism indicates that complete reduction in solid state reaction method requires uniform particle size with homogeneous distribution. Milling of the scheelite and activated charcoal served two purposes. Firstly, it reduced the particle size thereby increasing the surface area. The increase in surface area enhances the rate of reaction. Secondly, it reduces the reaction temperature as the activation energy required for diffusion is less. For solid state process the movement of atoms from one position to another, requires energy which can be divided into two parts. One part is the activation energy required to break the bonds with neighboring atoms and other is used to move atom to another place.

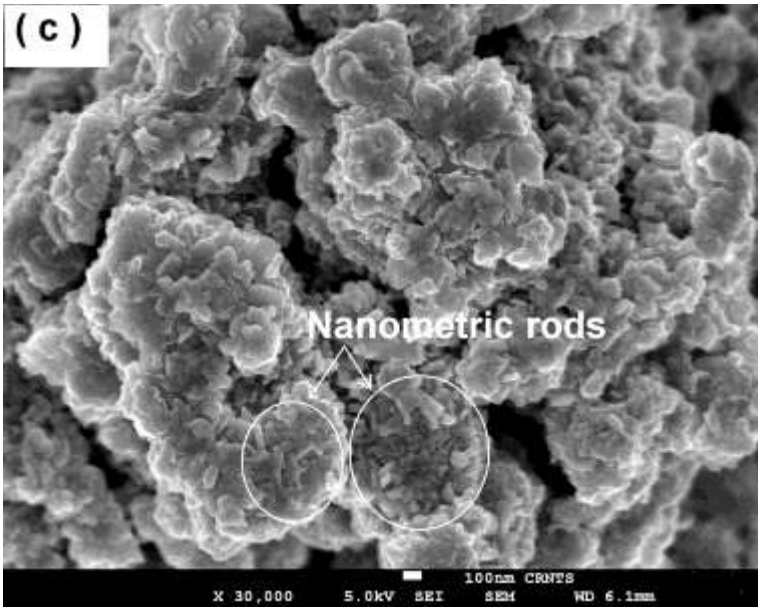

Figure 4.4: HRSEM of calcined (10h) and leached sample.

On surface, the first part of energy required is negligible. Thus milling enhances the rate of reaction and reduces the reaction temperature. For complete conversion of scheelite these parameters need to be optimized. Reduction of last traces of scheelite will be difficult especially for those which are present on the surface of the pellet. Fig. 4.4 shows HRSEM of 10h calcined sample (acid and base leached). An interesting feature observed in the sample is presence of nanometric rods. The sample was examined for further analysis under transmission electron microscope (TEM).

4.1.1.5 TEM analysis

Fig. 4.5(a) shows the low magnification TEM micrograph of 10 h calcined and leached sample. In our X-Ray analysis we could observe WC, W and H_2WO_4 (converted from unreacted scheelite phase while leaching with HCl). Powder mixture contained nanosized rods, faceted particles and agglomerated rods. Importantly these rods were seen in entire powder. In Fig. 4.5(a), we could observe nucleation and growth of nano rods marked as X1, X2 and X3 which depicts their sequential growth respectively. Further these rods merged into each other (X4 and X5). These rods grew in due course of time to attain faceted structure (X6). Similar mechanism was also observed from other area of the sample as shown in Fig. 4.5(b). Here different size of rods merged to form faceted particles (marked as Y1, Y2, Y3 and Y4). Figure 4.5(c) also shows individual rods of size between 5 to 7 nm thicknesses. The X-ray diffraction peaks of H_2WO_4 showed larger broadening in comparison to other phases which is an indicative of the smallest size amongst the three phases. Also there is large increase in intensity of diffraction peaks corresponding to (111) plane relative to (0 2 0) plane in comparison to the standard card values (ICDD card no. 01-084-0886). These facts confirm that smallest rods of 5 to 7 nm shown in Fig. 4.5(c) are of tungstic acid. Fig. 4.5 (d) shows high magnification TEM of the nano rod marked as Y1 in Fig. 4.5(b). The lattice fringe spacing of 0.26 nm is very close the actual value of 0.251 nm of (1 0 0) plane of tungsten carbide. These facts confirm that final product contains nano sized rods of H_2WO_4 and WC. Fig. 4.5(e) shows the selected area diffraction pattern of the sample. The diffraction rings corresponding to the all the three phases present in the sample have that been marked.

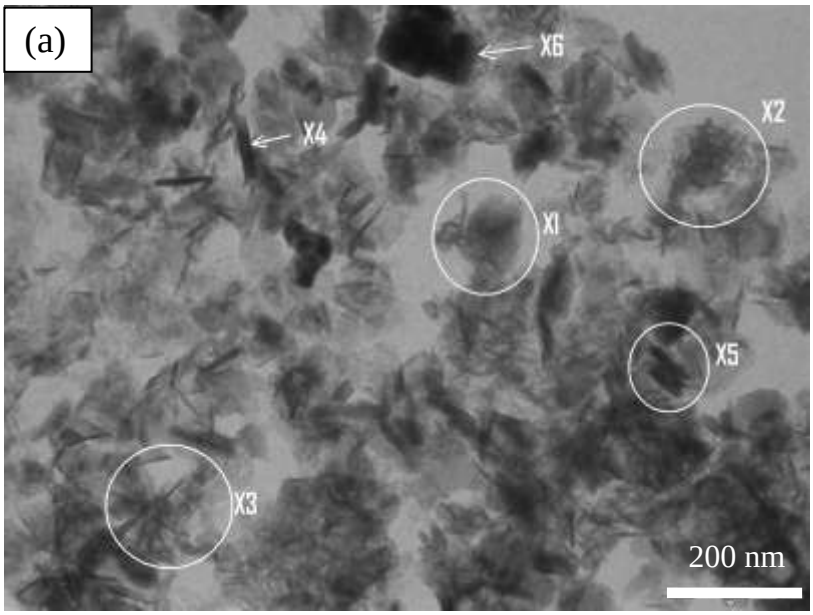
(a)
X6
X4
X2
X1
X5
X3
200 nm

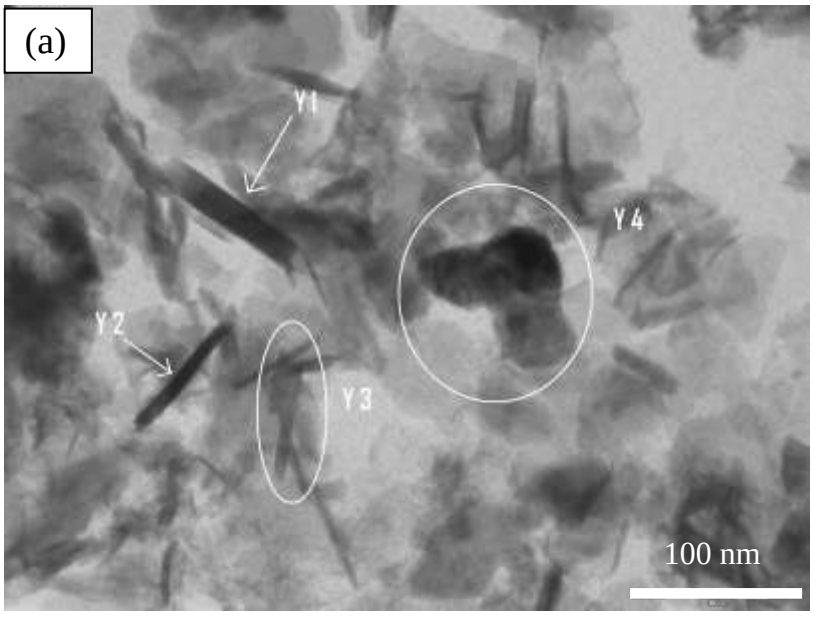
(a)
Y 1
Y 4
Y 2
Y 3
100 nm

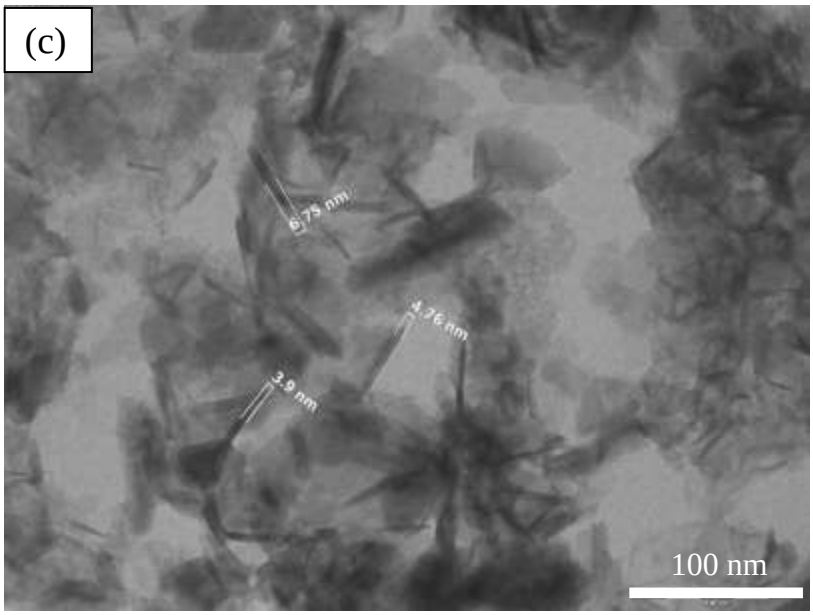
(c)
6.75 nm
4.76 nm
3.9 nm
100 nm

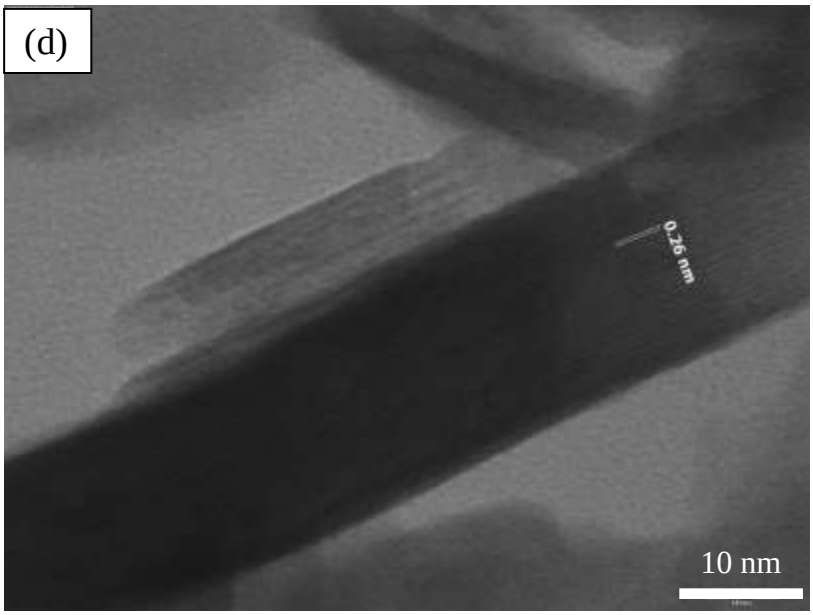
(d)
0.26 nm
10 nm

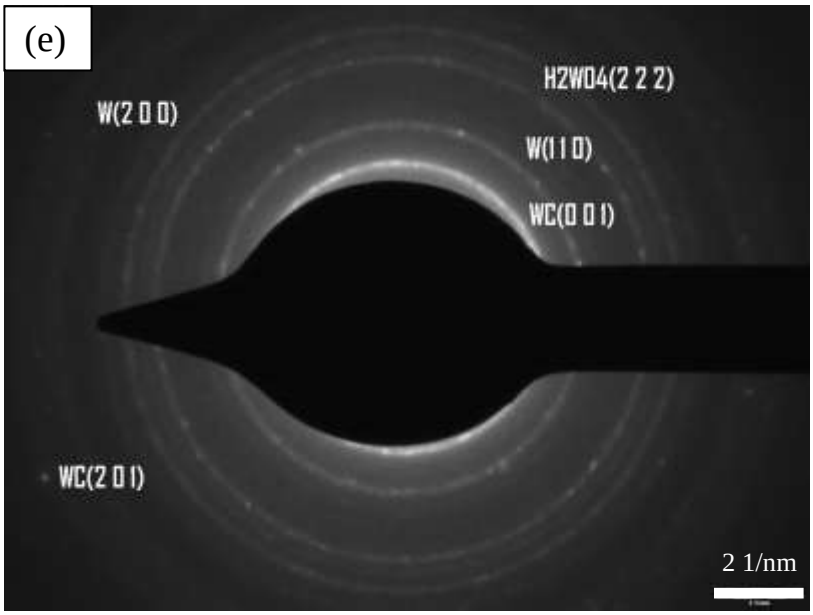

Figure 4.5: Transmission electron micrographs (a & b)of 10 h calcined sample after leaching showing nucleation and growth mechanism for WC (c) showing rods of tungstic acid (d) showing single WC nano rod (e) selected area electron diffraction (SAED) pattern showing presence of WC, W and H_2WO_4.

4.1.2 Synthesis of single phase nanocrystalline WC powders

The results described in previous section could lead to synthesis of mix phases. However, pure WC could not be observed. This section describes the experimental results with the aim to synthesize single phase nanocrystalline WC. The procured scheelite ore was milled for 40 h to reduce the particle size (Fig. 4.7(a & b)). The ball to powder ratio (BPR) was kept as 10:1 and this powder is termed as milled scheelite. The mixtures of milled scheelite and activated charcoal (1:2 weight ratios) were prepared. Powders were loaded in 250 ml capacity tungsten carbide jar and milled in air with WC balls (Retsch PM 100). The ball to charge weight ratio was kept at 50:1. The mixtures were milled for 50 h and 100 h. These powders are termed as 50h milled and 100h milled samples in this work. After milling, the powders were taken out and pellets were made. The powders were loaded in a die of 15 mm diameter and a pressure of 115 kg/cm^2 was applied on the plunger of the die. The pressure was maintained for one minute and after that pressure was released. These pellets were taken out and calcined in a tubular furnace at different temperatures under flowing argon gas.

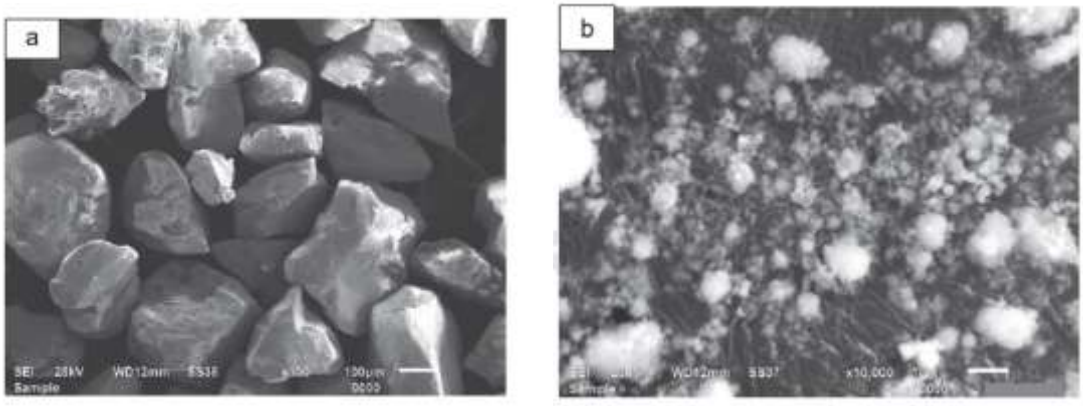

Figure 4.6: Scanning electron micrograph of (a) raw scheelite (b) raw scheelite milled for 40h.

4.1.2.1 X-ray diffraction and thermal analysis

Fig. 4.7 (a & b) shows the X- ray diffraction pattern of raw and milled scheelite (matched with ICDD card no. 01-072-1624). The broadening of the peaks in Fig. 4.7(b) can be attributed to reduced particle size and induced strain in the scheelite. Figs. 4.7(c & d) show X-ray diffraction patterns of 50h and 100h milled samples.

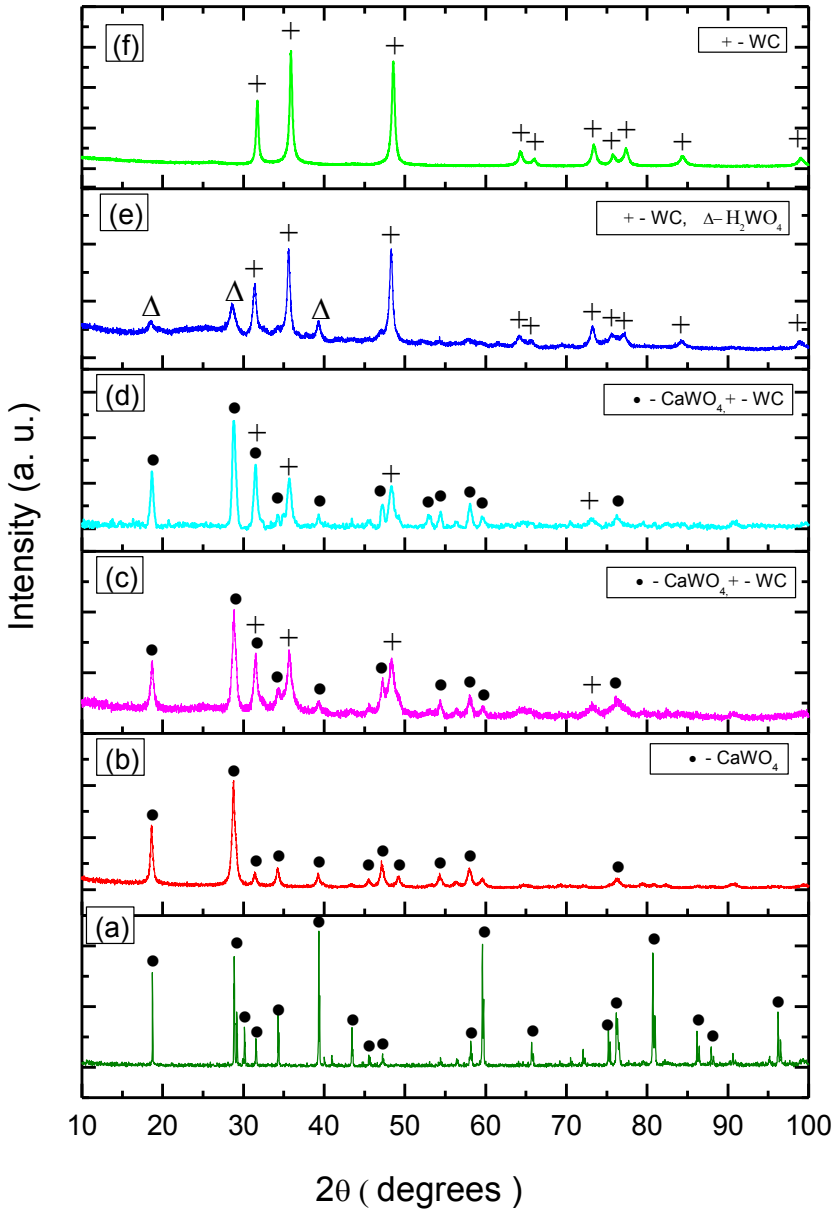

Figure 4.7: X-ray diffraction pattern of (a) raw scheelite (b) raw scheelite milled for 40 h (c) 50h milled sample (d) 100h milled sample (e) Sample (c) calcined (1025 °C for 4h) and leached (f) sample (d) calcined (1025 °C for 4h) and leached.

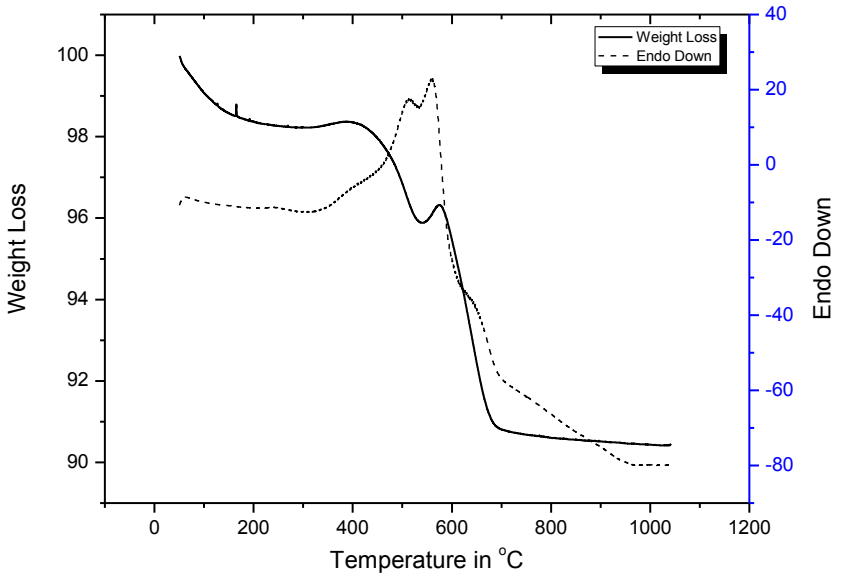

Figure 4.8: DTA/TG curves of 100h milled powder calcined at 1025 °C for 4h (without leaching).

The X-ray diffraction of 50h milled sample showed medium intensity peaks corresponding to WC phase and high intensity peaks of $CaWO_4$ phase. This indicates that some reduction had occurred during milling itself. Since the loading of the scheelite and activated charcoal powders in milling jar were done in air only, some of the activated charcoal might have formed CO inside the jar during milling. The activated charcoal/CO would have reduced some scheelite particles to WC during milling operation. Similar results were also observed for 100h milled powders as can be seen in Fig. 4.7 (d). We found no substantial increase in the WC phase formation in comparison to 50h milled sample.

Fig. 4.7(e) shows the X-ray diffraction pattern of 50h milled and calcined (1025°C for 4h) sample which was first leached by acid (1:1 HCl) and then subsequently by base (0.25M NaOH). Diffraction pattern could be indexed to WC and tungstic acid (H_2WO_4) phases. Tungstic acid peaks came from residual scheelite which got converted to H_2WO_4 during leaching with HCl. Fig. 4.7(f) shows the X-ray diffraction pattern of 100h milled and calcined (1025 °C for 4h) sample which was both acid and base leached. The peak

positions and intensities matched with WC (ICDD card no. 01-073-9874). The lattice constants calculated from X-ray diffraction peaks were a = 2.898 Å, c = 2.835 Å, which were close to reported values (a = 2.900 Å, c = 2.831 Å, ICDD card no. 01-073-9874) confirming the presence of nanocrystalline WC (hexagonal phase, space group $P\text{-}_6m2$). To check the presence of residual carbon, thermal analysis of the unleached sample was done. Fig. 4.8 shows the DTA/TG curves of the 100h milled and calcined (1025 °C for 4h) sample. There is around 8% wt. loss in the sample in two steps. The corresponding exothermic peaks indicate the burning of the carbon in the sample. The free carbon burns first followed by wrapped carbon on the surface of WC. There is 0.5 % weight increase from 540 to 570°C; this increase in weight may be due to oxidation of other impurities.

4.1.2.2 TEM analysis of milled powders

Fig. 4.9(a) shows transmission electron micrograph of 50h milled sample. The scheelite particles were reduced to the nano range and they appeared in agglomerated state. Because of this agglomerated state, some of scheelite particles were not reduced and got converted to tungstic acid during acid leaching. Fig. 4.9(b) shows TEM of 100 h milled sample. The major difference in comparison to the 50h milled sample is that here particles are well distributed (not in agglomerate state). This might be the reason of complete reduction of scheelite particles in 100h milled sample. The other interesting feature in 100h milled powder is that scheelite particles were reduced to nano sized capsules and spherical shapes as can be seen in Figs. 4.9 (c & d).

4.1.2.3 Structural analysis of calcined samples

Fig. 4.10 (a & b) shows HRSEM of 100h milled sample calcined (1025 °C for 4h) subsequently acid and base leached. Well faceted WC nanoparticles can be seen in the micrographs. Fig. 4.11(a) shows the HRTEM of same sample. Well faceted nanocrystalline WC particles can be seen in the micrograph. Fig. 4.11(b) shows HRTEM of 35 nm size WC particle. Fig. 4.11(c) shows the corresponding diffraction pattern of single WC particle. The diffraction spots could be indexed as (200) and (002) planes of WC.

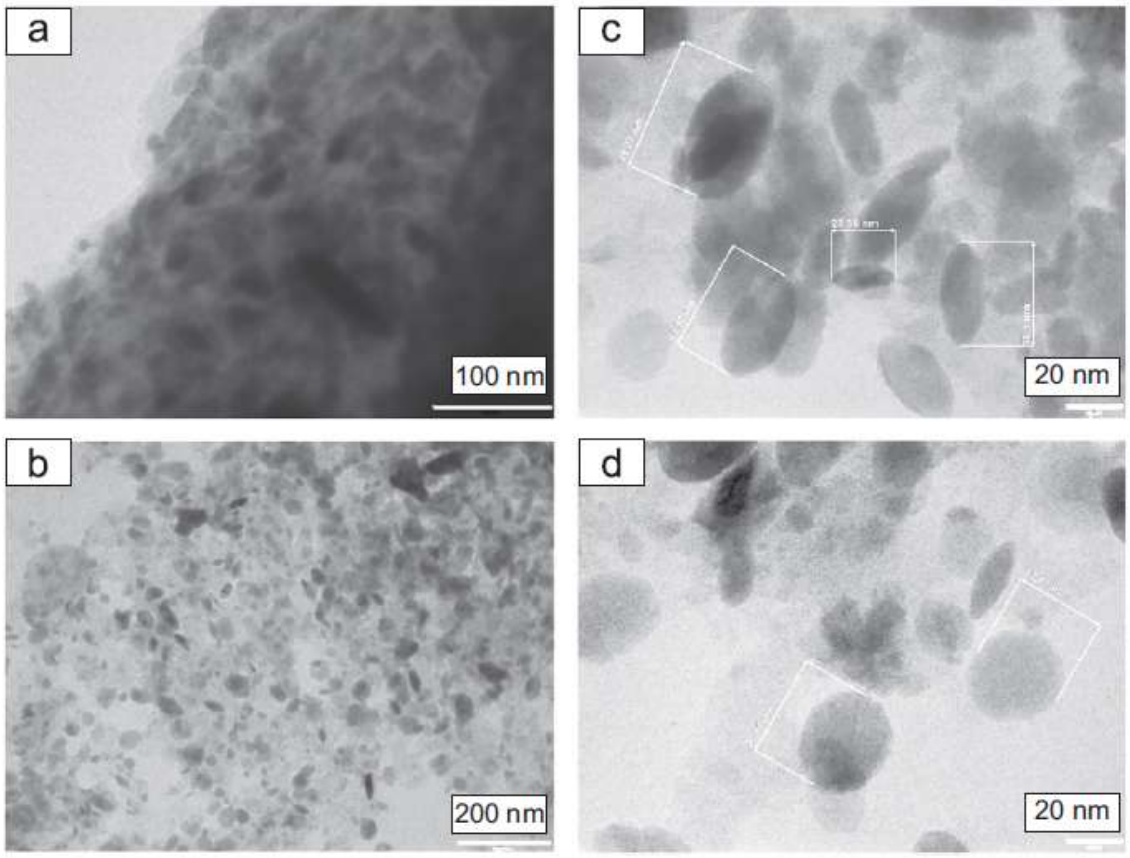

Figure 4.9: Transmission electron micrograph of (a) 50h milled sample (b, c and d) 100h milled sample showing nano sized capsule and sphere shaped $CaWO_4$ particles produced in 100h milled sample.

The decomposition of scheelite ore at high temperature occurs as per the following reaction:

$$CaWO_4 \longrightarrow CaO + WO_3 \quad (4)$$

Activated carbon further helps in reducing WO_3 to W as per the following reactions:

$$WO_3 + 3C \longrightarrow W + 3CO \quad (5)$$

$$CO_2 + C \longrightarrow 2CO \quad (6)$$

As we know formation of carbides is the process of diffusion of carbon through the surface. At high temperature carbon diffuses inside WO_3 and reduces it to elemental tungsten (W).

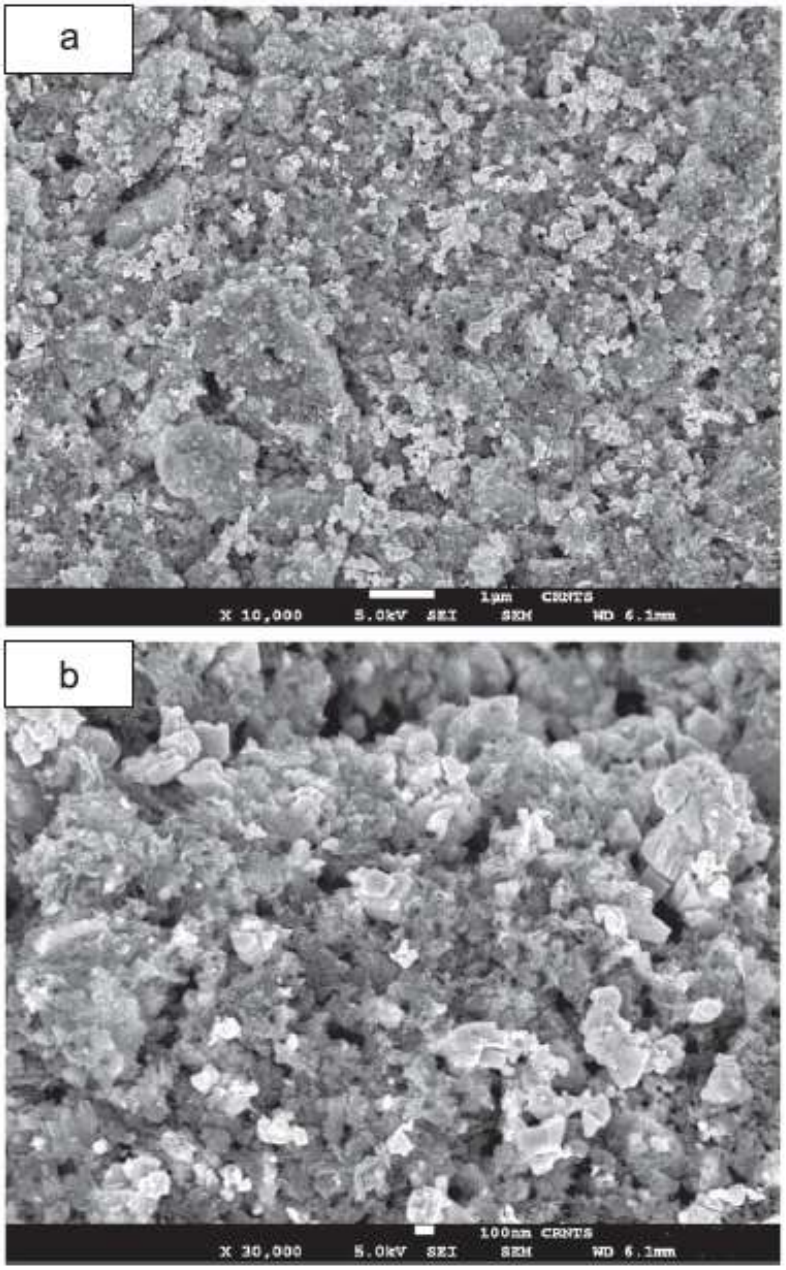

Figure 4.10: (a & b) HRSEM of 100h milled sample calcined (1025 °C for 4h) subsequently acid and base leached.

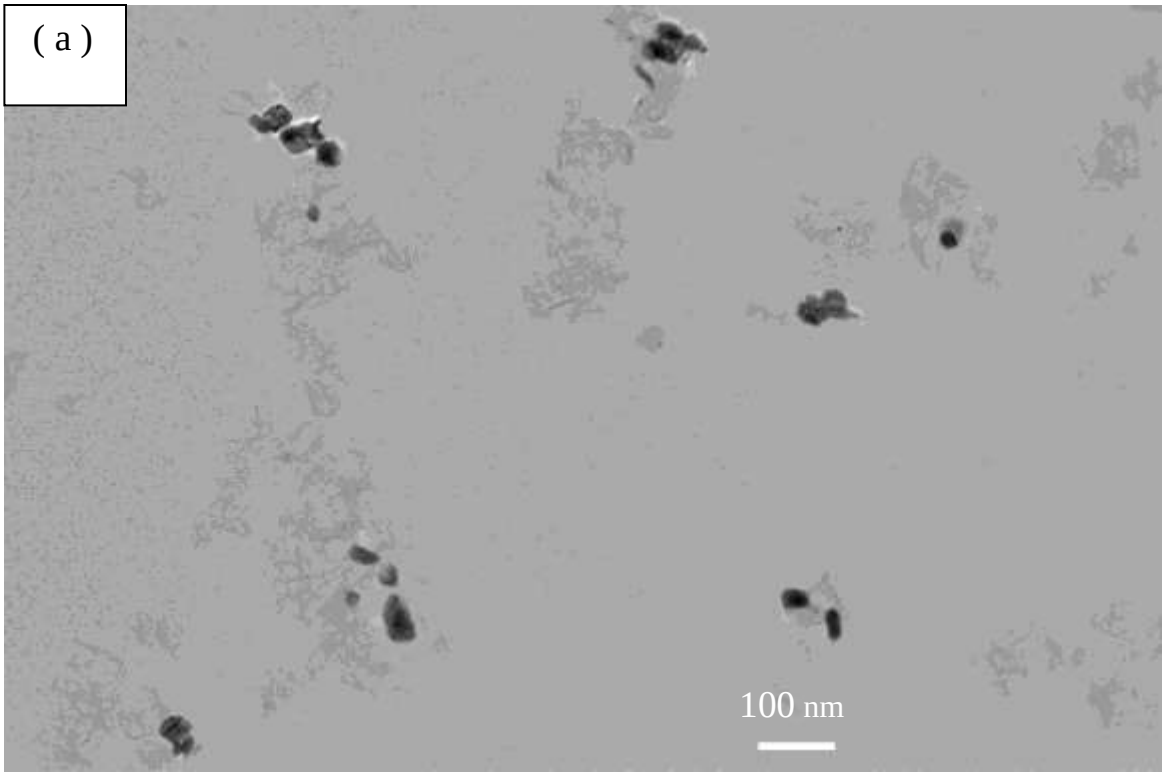
(a)
100 nm

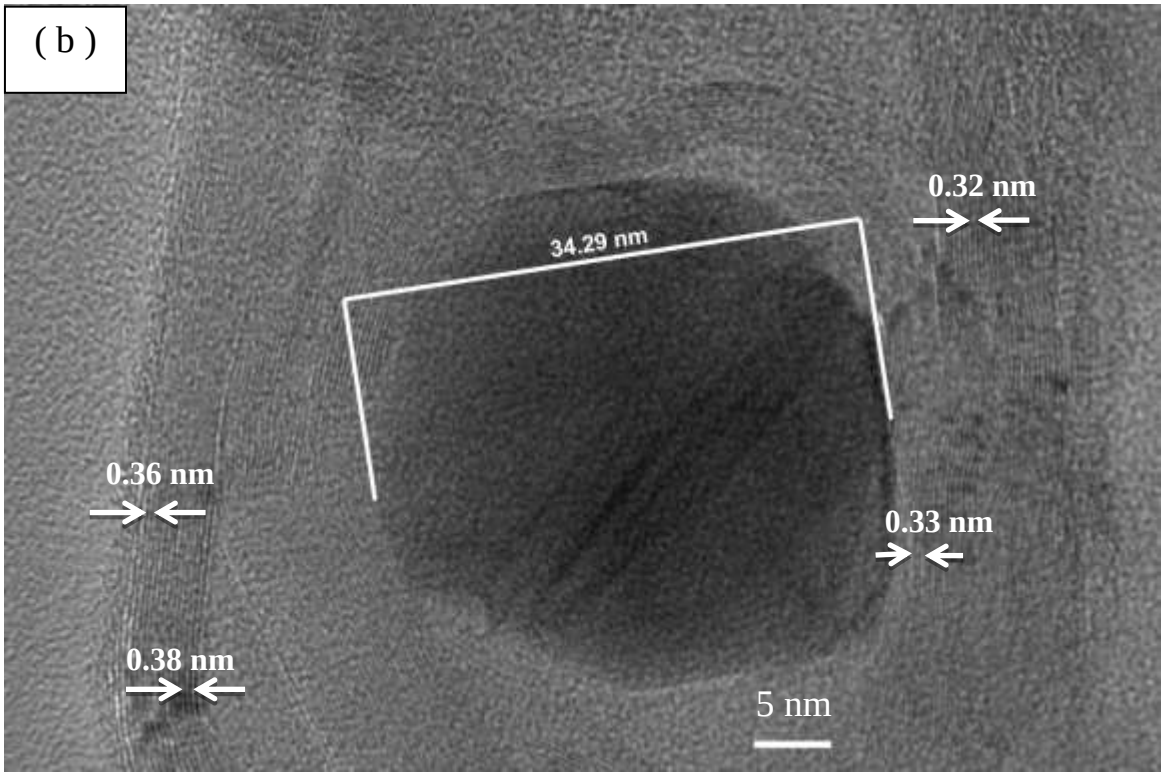
(b)
0.32 nm
34.29 nm
0.36 nm
0.33 nm
0.38 nm
5 nm

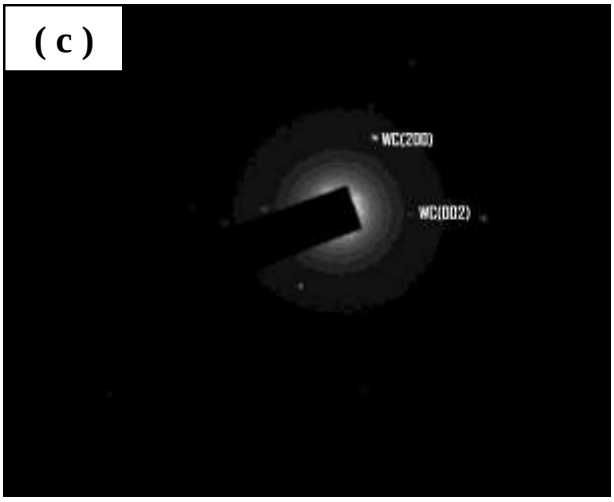

Figure 4.11: (a) HRTEM of 100h milled sample calcined (1025 °C for 4h) subsequently acid and base leached (b) single nanocrystalline WC particle (c) diffraction pattern of single nanocrystalline WC particle.

Because of high reactivity of carbon and W they combine leading to the formation of WC. Since the diffusion occurs from high concentration to low concentration so amount of carbon deposited on surface is higher. This can be further confirmed from the lattice fringes obtained on the surface of WC as shown in Fig. 4.11 (b). The measured value of lattice fringes is 0.33 nm which corresponds to the d-spacing of carbon [11]. However, at some places the value of d-spacing varies from 0.33 to 0.38, which might be due to the trapping of WC inside carbon layers. The selected area diffraction pattern obtained from the inner zone of Fig.4.11(c) clearly shows the presence of WC. The trapped molecule inside the carbon layers caused swelling of the layer causing graphitic layers to move away from the walls that causes an increase in the lattice spacing from 0.33 to 0.38 nm at the outer edges [12].

In order to find the mechanism of reduction phenomenon for formation of nanocrystalline WC, series of systematic experiments were conducted. Powders milled for 50 h were calcined for 4 h at 700, 800, 900, 1000, and 1100°C**.** The XRD pattern of the calcined powders is shown in Fig. 4.12. The X-ray diffraction patterns indicated that no reaction had occurred at 700, 800 and 900°C; rather reactant scheelite retained its initial state.

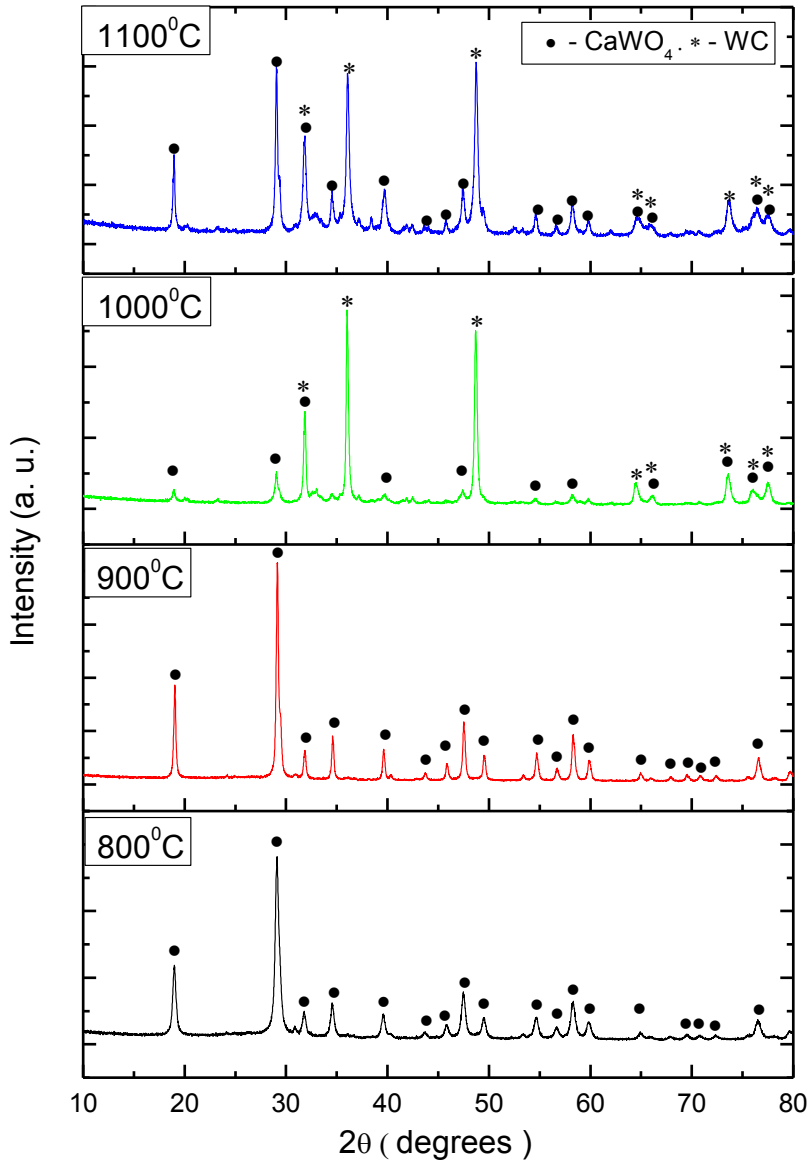

Figure 4.12: X-ray diffraction patterns of 50 h milled samples calcined for 4 h at 800, 900, 1000, and 1100 °C.

Only two crystalline phases WC and $CaWO_4$ were observed at 1000 and 1100°C. In order to find exact milling time and temperature for the reduction more calcination experiments were conducted with 50h and 100h milled samples each at 950°C and 1025°C. The X-ray diffractogram of these samples is shown in Fig.4.13.

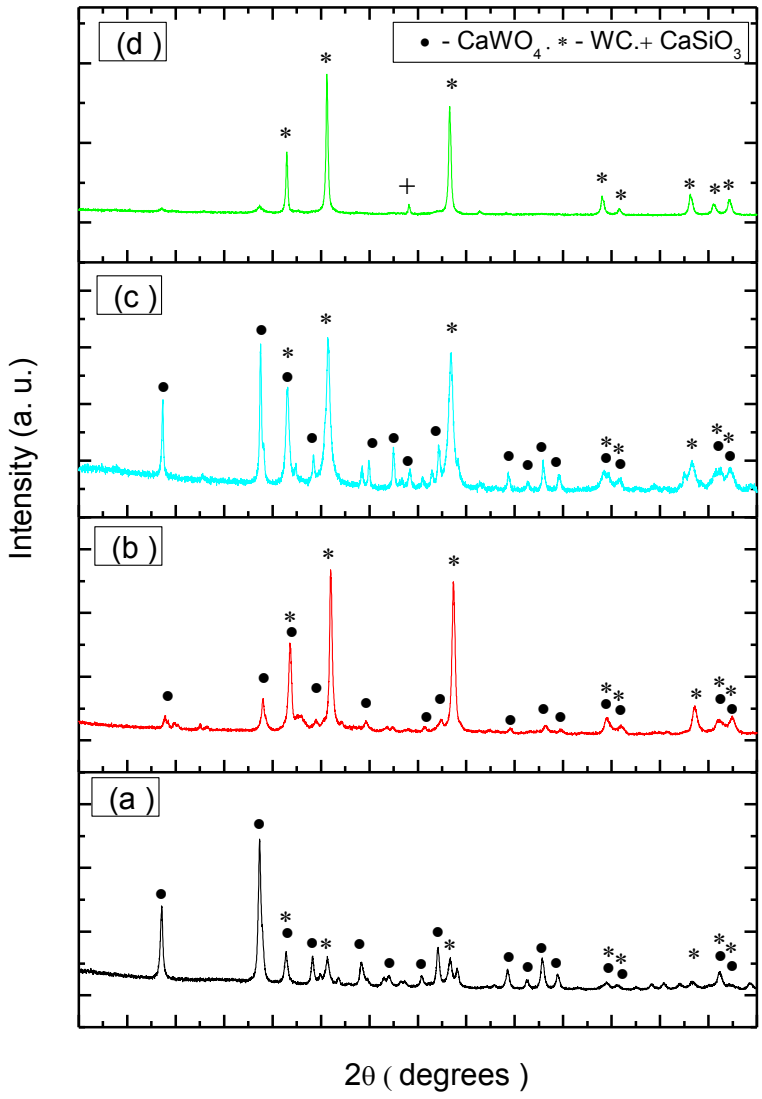

Figure 4.13: X-ray diffraction patterns of 50 h milled sample calcined for 4 h at (a) 950°C (b) 1025°C; 100 h milled sample calcined for 4 h at (c) 950°C (d) 1025°C.

The best results were observed for 100 h milled samples calcined at 1025°C. The X-ray diffraction pattern of this sample showed traces of unreacted scheelite and a very low intensity single peak of calcium silicon oxide ($CaSiO_3$). This $CaSiO_3$ was formed by the following reactions:

$CaWO_4 + 4C \longrightarrow WC + CaO + 3CO$ (given on page 56) (1)

$CaO + SiO_2 \longrightarrow CaSiO_3$ (7)

The scheelite ore consisted of SiO_2 as one of its impurity. This SiO_2 reacted with CaO (reaction 1) at 1025°C and formed $CaSiO_3$. These undesired products CaO, $CaSiO_3$ and other impurities were leached out by dilute HCl (1:1) followed by base leaching with 0.25M NaOH solution. The above experiments revealed two interesting facts. Firstly, the peaks of WC phase which were observed in 50 h milled powders of scheelite and activated charcoal disappeared when calcined at 700, 800 and 900°C, implying that WC phase formed during milling was unstable as there was slight reduction on the outer surface of the some of the scheelite particles.

Secondly, no intermediate phase like W, W_2C and Ca_3WO_6 were observed in the calcined samples. Only two phases $CaWO_4$ and WC were observed when powders were calcined above 900°C. This behaviour was in contrast to the general solid state reactions which usually proceed with the formation of intermediate phase followed by final product, whereas in our experiments final phase is formed directly without formation of any intermediate products. The probable reason for this variation could be the existence of scheelite particles in nano range and its homogeneous mixing with activated charcoal, along with sufficient heating time of 4 h. However, shorter heating time may produce intermediate phase(s).

4.1.3 Effect of extended milling of scheelite ore

As described in the previous section, single phase nanocrystalline WC particles (35 to 100 nm) were obtained by calcining the 100h milled sample. This study indicates that milling time influences the kinetics of reaction. In order to obtain still smaller with narrow range of particle size the mixture of scheelite ore and activated charcoal was milled for 150h. Except for milling time all other experimental conditions like compaction, calcining and leaching conditions were kept same as was done earlier (section 4.1.2)

4.1.3.1 X-ray diffraction analysis

Fig. 4.14 (a) shows the X-ray diffraction pattern of raw scheelite. Fig. 4.14(b) shows the X-ray diffraction pattern of 150 h milled sample of scheelite and activated charcoal. The X-ray diffraction pattern shows medium intensity peaks of WC phase and high intensity peaks of $CaWO_4$. The presence of WC phase in the milled sample indicates that reaction has occurred during milling itself. Similar results were also observed in the 100h milled sample. The extended milling of 150h did not carry the reaction further to its complete reduction. The X-ray diffraction pattern of 150 h milled and calcined (1025°C for 4h) sample after leaching is shown in Fig 4.14(c). We could observe the major phase WC with some minor quantity of $CaWO_4$.

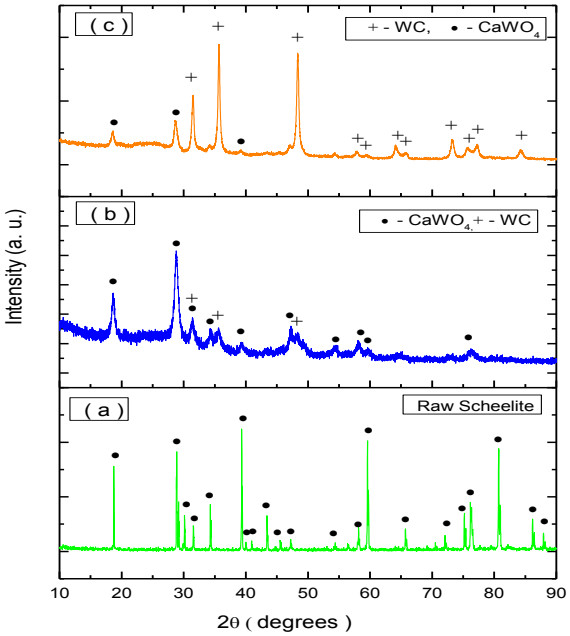

Figure 4.14: X-ray diffraction pattern of (a) raw scheelite, (b) 150 h milled sample of scheelite and activated charcoal (c) 150 h milled, calcined (1025° C for 4 h) and leached.

The results were surprising in a manner that 100 h milled sample got completely converted to WC during calcination, whereas, 150 h milled sample showed some unreacted traces of scheelite. This phenomenon was also observed for 50 h milled sample which requires further investigation.

The X-ray diffraction pattern was refined for WC phase by Rietveld method using Fullprof.2k (Version 5.0) [13]. The crystal structure was refined using *P-$_6$m2* symmetry and 187 space group as shown in Fig. 4.15. The refined parameters are a= 2.9004 Å and c = 2.8356 Å with cell volume V = 20.68 Å^3. These cell parameters are close to the reported values a= 2.9065 Å and c = 2.8366 Å (ICDD card no. 01-072-0097).

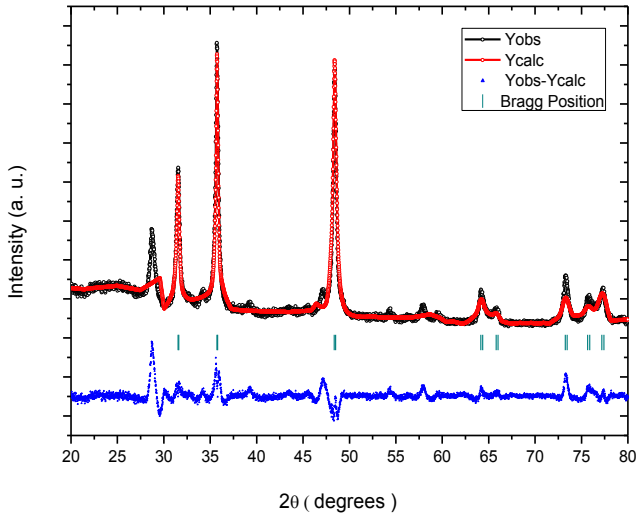

Figure 4.15: Rietveld refinement plot of observed, calculated and difference profile of nanocrystalline WC.

4.1.3.2 TEM and SEM analysis

Fig. 4.16 shows the TEM of 150 h milled sample of scheelite and activated charcoal. The extended milling of 150 h has reduced the scheelite particle size in the range of 10 to 30 nm. Fig.4.17 shows the back scattered scanning electron micrograph of 150h milled and calcined sample (after leaching). The white spots indicate agglomerated nano WC particles. Fig. 4.18 (a) and (b) shows the TEM of 150h milled and calcined sample (after leaching). The particle size of the WC powders was in the range of 10 to 25 nm. The increased milling time of 150h has facilitated to reduce particle size as compared to reported earlier. Moreover, pure WC can be easily obtained after increasing the leaching time.

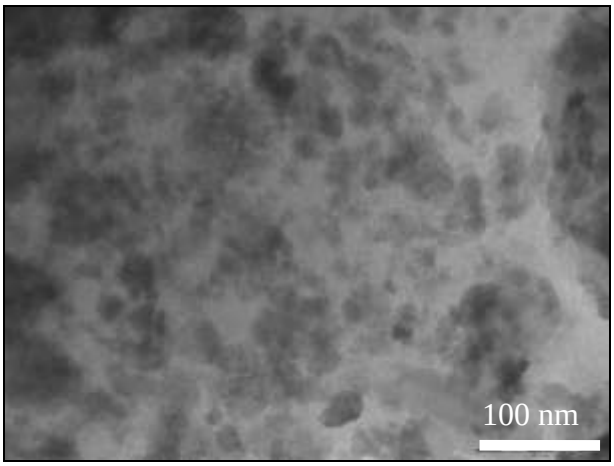

Figure 4.16: TEM of 150 h milled sample

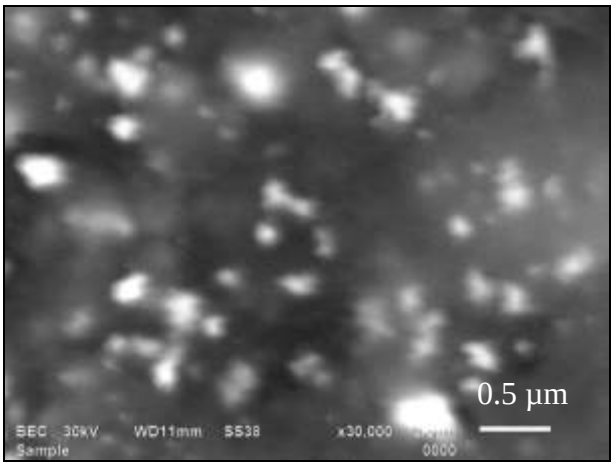

Figure 4.17: SEM of 150 h milled sample calcined at 1025°C (after leaching).

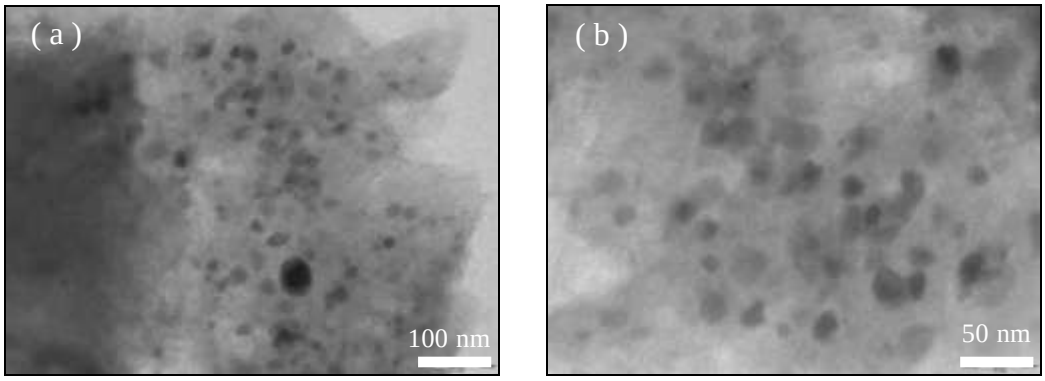

Figure 4.18: TEM of 150 h milled sample calcined at 1025°C (after leaching).

4.2 Thermo chemical route

In section 4.1 the results obtained from milled and calcined powders where the reduction was done in argon atmosphere. In this section the reduction was done at high temperature by taking activated charcoal and acetone (liquid) carbon source.

4.2.1 Single phase synthesis of nanocrystalline WC at 800°C

In the solid state reaction method, we observed that there was no reaction of scheelite with activated charcoal in 50 h milled sample below 900°C (Fig. 4.9). In a quest to find out lower temperature method from an ore, a new route has been attempted. The experiment was performed using 1 g of milled scheelite**,** 2 g of activated charcoal and 1 g of Mg in an autoclave. The sealed autoclave was kept in a furnace at 800 °C for 20 h. The furnace was heated at the rate of 5°C/min. After the experiment, autoclave was allowed to cool in the furnace. The powders were taken out and washed with dilute HCl (1:1) to remove CaO, MgO and other impurities. The acid washed powders are designated as sample A. Finally the sample A was base treated (0.25 M NaOH) to remove traces of silica and designated as sample B.

4.2.1.1 X-ray Diffraction Analysis

Fig. 4.19(a) and (b) shows the X-ray diffraction pattern of raw scheelite and scheelite milled for 50 h. Fig. 4.19 (c) shows the X-ray diffraction pattern of the sample A. The X-ray diffraction pattern matches well with WC (ICDD card no. 01-072-0097) and confirms the direct formation of nanocrystalline WC from scheelite. The crystallite size calculated from scherrer formula is 16 nm. The X- ray diffraction pattern of sample A also showed traces of SiO_2. This silica was removed by further washing with 0.25M NaOH solution (Fig. 4.19(d). The X-ray diffraction pattern was refined by Rietveld using Fullprof setup. The crystal structure showed $P\text{-}_6m2$ symmetry with space group 187. The refined parameters are a =2.9032 Å and c = 2.8400 Å with cell volume V= 20.73 $Å^3$, the parameters shows good fit with Chi Square (χ^2) = 2.01 as shown in Fig. 4.20.

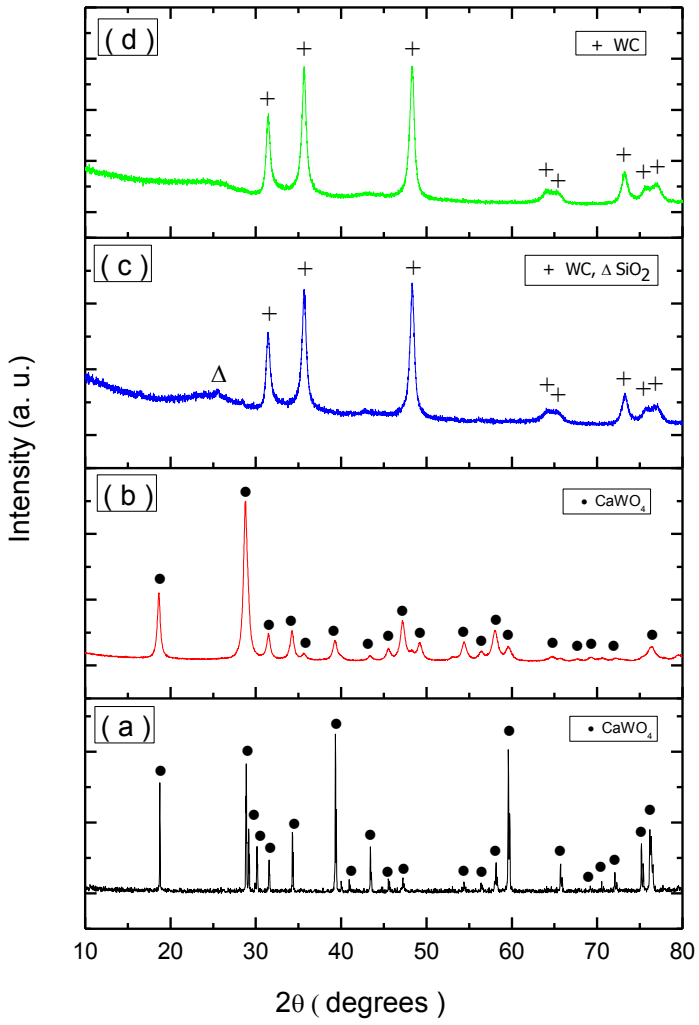

Figure 4.19: X-ray diffraction pattern of (a) raw scheelite (b) scheelite milled for 50 h (c) sample A showing presence of WC and minor SiO_2 phase (d) sample B showing single phase nanocrystalline WC.

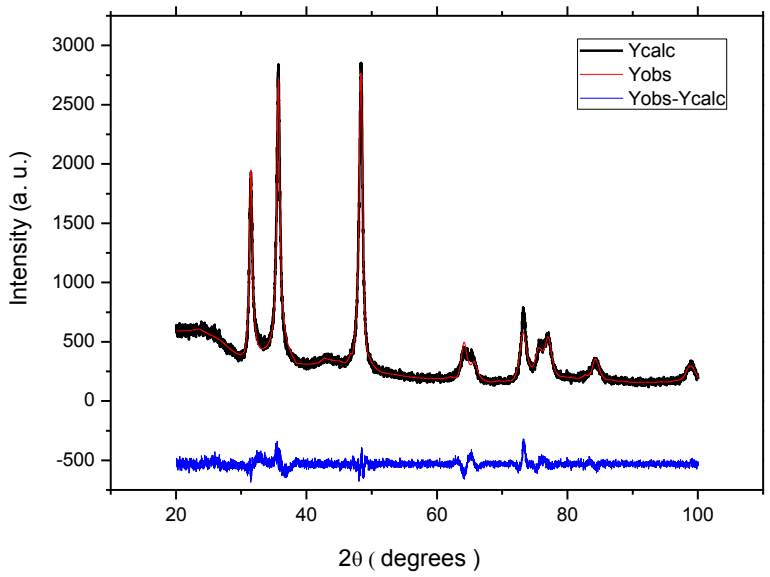

Figure 4.20: Rietveld refinement plot of observed, calculated and difference profile of single phase nanocrystalline WC (sample B).

4.2.1.2 HRSEM and EDAX analysis

Fig. 4.21(a) and (b) shows HRSEM of sample B. The two different types of structural features are visible in the micrographs. The dark color particles having flake type features is charcoal. The white colored nanoparticles are of tungsten carbide. The solid gas phase reaction taking place in the autoclave has led to formation of nanocrystalline WC. The possible reaction mechanism is given below:

$$CaWO_4 + 3Mg \longrightarrow W + 3MgO + CaO \quad (8)$$

$$2C + O_2 \longrightarrow 2CO \quad (9)$$

$$2W + 2CO \longrightarrow 2WC + O_2 \quad (10)$$

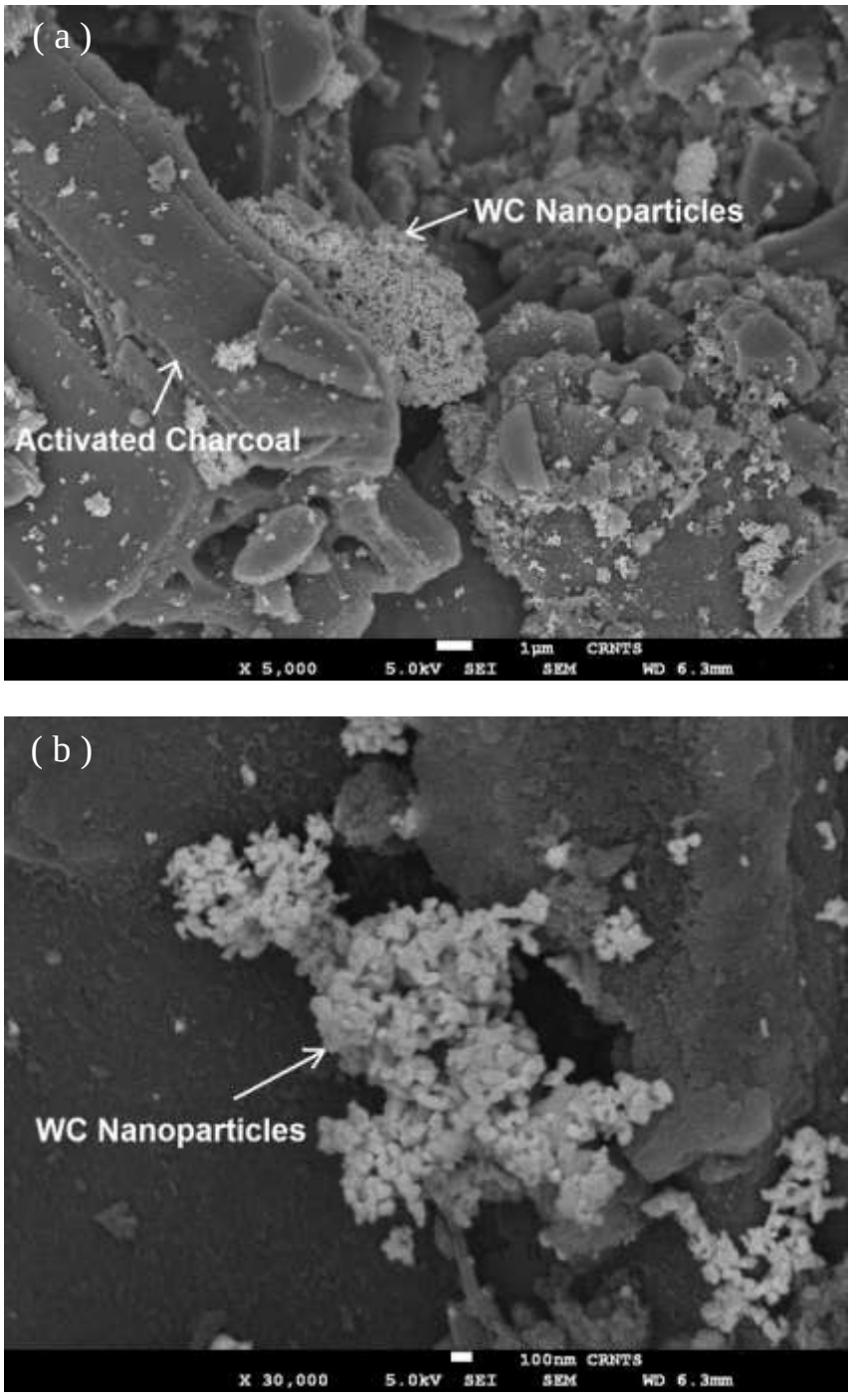

Figure 4.21(a & b): HRSEM of sample B showing WC nanoparticles and activated charcoal.

Figure 4.22 shows the EDX pattern taken on white particles. Peaks corresponding to C and W confirm the presence of WC phase. Also, EDX pattern shown in Fig. 4.23 confirms that the black colored flakes are of charcoal.

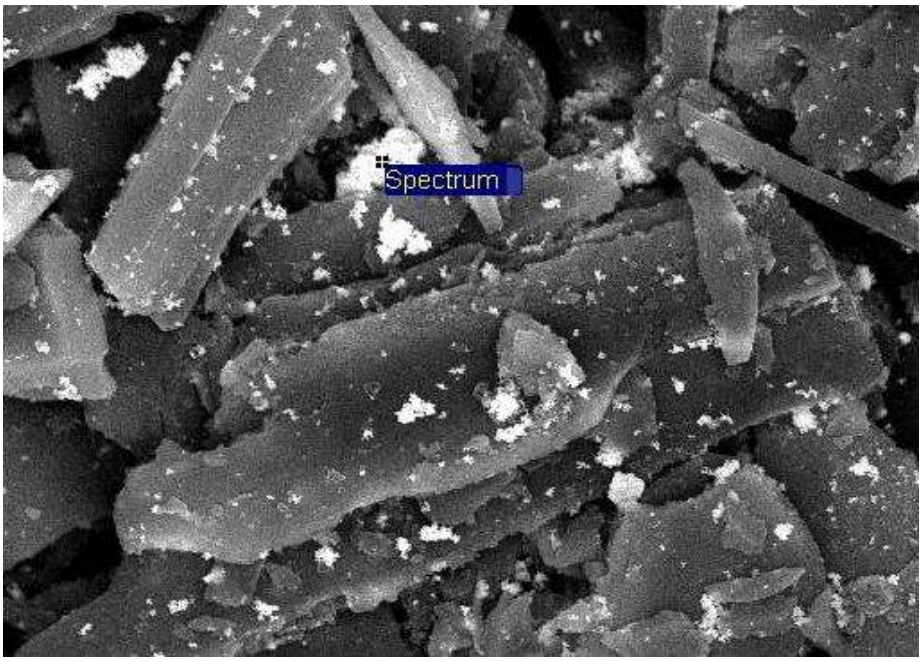

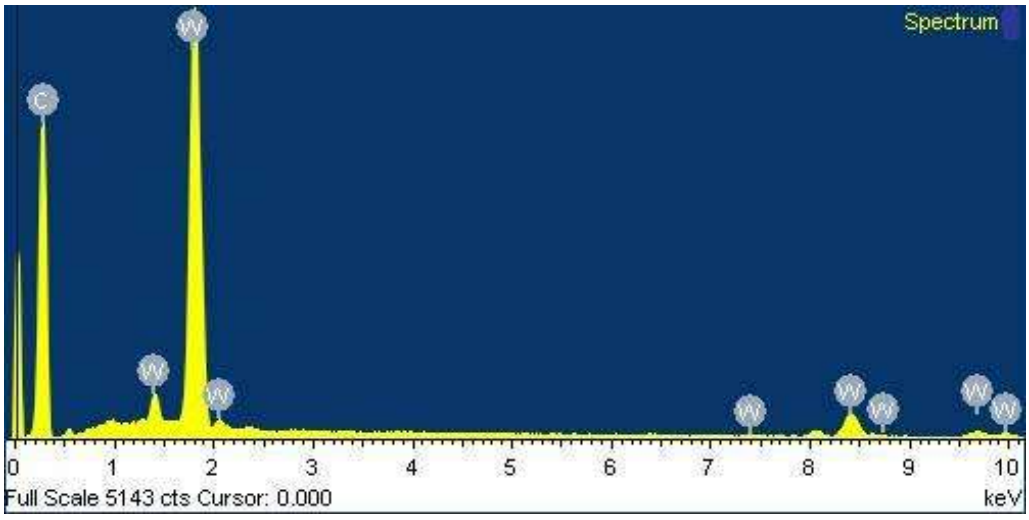

Figure 4.22: EDX of sample B on white particles (WC) nanoparticles.

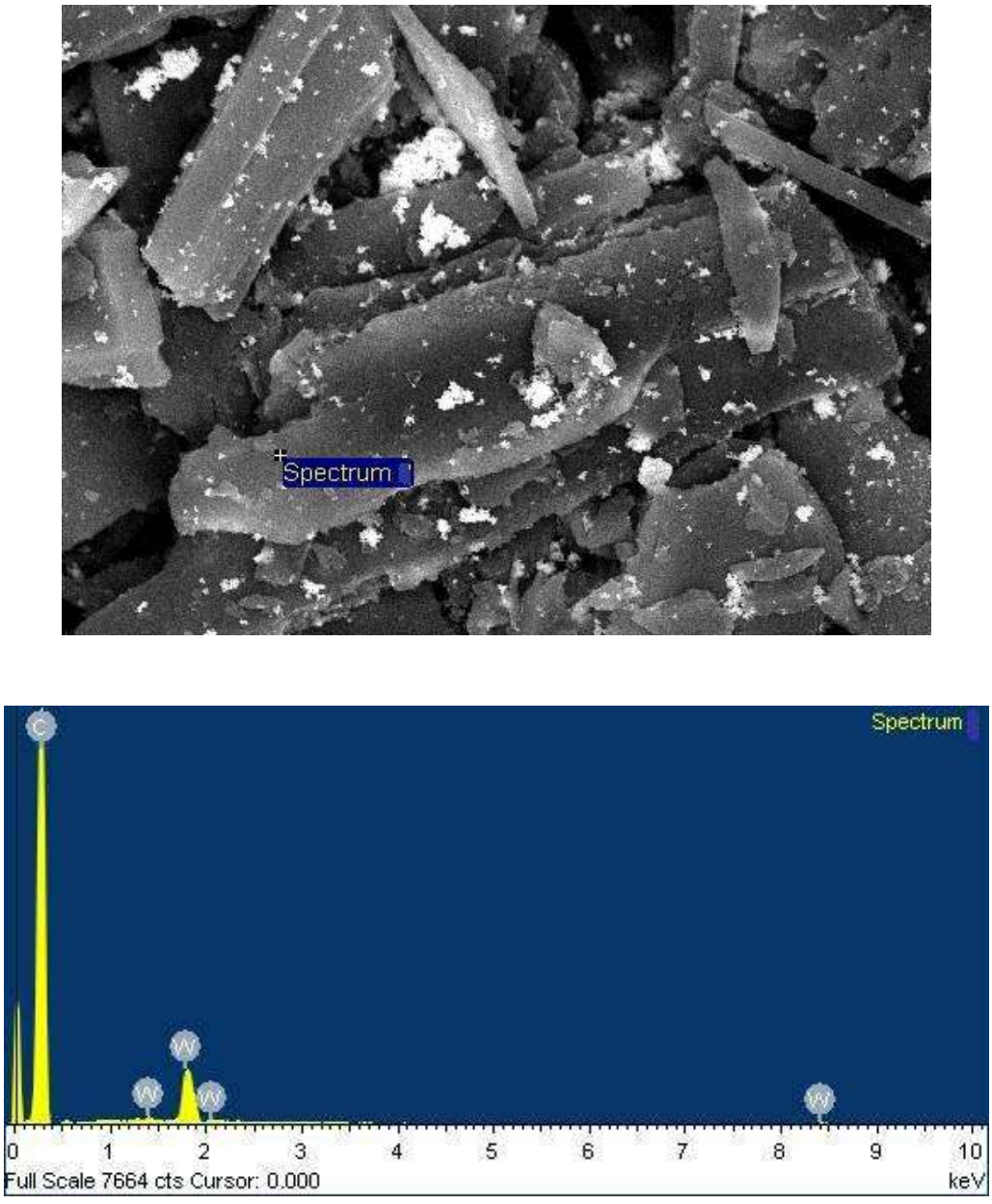

Figure 4.23:EDX of sample B showing on black particles (activated charcoal).

The magnesium is reducing the $CaWO_4$ to W at 800 °C. As there is excess carbon in the autoclave so activated charcoal forms CO gas. This CO reacts with elemental tungsten to produce WC. The oxygen evolved further reacts with C to form CO and this cycle goes on till the entire W is carburized. The impurities present in the ore provide the site for breakage of scheelite at high temperature and pressure. The high pressure developed in the autoclave facilitated diffusion of carbon to get WC nanoparticles [14-16].

4.2.1.3 HRTEM analysis

Fig. 4.24(a) and (b) shows the HRTEM of sample B. The tungsten carbide crystals are in agglomerated form due to high surface area. Fig. 4.24 (c) and (d) shows the lattice fringes of nanocrystalline WC particles. The d-spacing is found to be 0.26 nm and 0.18 nm which is for (100) and (101) plane of WC (ICDD card no. 01-072-0097) respectively.

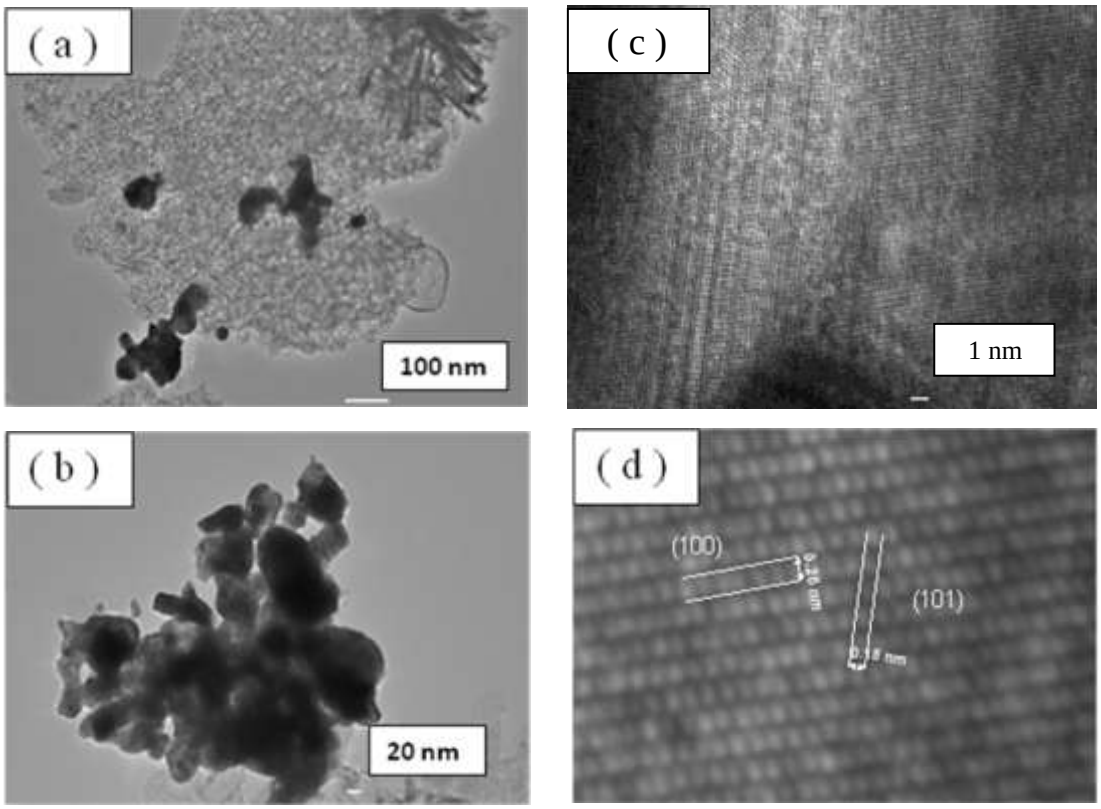

Figure 4.24: HRTEM of acid and base washed sample S5 (a) and (b) nanocrystalline WC (d) and (e) lattice fringes of nanocrystalline WC.

We carried out control experiments to find the effect of carbon, nascent carbon, H_2 and Mg on the reduction and carburization of $CaWO_4$ to produce nanocrystalline WC. Table 4.2 shows the reactants with their quantity and products obtained after HCl (1:1) washing. During experiment S1, nanocrystalline WC was produced but there was substantial quantity of unreacted $CaWO_4$ even after 20 h heating time. To find the effect of nascent carbon and H_2, experiment S2 with acetone carbon source was conducted, since pyrolysis of acetone produces C and H_2 [17]. The results were better than activated charcoal, again substantial quantity of $CaWO_4$ phase was there in final product. Further experiments S3 and S4 were conducted by taking 10 ml and 20 ml respectively of acetone along with Mg.

Table 4.2 Summary of different reactants, reaction conditions and products obtained.

Sample Name	Reactants	Reducing/Carburising Elements	Temperature	Time	Products (Acid Washed)
S1	Scheelite (1gm) + Activated Charcoal (2gm)	C	800 °C	20h	*$CaWO_4$, WC (*unwashed sample)
S2	Scheelite (1gm) + Acetone (20ml)	C(nascent), H_2	800 °C	20h	$CaWO_4$, WC
S3	Scheelite(1g) + Acetone(10ml) + Mg (1gm)	C(nascent), H_2, Mg	800 °C	20h	$CaWO_4$, WC, MgO, H_2WO_4
S4	Scheelite(1gm) +Acetone (20ml) + Mg (1gm)	C(nascent), H_2, Mg	800 °C	20h	$CaWO_4$, WC, MgO, H_2WO_4
S5	Scheelite (1gm) + Activated Charcoal (2gm) + Mg (1gm)	C, Mg	800 °C	20h	Single phase WC

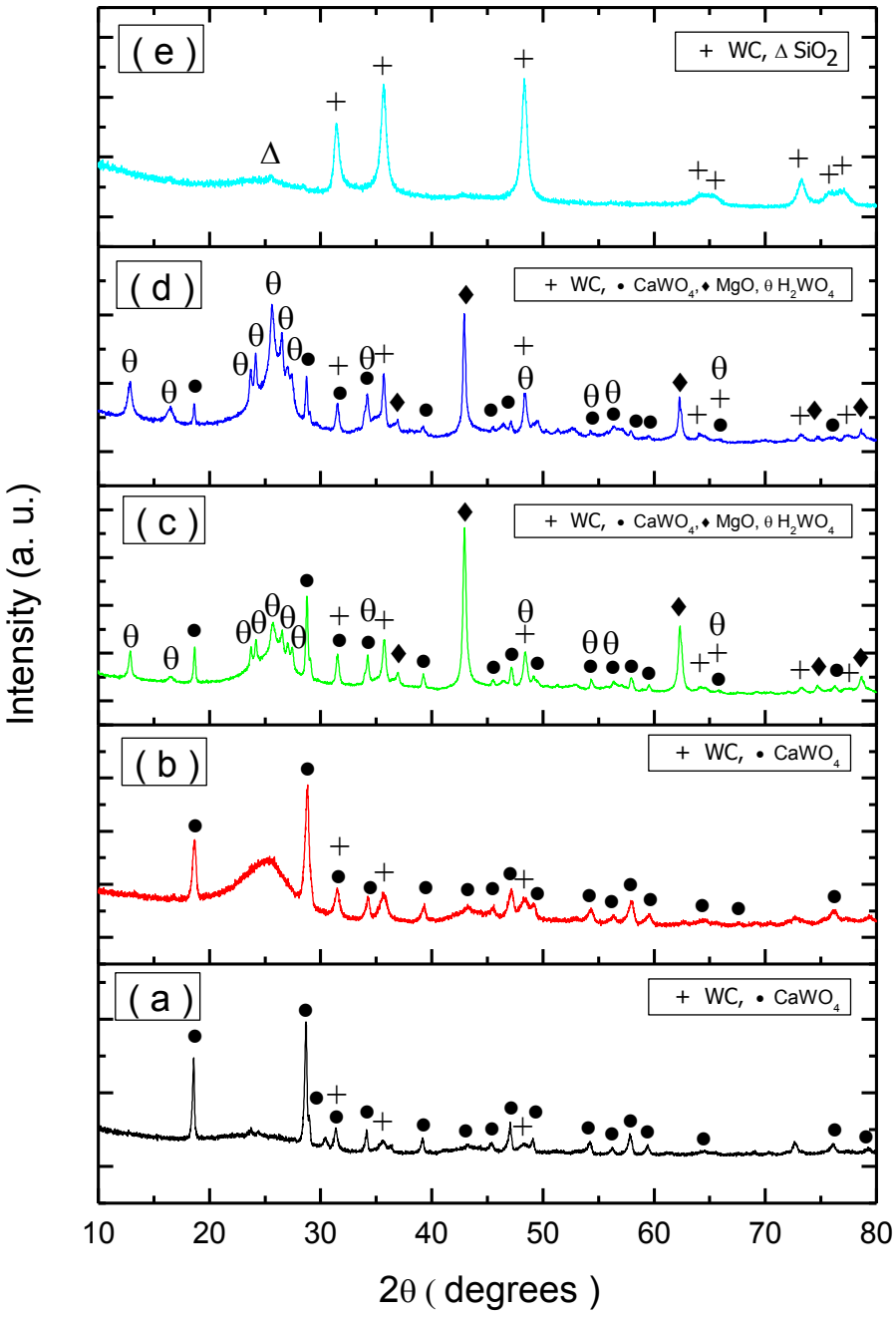

Figure 4.25: X-ray diffraction patterns of acid washed samples (a) S1 (b) S2 (c) S3 (d) S4 and (e) S5.

The final products after HCl (1:1) washing contained the $CaWO_4$, WC, MgO and H_2WO_4. Some of the $CaWO_4$ got converted to H_2WO_4 during leaching with HCl. There is a tendency of formation of layer of tungstic acid on $CaWO_4$ particles which stop further complete leaching [6]. The peak intensities of WC phase were more than experiment S2 with impurities. Experiment S5 was conducted by taking activated charcoal along with Mg. The product after acid washing contained single phase WC with traces of SiO_2. The SiO_2 was removed by further leaching with dilute 0.25M NaOH base.

In these experiments we found dry autoclaving is better than usage of acetone (liquid) in two ways. Firstly system works under only in autogenic pressure in comparison to liquid carbon source which generates very high pressure in autoclave [18-19], Secondly it requires lesser quantity of Mg than solvothermal method (acetone usage), since additional Mg to reduce acetone to C and other elements. In experiments S3 and S4 scheelite was not completely reduced to WC inspite of presence of H_2 and Mg as strong reducing agent and higher system pressure than S5 experiment. Another interesting thing observed in the sample S3 and S4 that even HCl (1:1) could not remove MgO from the powders. These behaviors needs further investigation.

4.2.2 Optimization of time and temperature

The experiments described in previous section could lead to synthesis of pure WC phase with solid charcoal at 800°C. In order to bring down the temperature further, experiments were carried out at lower temperature with variation in holding time. Same milled sample was used in these optimization experiments. The milled mixture was heated for constant time period (4h) at 650, 700, 800°C. In order to optimize the conditions further some independent experiments with variation in time and temperature was also done.

4.2.2.1 X-ray diffraction analysis

Figure 4.26(a) shows the X-ray diffraction pattern of the milled scheelite (50 h). The peak broadening is indicative of reduced particle size of scheelite and induced strain in the

lattice caused during milling operation. Figure 4.26 (b) demonstrates the XRD pattern of acid and base washed powders obtained by heating at 650 °C (4 h). The X-ray diffraction pattern contains peaks corresponding to WC phase along with unreacted scheelite. It reveals the nucleation and growth of WC phase. Figure 4.26(c & d) depicts the X-ray diffraction pattern of sample heated at 700 °C (4 h) and 800°C (10 s) respectively. These X-ray traces shows similar features as previous sample with noticeable drop in the quantity of unreacted scheelite. The growth of the WC phase is found to complete in the sample heated at 800 °C (4 h). However, it shows traces of residual scheelite as illustrated in Fig. 4.26(e). Finally the complete phase transformation of scheelite to nanocrystalline WC was achieved with increased heating time of 10 h at 800 °C. This has been very well authenticated by XRD pattern of Fig. 4.26(f).

Since high temperature synthesis causes grain growth, so it was essential to optimize the condition at low temperature. Synthesis at 650°C could lead to formation of WC phase. However, low holding time could not lead to complete conversion to WC phase as shown in Fig 4.26(b). Experiment conducted at 650 °C with increased reaction time of 20 h could lead to single phase nano WC as shown in Fig. 4.26(g), where complete phase transformation to WC was attained without any residual scheelite or any intermediate phase. Peak broadening was an indicative of WC nano size.

In the XRD pattern as shown in Fig. 4.26(g) there is slight background slope that was observed between peaks at 2θ angles 30° to 36°, indicating that minor quantity of amorphous WC might be present [20]. The WC crystallite size were observed to increase with the increase in synthesis temperature and time (Table 4.3). The X-ray diffraction patterns shown in Fig. 4.26(b) to (g) indicate two distinct features; one is broad halos for amorphous carbon and sharp and broad peaks of nanocrystalline WC. The crystallinity of WC phase was found to increase with the increase in synthesis temperature from 650 °C to 800°C and also with time.

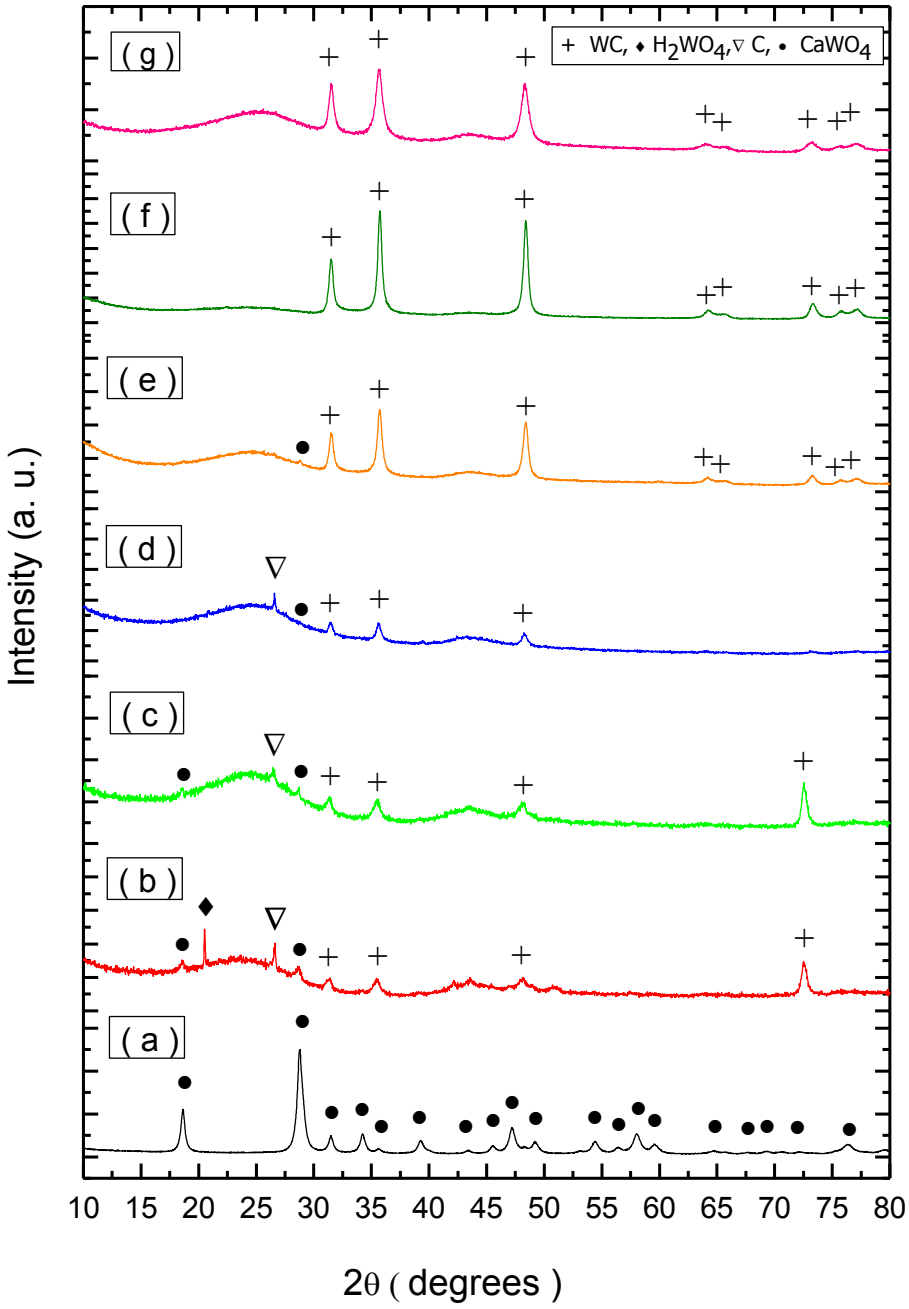

Figure 4.26: X-ray diffraction pattern of (a) milled scheelite; acid and base washed powders obtained after heating at (b) 650 °C (4 h) (c) 700 °C (4 h) (d) 800 °C (10 S) (e) 800 °C (4 h) (f) 800 °C (10 h) (g) 650 °C (20 h).

The schematic illustration of the reaction mechanism is shown in Fig.4.27. Since ore contains various impurities trapped in $CaWO_4$ grains, these impurity layers act as stress centers during heating as each impurity will have different thermal expansion coefficient. These impurities break the $CaWO_4$ particles into smaller particles. Activated charcoal formed CO gas in the sealed autoclave. The undesired reaction products and impurities were easily removed by dilute acid and base leaching. Mg absorbs the oxygen from the autoclave atmosphere and is converted to MgO which acts as catalyst for reaction to proceed. In all the experiments conducted for finding the mechanism, we could not observe any intermediate phase like elemental W, W_2C or WC_{1-x} as reported by Reddy et al. [21, 22]. The probable reason for this behavior could be the very small size of freshly produced active tungsten during reduction of $CaWO_4$, which got carburized completely in short period of holding time even as that of 10 second. The autogenic pressure helped in disintegeration and carburising process. However, it is possible that during heating some intermediate phase might have formed because the heating rate of the furnace was (5°C/min) slow enough which could take nearly 3h to attain 800°C temperature.

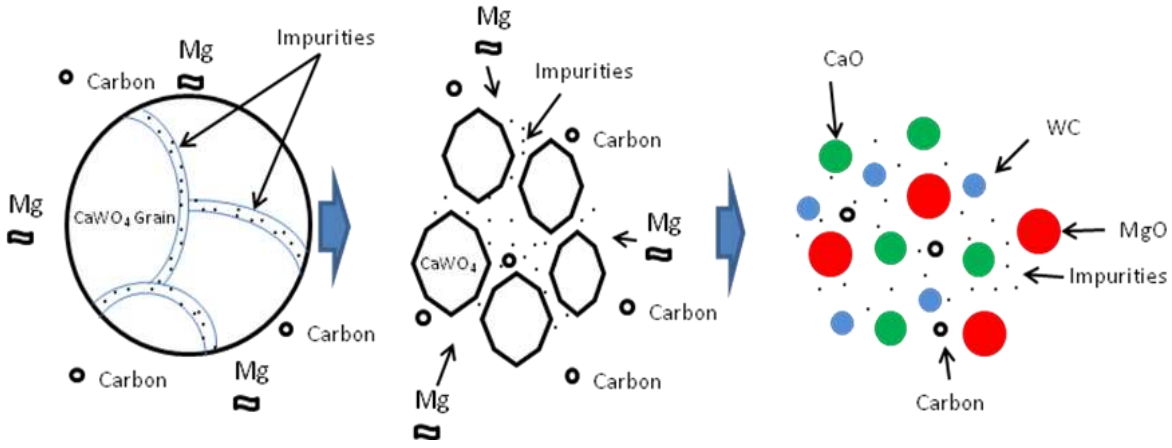

Figure 4.27: Schematic illustration of direct conversion of scheelite ore to nano tungsten carbide.

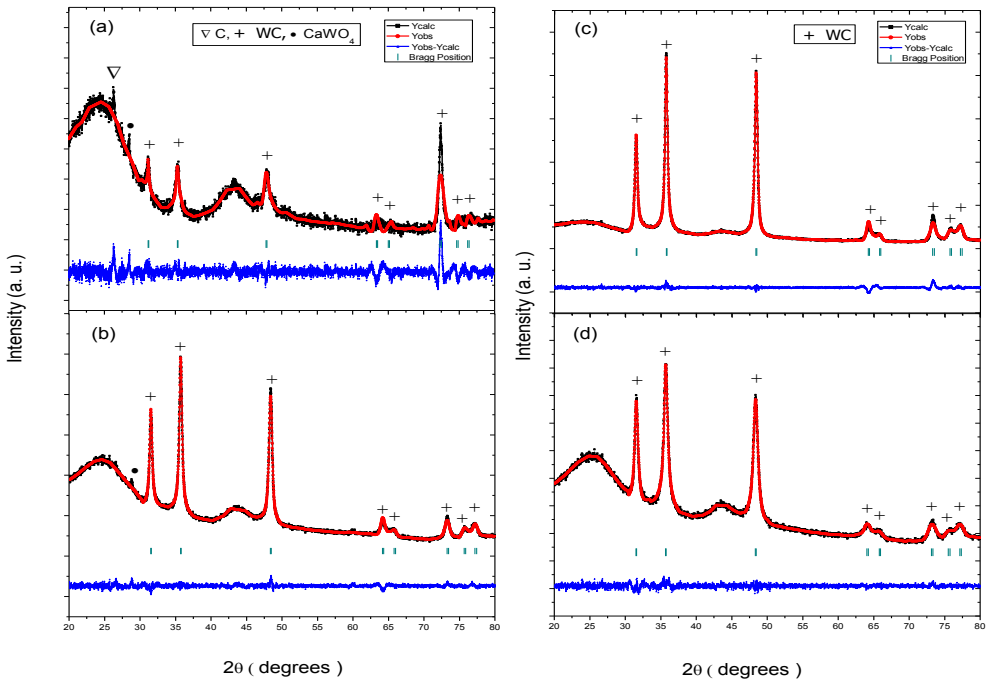

Figure 4.28: Rietveld refinement plot of observed, calculated and difference profile of nanocrystalline WC (acid and base washed) obtained at (a) 700 °C (4h) (b) 800 °C (4h) (c) 800 °C (10h) (d) 650 °C (20h).

It is evident from the XRD patterns of Fig. 4.26 (b to f) that time duration of 4 h was sufficient enough to completely carburize the elemental tungsten produced (reaction 3) in all sets of experiments. However, higher temperature of 800 °C with 10 h heating time or increased heating time of 20 h at lower temperature 650°C was required to completely reduce the $CaWO_4$ to W followed by carburization of WC. So, the reaction 5 is found to be limiting reaction.

$$CaWO_4 + 3Mg \longrightarrow W + 3MgO + CaO \quad (8)$$

$$2C + O_2 \longrightarrow 2CO \quad (9)$$

$$2W + 2CO \longrightarrow 2WC + O_2 \quad (10)$$

The X- ray diffraction pattern matches well with WC (ICDD card no. 01-072-0097) as shown in Fig. 4.26 (b to f), that confirms the direct formation of nanocrystalline WC from scheelite. The X-ray diffraction pattern was further refined by Rietveld method using Fullprof.2k (Version 5.0). Figure 4.28 shows full profile of Rietveld refinement of selected samples. The crystal structure was refined with *P-$_6$m2* symmetry and 187 space group. The cell parameters obtained after refinement are shown in the Table 4.4. As the growth of the WC phase is completed for the reaction at (800 °C (10 h) and 650°C (20 h)), the cell parameters approach the reported card values a =2.9065 Å, and c = 2.8366 Å with cell volume V= 20.75 Å^3 (ICDD card no. 01-072-0097). The best refinement, (Chiχ^2= 0.90) and very close values of cell parameters were found to be of WC phase synthesised at lower temperature 650°C (20 h). The results indicate that the low temperature is good for synthesis of nano size compounds as high temperature promotes the grain growth. Fig. 4.29 shows the HRTEM of acid and base washed sample heated for 20 h at 650 °C. Fig 4.29 (b) shows the WC particles of around 20nm size which is close to the crystallite size of 14.1 nm calculated from XRD. Fig. 4.30 shows the lattice fringes of nanocrystalline WC particle. The d-spacing found to be 0.18 nm which is in consistence with (101) plane of WC (ICDD card no. 01-072-0097) respectively. This confirms the crystalline nature of WC particles formed at 650°C.

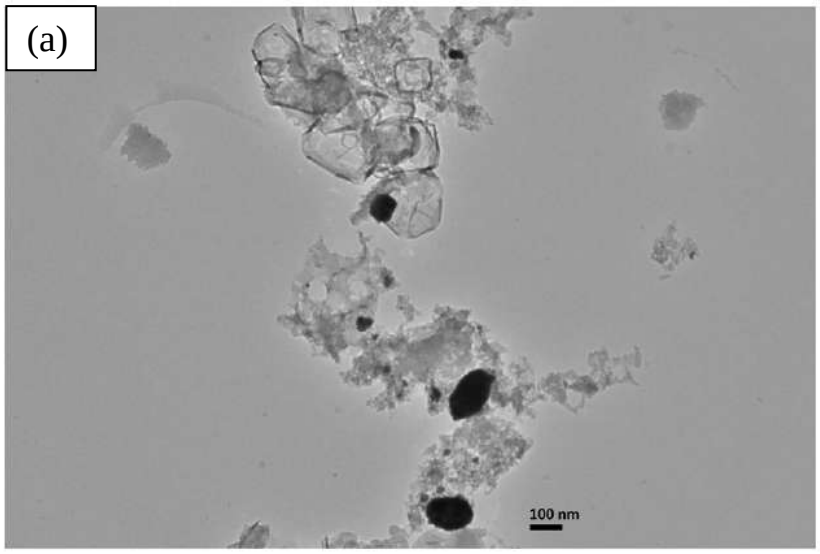

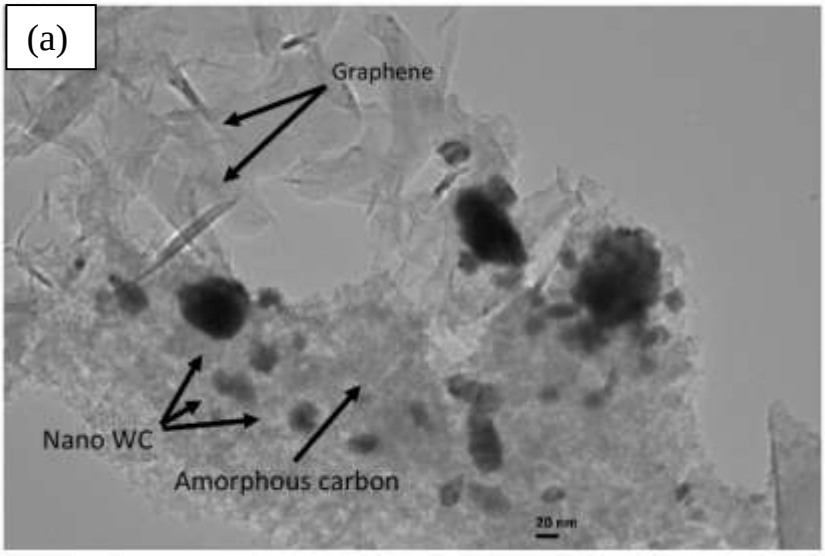

Figure 4.29: (a and b) HRTEM of WC nanoparticles obtained at 650 °C.

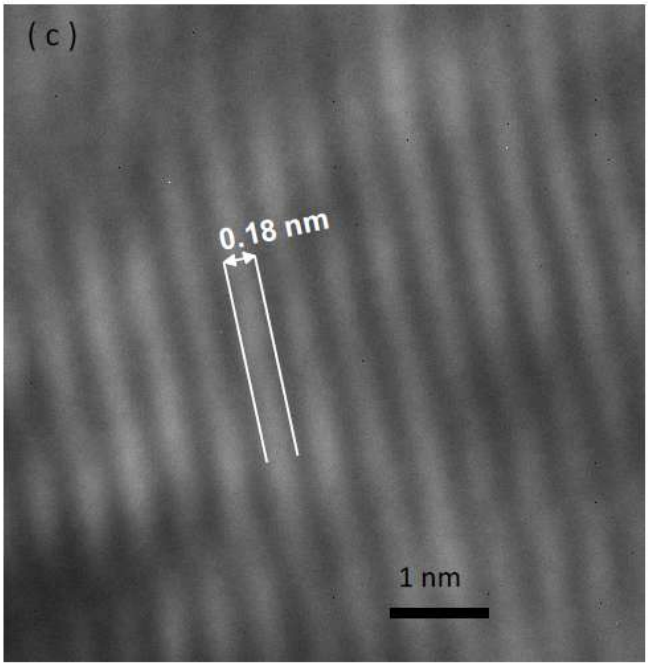

Figure 4.30: Lattice fringes of WC nano particle.

Table 4.3

Variation in WC crystallite size with temperature and time.

Temperature (°C)	Time	WC Crystallite size (nm)
700	4h	14.1 ± 0.1
800	4h	20.2 ± 0.1
800	10h	22.1 ± 0.1
650	20h	14.1± 0.1

Table 4.4

WC lattice parameters obtained by Rietveld refinement.

Temperature (°C) /Time	Cell parameters				R- factors			
	a (Å)	c(Å)	c/a	Volume($Å^3$)	R_p	R_{wp}	R_{exp}	Chi(χ^2)
700(4h)	2.9341	2.8669	0.977	21.412	4.91	6.89	5.48	1.58
800(4h)	2.9006	2.8356	0.977	20.660	2.41	3.23	3.02	1.14
800(10h)	2.8988	2.8364	0.978	20.651	3.15	4.89	3.34	2.15
650(20h)	2.9051	2.8367	0.976	20.737	2.38	3.10	3.25	0.90

4.3 Experiments for higher yield of nano WC

In the results reported in the previous section for the synthesis of single phase nano WC, it is observed that there are six variable parameters that affect the reaction output for product phase formation. These are quantity of scheelite, milling time, ball to powder weight ratio, quantities of Mg and activated charcoal and lastly temperature. In order to increase the quantity of synthesized nano WC experiments were conducted with more than 1g of scheelite milled for 10 h with ball to powder weight ratio (BPR)5:1 and 50:1 for which details are summarised in Table 4.5.

Table 4.5 Summary of the optimization experiments conducted for higher yield of nano WC.

Sample	Scheelite (Milling Time/BPR)	Mg	Activated Charcoal	Time	Temp (°C)	Phases (after acid & base leaching)
Earlier Optimized conditions	1g (50/(50:1)	1g	2 g	10h	800	Single Phase Nano WC
S1*	1g (50/(50:1)	0.75g	0.5 g	10h	700	Single Phase Nano WC
S2*	1.5g (10/(50:1))	1.15g	0.75g	20h	800	Single Phase WC
S3	3g (10/(5:1))	1.5g	-	4 h	500	No Reaction
S4	3g (10/(5:1))	1.5g	-	4h	700	H_2WO_4, Gasket leak
S5	3g (10/(5:1))	1.15g	-	4h	700	H_2WO_4
S6*	3g (10/(5:1))	1g	0.124g	4h	700	W,H_2WO_4
S7*	3g (10/(5:1))	1g	0.186g	4h	700	W, W_2C, H_2WO_4
S8*	3g (10/(5:1))	1.15g	0.5g	20h	800	WC, W_2C, H_2WO_4
S9*	3g (10/(5:1))	1.15g	0.75g	20h	800	WC, W_2C, H_2WO_4

(* All the experiments were done 3 times to confirm the feasibility of product phases)

S1 experiment was carried out with reduced quantities of Mg and activated charcoal at 700°C for 10h and it could successfully produce single phase nano WC (Fig. 4.25(a)). After studying literature another study (S2) was attempted by further decreasing the quantities of Mg and activated charcoal along with substantial drop in milling time and increased temperature. Here, also single phase WC was obtained. Other experiments given in the table 4.4 could not lead to single phase WC powder. Moreover, experiments S1 and S2 was conducted three times to confirm the feasibility.

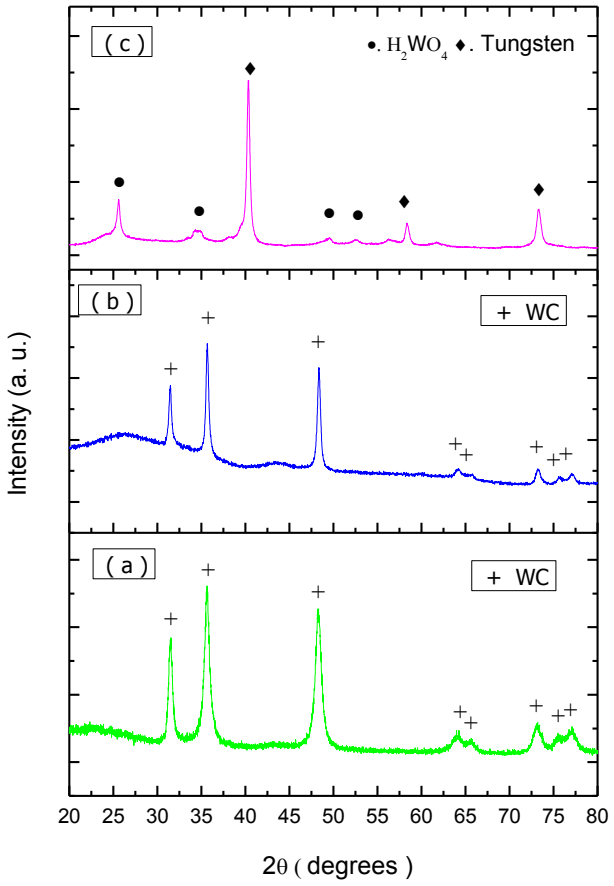

Figure 4.31: X-ray diffraction pattern of (a) sample S1 showing single phase nano WC (b) sample S2 showing single phase nano WC (c) sample S8 (W and H_2WO_4).

It is important to note that an all other experiments with variation in processing parameters could lead to formation of intermediate products as reported in literature [21-22]. The above experiments indicate that particle size, quantity of scheelite, carbon source, Mg along with temperature and holding time plays important role to get WC phase.

References

[1] G.S. Upadhyaya, Cemented tungsten carbides: production, properties and testing.Westwood, New Jersey, USA: Noyes publications; 1998.

[2] E. Lassner, W.D. Schubert, Tungsten Properties, Chemistry, Technology of the Element, Alloys, and Chemical Compounds. Kluwer Academic/Plenum Publishers, New York, 1999.

[3] R.P.S Gaur, The J. The Min. Metals and Mater. Soc., 58 (9) (2006) 45-49.

[4] J. F. Paulinoa, J. C. Afonso, J. L. Mantovano, C. A. Vianna, J. W. S. D. Cunha, Hydrometal., 127-128 (2012) 121–124.

[5] Z. Zhao, J. Li, S. Wang, H. Li, M. Liu, P. Sun, Y. Li, Hydrometal., 108 (2011) 152–156.

[6] J.I. Martins, A. Moreira, S.C. Costa, Hydrometal. 70 (2003) 131–141.

[7] Z. Zhao, Y. Liang, H. Li, Int. J. Ref. Metals Hard Mat., 29 (2011) 289–292.

[8] N.J. Welham, N. Setoudeh, Lett. Edit., Car., 43 (2005) 855–894.

[9] NJ. Welham, Mater. Sci. Eng. A, 255(1-2) (1998) 81–89.

[10] A.W. Weeber, H. Bakker, Phys. B 153(1-3) (1988) 93–122.

[11] I. Morjan, I. Soare, R. Alexandrescu, LG Florescu, RE Morjan, G. Prodan, Infra. Phys. Tech., 51 (2008) 186-197.

[12] V.Z. Mordkovich, M. Baxendale, M. Yudasaka, R. Kikuchi, S. Yoshimura, J.Y. Dai, Springer, Berlin 1998.

[13] J. Rodriguez-Carvajal, Program Fullprof.2k Version 5.0, 2011 (LLB, CEA-CNRS).

[14] C. Guo, Y. Liu, X. Ma, Y. Qian, L. Xu, Chem. Lett. 35 (2006) 1210-11.

[15] A. Kumar, K. Singh, O.P. Pandey, Int. J. Ref. Metals Hard Mat., 29 (2011) 555-558.

[16] M. Mahajan, K. Singh, O.P. Pandey, Int. J. Ref. Metals Hard Mat. 36 (2013) 106-110.

[17] Akshay Kumar, Preparation and Characterization of Tungsten Carbide Micro/Nano Composites, Ph.D. Thesis, 2011.

[18] V.G. Pol, S.V. Pol, A. Gedanken, Adva. Mater., 23 (2011) 1179-1190.

[19] S.V. Pol, V.G. Pol, A Gedanken, Adv. Mater., 18 (2006) 2023-2027.

[20] V.K. Pecharsky and P.Y. Zavalij, Fundamentals of powder diffraction and structural characterization of materials. Springer, USA, 2005, pp. 342-343.

[21] K. Madhav Reddy, T. N. Rao, J. Joardar, Mat. Chem. Phys., 128 (2011) 121- 126.

[22] K. Madhav Reddy, T. N. Rao, J. Joardar, J. All. Compds., 494 (2010) 404-409.

Chapter 5

Results and Discussion (Wolframite ore)

Overview

This chapter presents the results of synthesis of different carbides of tungsten from wolframite ore by solid state reaction method. Also the results of synthesis of single phase nanocrystalline WC directly from the wolframite ore (containing nearly 50% impurity in as received form) by thermo-chemical route are described. The impurities were leached out after synthesis using dilute HCl (1:1) and concentrated HF, thus setting a reverse trend where prior removal of impurities is done. This chapter is divided into two parts. First one describes the results by solid state reaction method. The second part gives the account of experiments conducted by thermo-chemical route. The powders were characterized by X-ray diffraction and high resolution transmission electron microscope (HRTEM). The lattice parameters were calculated from Rietveld analysis using Fullprof program. This is a simple and economical method for synthesis of nanocrystalline WC.

The processing of the tungsten ore wolframite starts with alkali (NaOH) digestion or by alkali (Na_2CO_3) roasting [1-3]. The alkali roasting (Na_2CO_3) requires temperature range of 800 °C to 900 °C whereas digestion with NaOH is done at comparatively lower temperature range of 190 °C to 325 °C under the pressure of 10.0 to 24.0 bar [4]**.** Recent study has reported 98.6% recovery of tungsten from wolframite by fusion with NaOH at 650 °C [5]. Both the processes require excess amount of alkali than stoichiometry of the reactions. The digested solution is diluted for precipitation and filtration of impurities like silica, alumina, and iron oxide. If the concentration of impurities is high, they cause disturbance and hinder further processing to ammonium paratungstate [4]. The sodium tungstate solution is converted into pure ammonium tungstate through ion exchange process and further crystallized to ammonium paratungstate. The latter is calcined to produce WO_3 or blue oxide. The WO_3 is then reduced with hydrogen at high temperature to produce elemental tungsten. The other tungsten precursor(s) like WCl_4, WCl_6 and $W(CO)_6$ are obtained by further processing of elemental W at high temperatures [1].

5.1 Solid state reaction method

5.1.1 Reduction of wolframite ore with activated charcoal

The wolframite was mixed with activated charcoal in 1:2 ratio of the stoichiometry of the reaction 1. The powder was milled for 50h at ball to powder ratio of 1:50 in tungsten carbide jar and balls (Retsch PM100). After that powder was compacted into pellets. These pellets were calcined at 1000°C (4h) and 1100°C (4h) in the flowing argon gas. The scanning electron micrograph of the wolframite and activated charcoal are shown in Fig. 5.1. It shows that the particle size of wolframite varies from submicron to micron size and activated charcoal also has vide variation.

$$FeWO_4 + 5C \longrightarrow WC + Fe + 4CO \qquad (1)$$

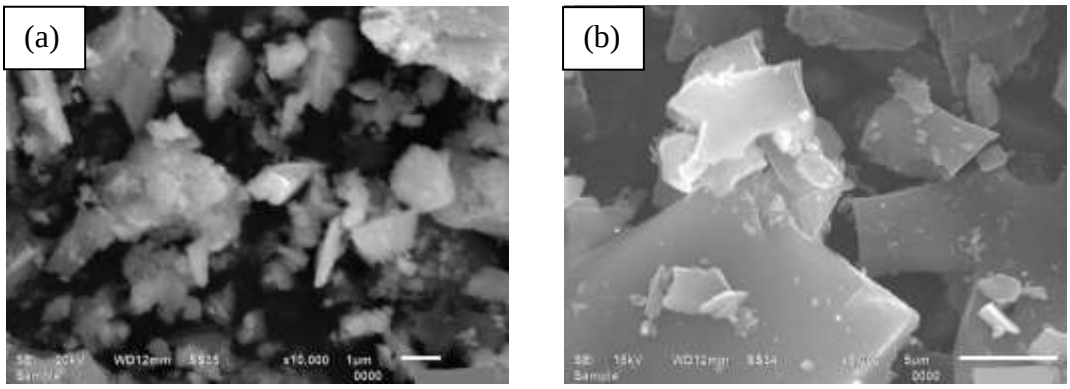

Figure 5.1: Scanning electron micrograph of the (a) wolframite and (b) activated charcoal.

5.1.1.1 X-ray diffraction analysis

Fig 5.2 shows the X-ray diffraction pattern of the wolframite. The major phases in the wolframite are $FeWO_4$ (ICDD card no. 01-074-1130) and SiO_2 (ICDD card no. 01-075-0443). The X-ray diffraction patterns of the calcined pellets are shown in Fig. 5.3. In the pellets calcined at 1000°C, majority of $FeWO_4$ got converted into Fe_2W_2C and W_2C. There was some residual $FeWO_4$ and SiO_2. Samples calcined at 1100°C showed

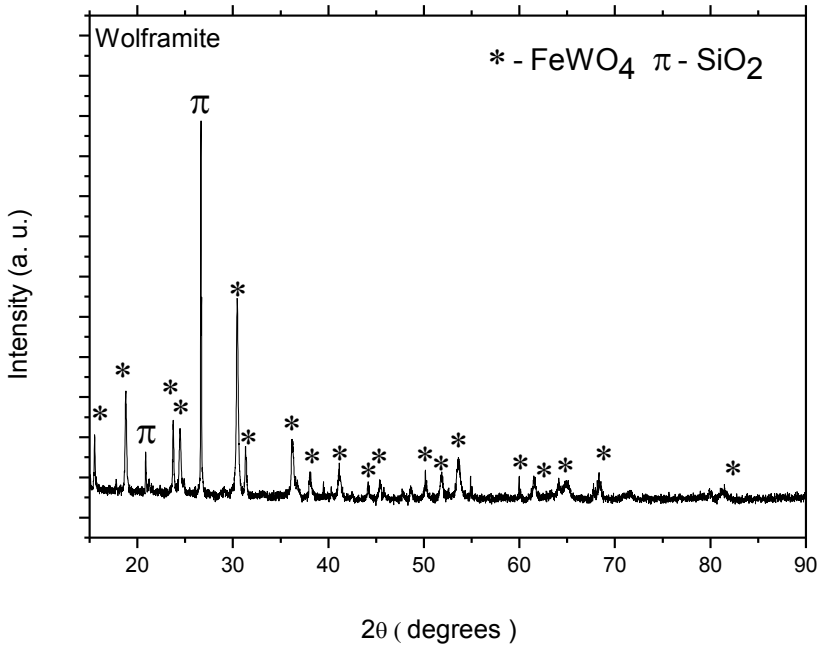

Figure 5.2: X- ray diffractogram of wolframite showing presence of $FeWO_4$ and SiO_2.

complete conversion of $FeWO_4$ to Fe_2W_2C and W_2C. This behavior was in contrast to the earlier study in which WC along with multiple impurities (Fe_3W_3C, Fe_7W_6, W, Fe_3C and Fe) was produced [6]. The crystallite sizes calculated from the XRD are 44 nm for Fe_2W_2C and 43 nm for W_2C. The calcination seems to proceed through reactions as given below:

$$2FeWO_4 + 9C \longrightarrow Fe_2W_2C + 8CO \quad (2)$$

$$Fe_2W_2C \longrightarrow W_2C + 2Fe \quad (3)$$

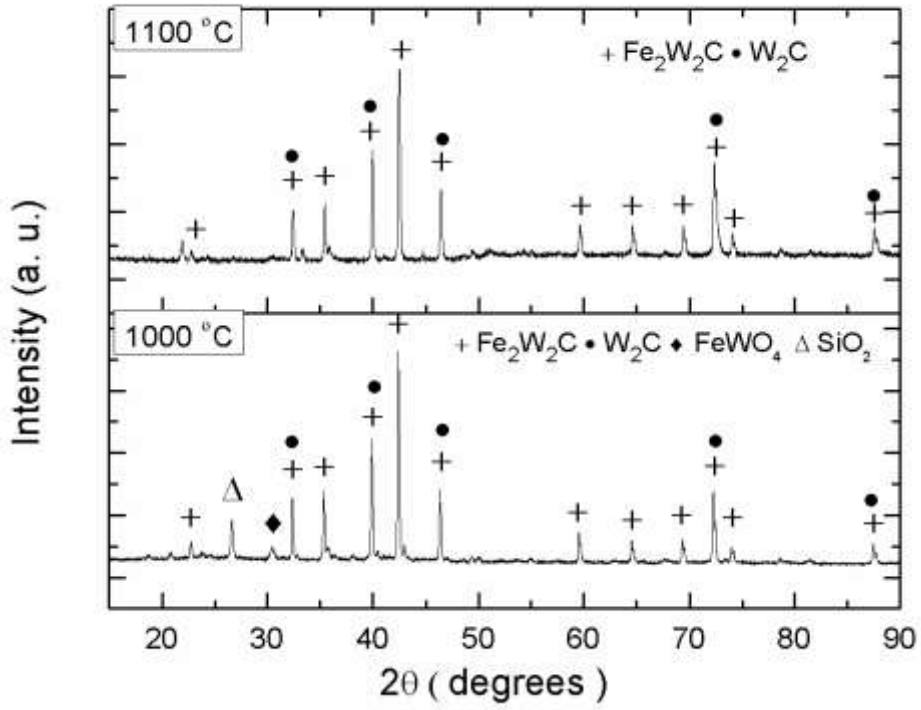

Figure 5.3: X-ray diffraction pattern of the milled powders calcined at 1000 °C and 1100°C.

5.1.1.2 SEM studies

The scanning electron micrographs of 1000°C calcined samples are shown in Fig. 5.4(a and b). Particles observed are in the range of 0.1 to 1μm as can be seen in the Fig. 5.4 (a). Figure 5.4(b) shows well faceted particles confirming formation of crystalline phases.

SEM of 1100°C calcined samples shows the particles in the range of 1 to 4µm. Samples calcined at 1100°C represents similar structural features as that of 1000°C.

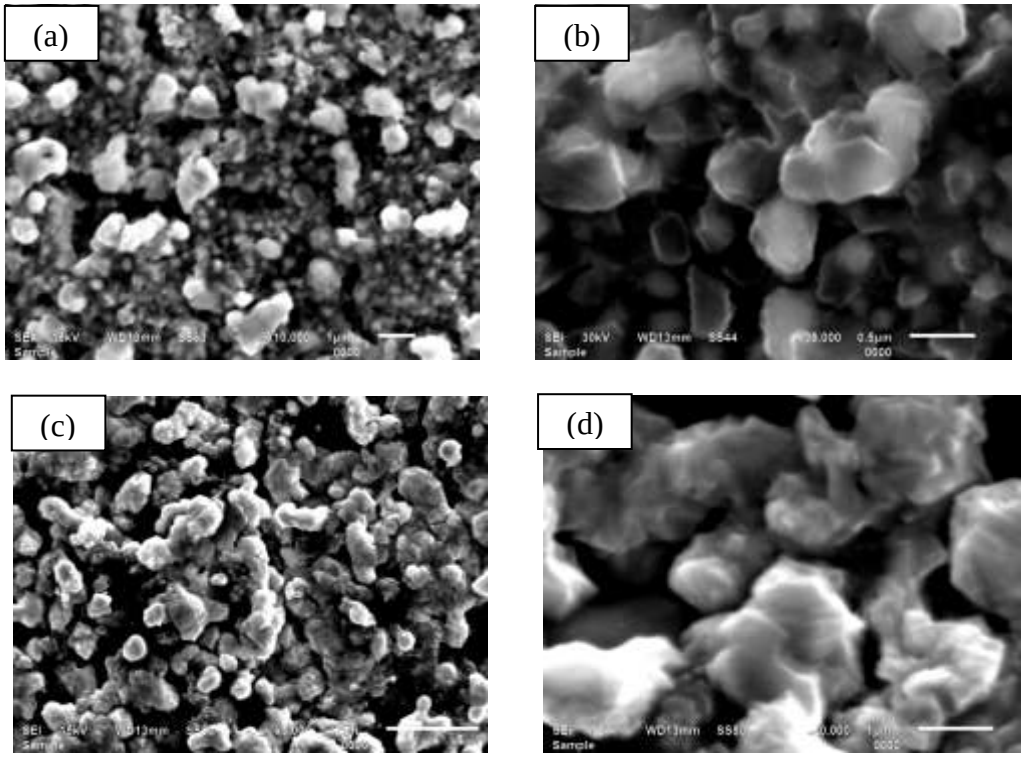

Figure 5.4: SEM micrograph of the milled powders calcined at 1000°C (a and b) and 1100°C (c and d).

The calcination done at 1100°C shows the feasibility of formation of carbide phases. The nano carbides Fe_2W_2C and W_2C have been observed in the product phase. Further, experiment at high temperature under variable ingradient content could not lead to formation of pure phase, rather Fe_7W_6 phase was observed. The study indicates that by taking excess of carbon the reaction may lead to formation of single phase WC. However, the role of impurities in the ore is not clear as it leads to formation of other constituents like Fe_2W_2C, Fe_7W_6. Since, the thermo chemical reduction route is more promising one, further experiments were performed by this process as the amount of impurity in wolframite is more as compared to scheelite.

5.2 Thermo-chemical Route

5.2.1 Synthesis of tungsten carbide

The schematic illustration of synthesis and purification is shown in Fig. 5.5. The experiment was performed using 1 g of wolframite**,** 2 g of activated charcoal and 1 g of Mg in the autoclave. The sealed autoclave was kept in a furnace at 800 °C for 20 h. The furnace was heated at the heating rate of 5°C/min. After the experiment, autoclave was allowed to cool at room temperature in the furnace. The powders were taken out and washed with dilute HCl (1:1) to remove Fe, MgO and other impurities. The powders were kept in 200ml dilute HCl solution for one hour and then washed with water several times followed by drying for 12 h in an oven at 70°C.

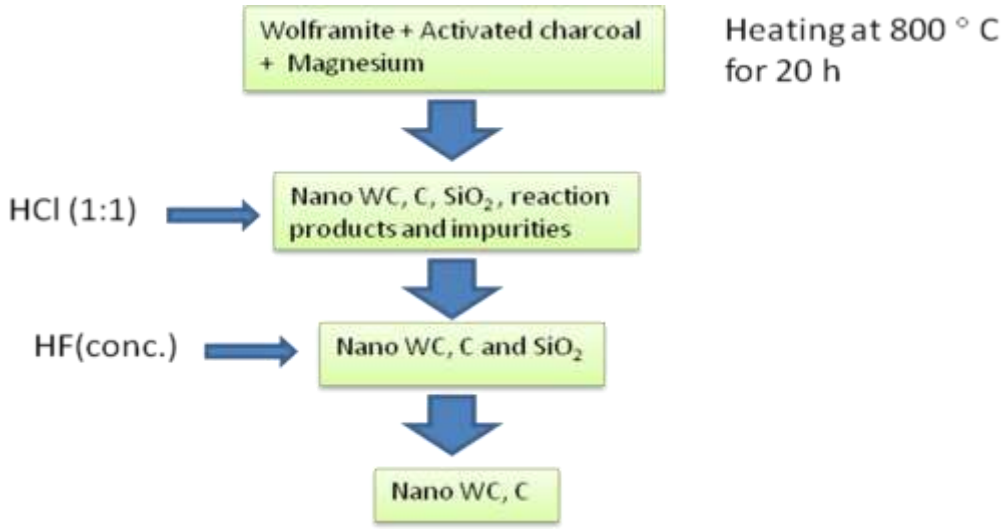

Figure 5.5: Schematic illustration of synthesis and purification of Nano WC from wolframite ore.

In order to remove silica impurity we performed systematic experiments where the products were first leached by 0.25 M NaOH solution (100 ml), then next set with 10% HF solution (100ml) with holding time for 1 h and finally we used concentrated HF (5ml) with variable holding time (detail given in the last section) for complete removal of silica.

5.2.1.1 X-ray diffraction analysis

Fig. 5.6(a) shows the X-ray diffraction pattern of raw wolframite. The peaks were indexed as $FeWO_4$ (ICDD card no. 01-074-1130) and SiO_2 (ICDD card no. 01-075-0443). Fig. 5.6(b) shows the X-ray diffraction pattern after complete removal of impurities. The X- ray diffraction pattern matches well with WC (ICDD card no. 01-072-0097) and confirms the direct formation of hexagonal nanocrystalline WC (*P-$_6$m2* symmetry with space group 187) from wolframite. The diffraction pattern also showed peak of graphitic carbon (ICDD card no. 00-012-0212). The broadening of peaks indicates that WC particles size are in the nano range. The crystallite size was calculated by Scherrer's formula.

$$D = \frac{0.9\lambda}{B\cos\theta}$$

where D is crystallite size, B (in radian) is full width at half maximum (FWHM) obtained by Gaussian fitting WC diffraction peak of (100) plane. The average crystallite size was found to be 27 nm. The X-ray diffraction pattern was refined by Rietveld method using Fullprof program as shown in Fig. 5.6(c). The refined lattice parameters are a= 2.901Å, c = 2.828 Å which is close to the reported values (a= 2.906Å c = 2.836 Å, ICDD card no. 01-072-0097). The parameters showed good fit with Chi Square (χ^2) = 2.74.

The solid gas phase reaction taking place in the autoclave led to formation of nanocrystalline WC. The possible reaction mechanism is given below:

$$FeWO_4 + 4Mg \longrightarrow W + 4MgO + Fe \quad (4)$$

$$2C + O_2 \longrightarrow 2CO \quad (5)$$

$$2W + 2CO \longrightarrow 2WC + O_2 \quad (6)$$

$$FeWO_4 + 3Mg + 2C \longrightarrow WC + 3MgO + Fe + CO + C \quad (7)$$

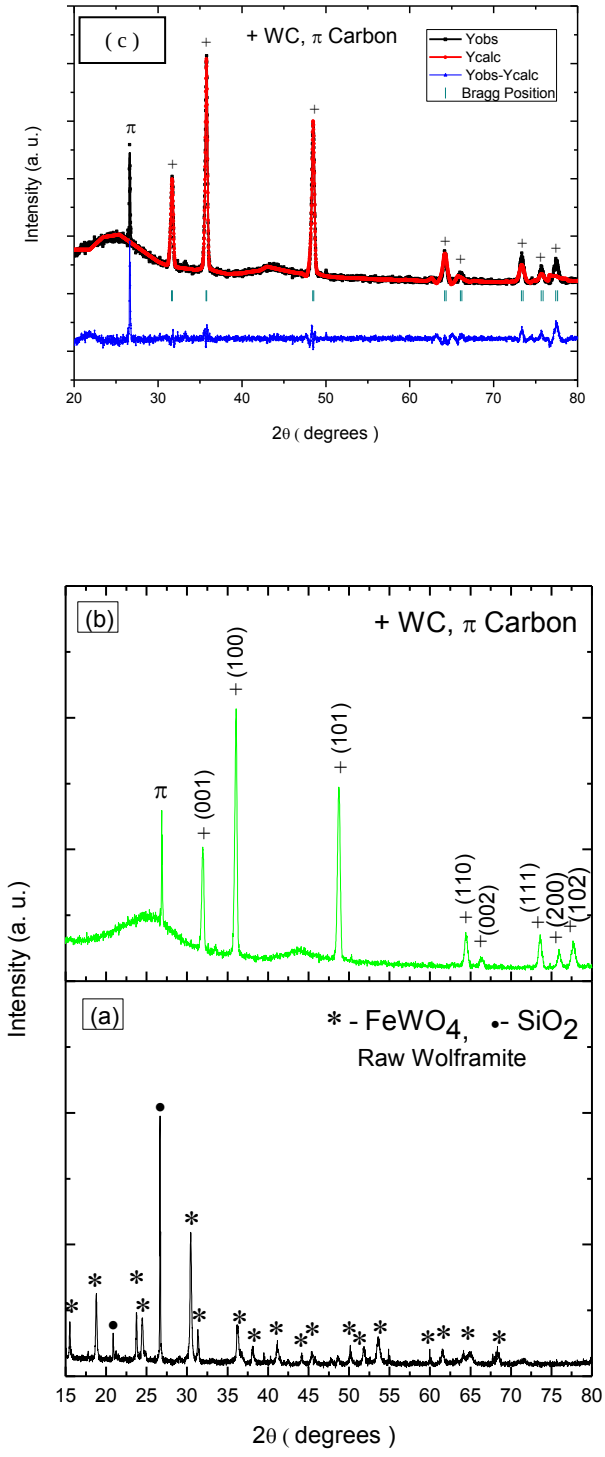

Figure 5.6: X-ray diffraction pattern of (a) raw wolframite (b) nanocrystalline WC synthesized from wolframite (c) Rietveld refinement plot of observed, calculated and difference profile of nanocrystalline WC.

The reduction of H_2WO_4 to W is reported at 900°C [7]. In our case magnesium reduces the $FeWO_4$ to W at 800 °C. The excess amount of activated charcoal forms CO gas in the autoclave. This CO reacts with elemental tungsten to produce WC. The oxygen evolved further reacts with C to form CO and this cycle continues till the entire W is converted to WC. The major factors which helped in retaining nano size of WC are comparatively lower synthesis temperature, presence of impurities and presence of the gas mixture at high temperature. This is known fact that some of impurities act as grain growth inhibitors for the synthesis of WO_3 and W [1]. The impurities present in the wolframite did not interfere in the synthesis process. However, the effect of individual impurity on the synthesis process of WC needs to be explored and is beyond the scope of this research.

5.2.1.2 HRTEM analysis

Fig. 5.7 shows the HRTEM of nanocrystalline WC obtained after complete removal of impurities. The WC particles are in the range of 50 to 100nm. WC crystal showed faceted morphology having hexagonal features.

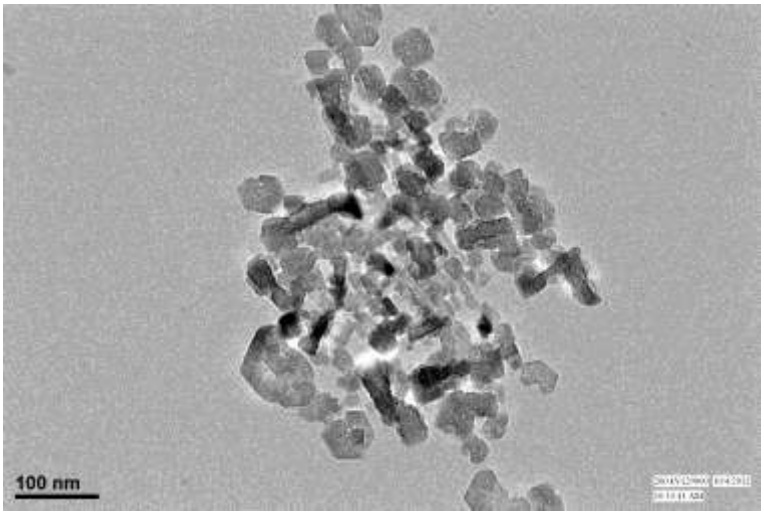

Figure 5.7: HRTEM of WC nanoparticles obtained after complete removal of impurities.

5.2.1.3 Removal of impurities

For the synthesis of nano WC, the reaction was carried out using wolframite in as received condition with all the impurities. The unreacted Mg, reaction by products (MgO, Fe) and other impurities (except silica) were leached out by dilute HCl (1:1) as shown in Fig. 5.8(a).

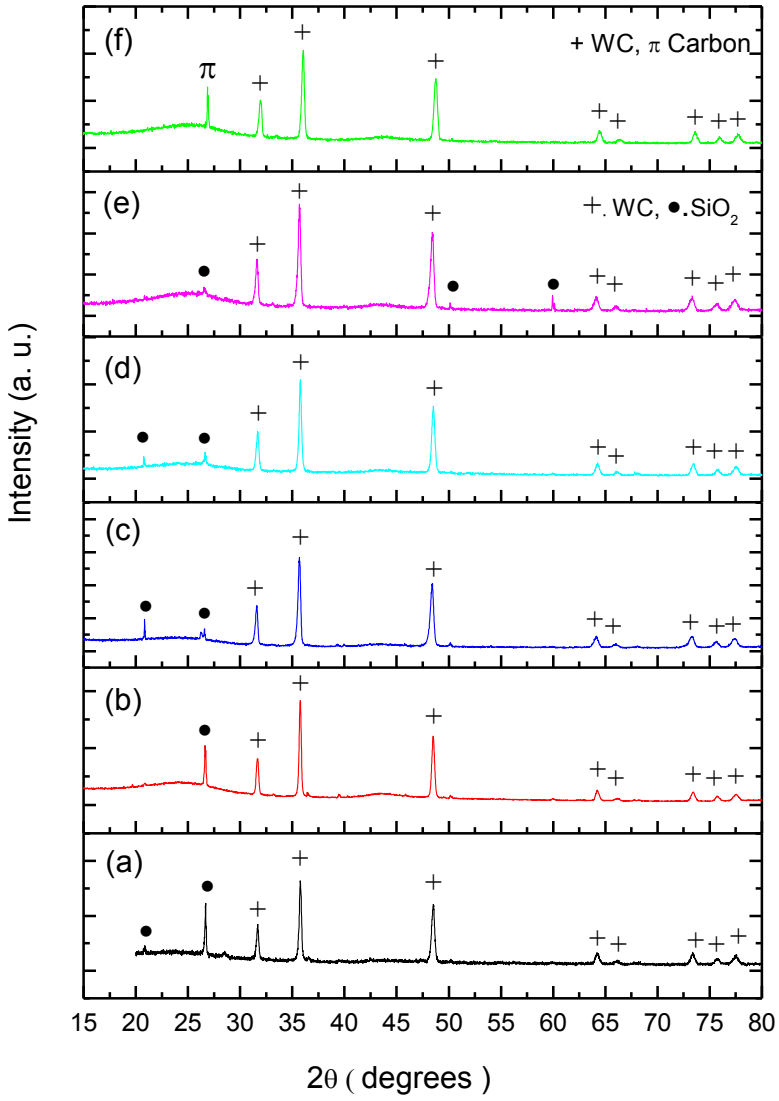

Figure 5.8: X-ray diffraction patterns after leaching with concentrated HF (a) zero time (without HF leaching) (b) 5 min leaching (c) 10 min leaching (d) 20 min leaching (e) 30 min leaching (f) 37 min leaching.

The major challenge to get pure WC phase was to remove most stable refractory impurity silica (SiO_2) in the mixture without affecting nanocrystalline WC. Firstly, we attempted to remove SiO_2 using dilute NaOH as per previous report [21], but to our dismay dilute NaOH was unable to do so. So, next trial was made with dilute HF and unfortunately it also proved to be unsuccessful. Finally, the concentrated HF was found to dissolve silica as per the reaction given below:

$$SiO_2 + 6HF \longrightarrow H_2SiF_6 + 2H_2O \quad (8)$$

It was also observed that reaction of HF with SiO_2 was time dependent and longer leaching time could probably affect WC. So, systematic leaching experiments were done to find optimal leaching time (Fig. 5.8 (a) to (f)). The powders (0.5g) were leached with concentrated HF (5ml), with continuous agitation. The samples for X-ray diffraction were taken after 5 min, 10 min and 1 h. It was observed that the quantity of SiO_2 reduced in powder sample with 5 min holding time and it showed further reduction with increase in holding time of 10 min as shown in Fig. 5.8(b and c). In the final sample (1 h holding time) not only silica was removed from the sample but also nano WC got converted to nano WO_3 (X-ray diffraction pattern not shown here). The next set of leaching experiment was performed under similar conditions. The samples were collected after 20 min and 30 min. The samples showed similar trend of silica reduction with increasing holding time of 20 min to 30 min as shown in Fig. 5.8(d & e). The 30 min leaching sample contained traces of SiO_2 (Fig. 5.8(e)). The complete SiO_2 leaching occurred in 37 min holding time as confirmed by X-ray diffraction pattern (Fig. 5.8(f)). The last leaching also converted amorphous carbon to graphitic carbon. The possible reasons could not be ascertained. However, experiments are still being done to establish leaching kinetics. The effect of leaching time on SiO_2 is shown in Fig. 5.9. The percentage of silica in the mixture was calculated by considering area of two intense peaks of SiO_2 and three high intensity peaks of WC.

There is general trend to use high purity compounds for research and particularly for synthesis of nanocrystalline WC. This study reveals that even larger quantity of impurities (approx. 50%) in the ore did not interfere the synthesis of nanocrystalline WC.

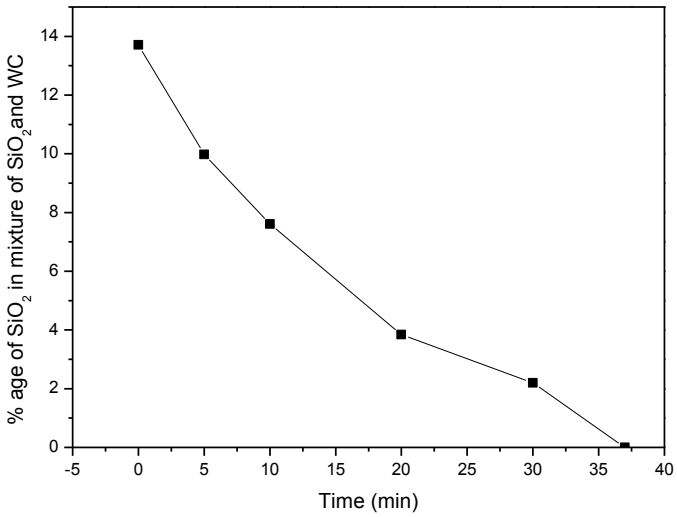

Figure 5.9: Effect of leaching time on the concentration of SiO_2.

In order to optimize the conditions, further systematic experiments were carried out at different temperatures. These are given at Table 1.

Table 5.1 Experimental conditions

Sr. No.	Sample Name	Temperature (°C)	Time(h)
1	S1	650	4
2	S2	700	4
3	S3	800	4
4	S4	800	20

Fig. 5.10 (b) shows the X-ray diffraction pattern of the HCL (1:1) washed sample S1. There is no peak corresponding to $FeWO_4$, confirming the completion of reaction 1 at 650°C. The wolframite has reduced to amorphous W or WC. As the temperature is increased to 700°C, the growth of WC becomes visible (Fig. 5.10 (c)). The growth of tungsten carbide phase is completed in sample S3 heated at 800°C (4h). Further increase in time from 4 h to 20 h the crystallite growth has occurred where the peak intensities got increased as shown in Fig. 5.10(e).

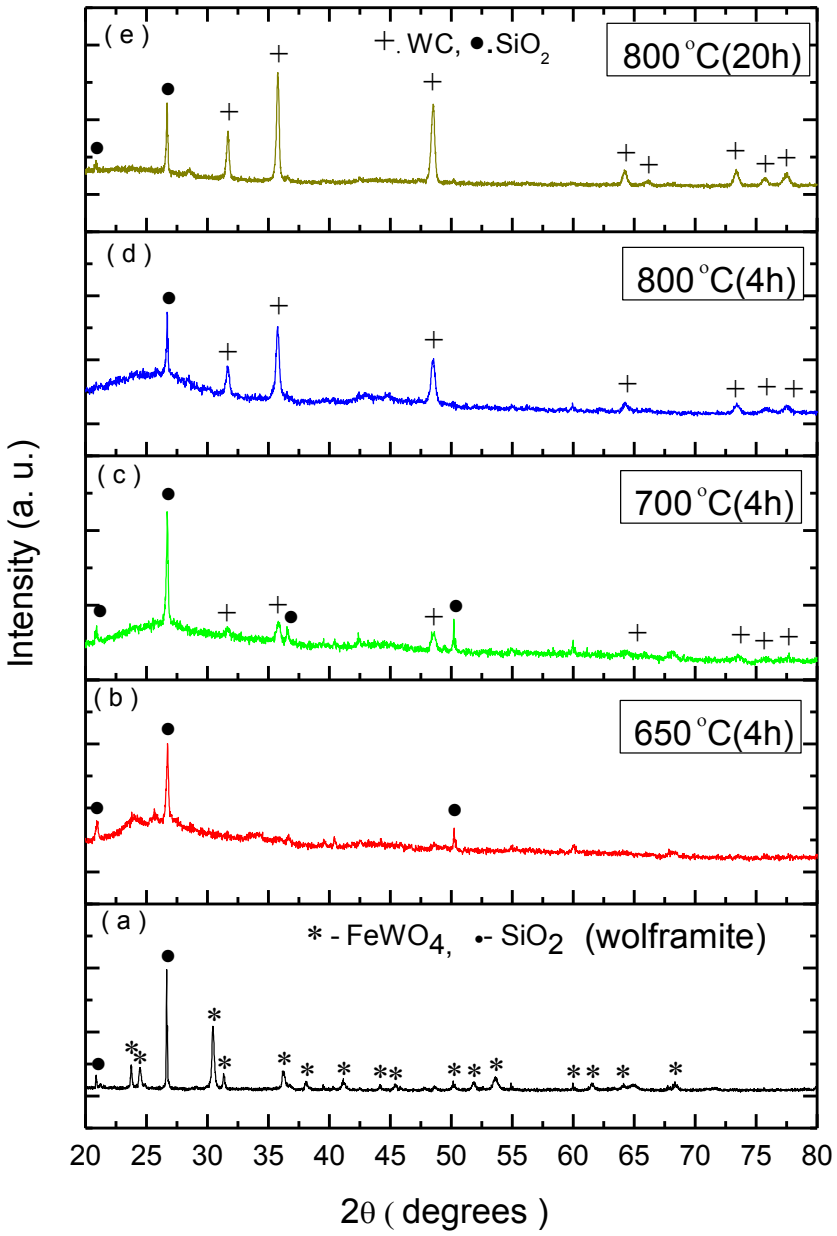

Figure 5.10: X- Ray Diffraction Patterns of (a) raw wolframite and acid washed samples heated at (b) 650°C(4h) (c) 700°C(4h) (d) 800°C(4h) (e) 800°C(20h).

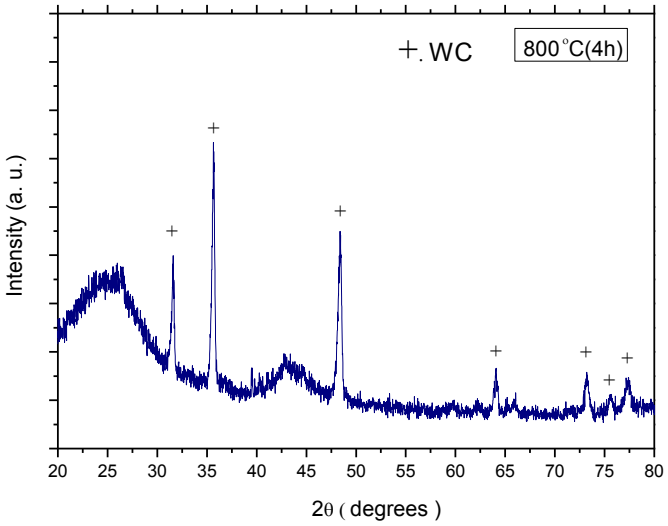

Figure 5.11: X- Ray Diffraction Patterns of S3 heated at 800 °C (4h).

Sample S3 was further leached with HF for 40 min holding time using the same procedure. The silica was completely removed confirming the repeatability of the procedure as shown in Fig.5.11. Fig. 5.12 shows the HRTEM of sample S3 after complete removal of impurities. The WC particles of a very narrow range of 3 to 7 nm have been observed in TEM.

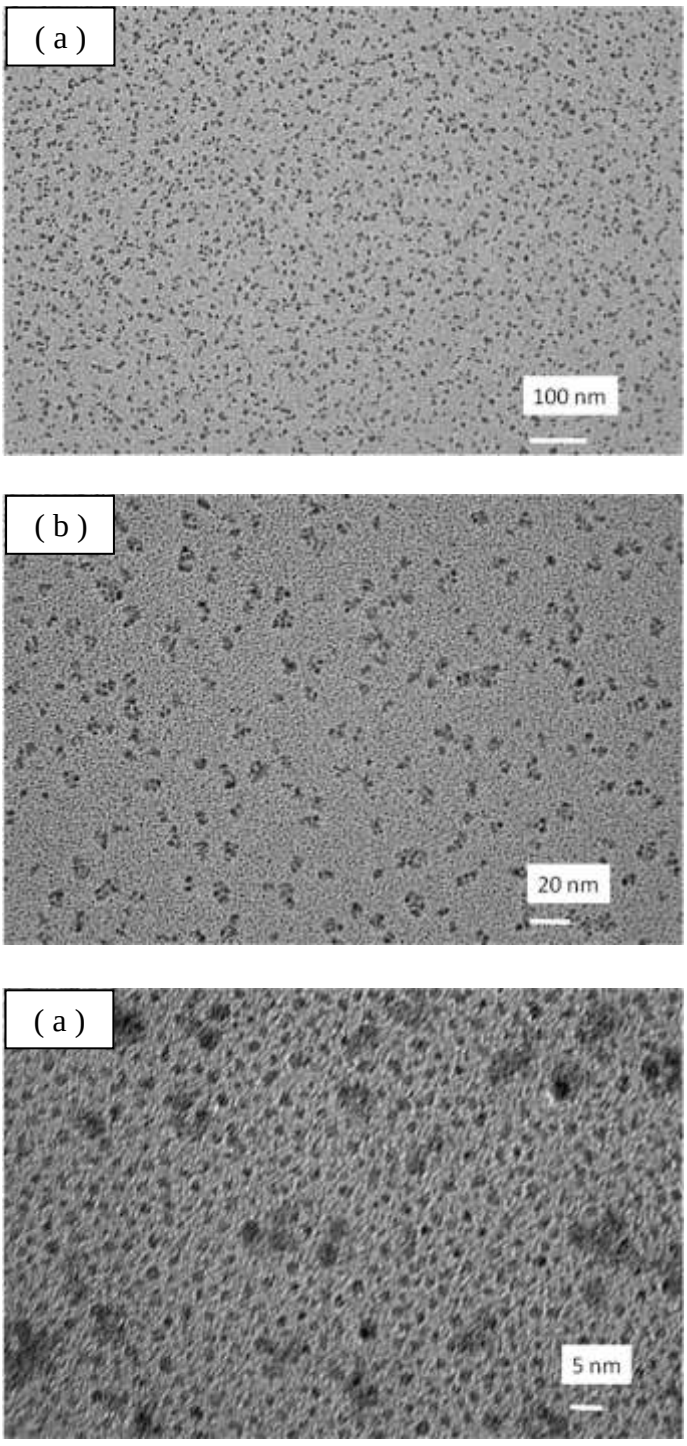

Figure 5.12: HRTEM of WC nano particles, after complete removal of impurities of sample S3.

References

[1] G.S. Upadhyaya, Cemented tungsten carbides: production, properties and testing. Westwood: Noyes publications; 1998.

[2] E. Lassner, From tungsten concentrates and scrap to highly pure ammonium paratungstate (APT). Int J Refract Met Hard Mater 13 (1995) 35-44.

[3] R.P. S. Gaur, Modern hydrometallurgical production methods for tungsten. The J. The Miner. Met. & Mat. Soc. 58(9) (2006) 45-49.

[4] M. Shamsuddin , H.Y. Sohn, Extractive metallurgy of tungsten. Proceedings TMS AIME Symposium. TMS, Warrendale, Chicago (1981) 205–230.

[5] J.F. Paulino, C.J. Afonso, J.L. Mantovano,C.A. Vianna, J.W.S.D.D. Cunha, Hydrometall 127-128 (2012) 121-24.

[6] J. Temuujin, M. Senna, T. Jadambaa, D. Byambasuren, J. Amer. Cera. Soc. 88 (2005) 983–985.

[7] S.V. Pol, V.G. Pol, A Gedanken, Adv. Mater., 18 (2006) 2023-2027.

Chapter 6

Results and Discussion (Preparation of WC-Co Composite)

Overview

The nanopowders synthesized in this work were further used for making WC-Co composites. For it nanopowders synthesized by thermo-chemcial route and solid state reaction method from scheelite ore were used. The composite was made by P/M route by taking 10 to 15 wt% Co binder. The sintering behavior of these composites at different temperatures (1100, 1200, 1300 and 1400°C) is discussed in detail. Microstructural examinations of the composites were done using optical and scanning electron micrographs. The variation in hardness of the developed composite was also studied.

6.1 Preparation of WC-Co composite

The as synthesized WC nano particles from scheelite ore by solid state reaction method and thermo-chemical route were used for the preparation of WC-Co composites for its end applications. Ultrafine Co powders have been used as a binder for making the composites. The amount of binder (Co) was varied from 10 to 15 wt.%. The details about it are described in experimental section. The consolidations of WC-Co powders were done by conventional method [1-3].

The WC nanopowders were prepared using two different ores with two different methods as described in Chapters 4 and 5. The removal SiO_2 impurities from wolframite requires HF leaching, which needs very careful handling and moreover, the process takes more time. So, the WC nanopowders obtained from scheelite ore by both the methods are used for composites. The details of the composition, sintering time and temperature are given in Table 6.1.

Table 6.1 Sample labels with sintering time, temperature and composition.

Sample Labels	Composition of composite (WC/Co)	Sintering Temperature(°C)	Sintering Time (in h)
WTC1	90/10	1100(in argon)	1
WTC2	90/10	1350 (in argon)	1
WTC3	90/10	1100(in air)	1
WTC4	90/10	1350(in air)	1
WSS1	90/10	1100 (in argon)	1
WSS2	90/10	1200 (in argon)	1
WSS3	90/10	1300 (in argon)	1
WSS4	90/10	1400 (in argon)	1
WSS5	90/10	1200 (in argon)	1
WSS6	85/15	1300 (in argon)	1
WSS7	85/15	1400 (in argon)	1

The samples WTC1, WTC2 and WTC3, WTC4 were obtained by thermo-chemical route from the experimental conditions of sample S2 and S8 respectively as given in table 4.4. Samples WSS1 to WSS7 were obtained by solid state reaction method as described in section 4.1.2.

6.1.1 Microstructural examination

6.1.1.1 WC-Co composites (WC obtained by thermo-chemical route)

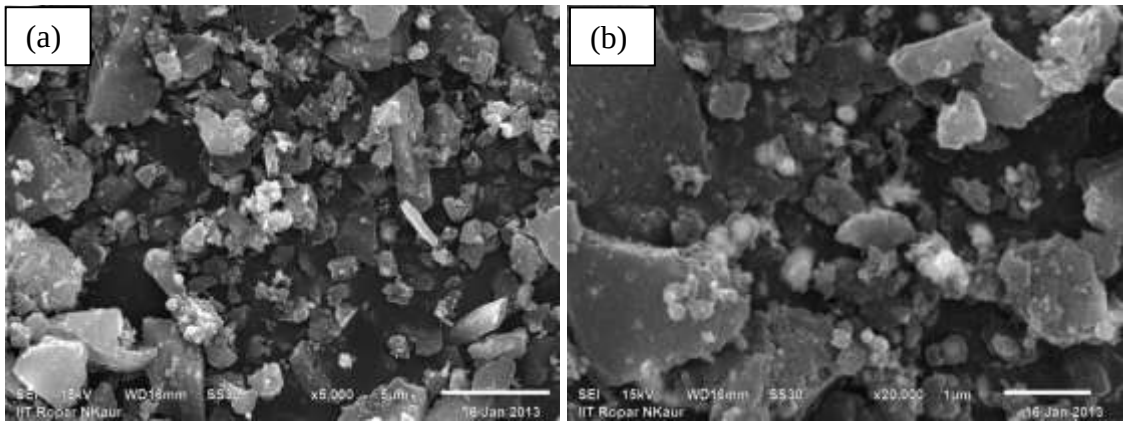

Figure 6.1: SEM of tungsten carbide-cobalt (WC- 10wt.%Co) composite (WTC1) sintered at 1100°C (in argon).

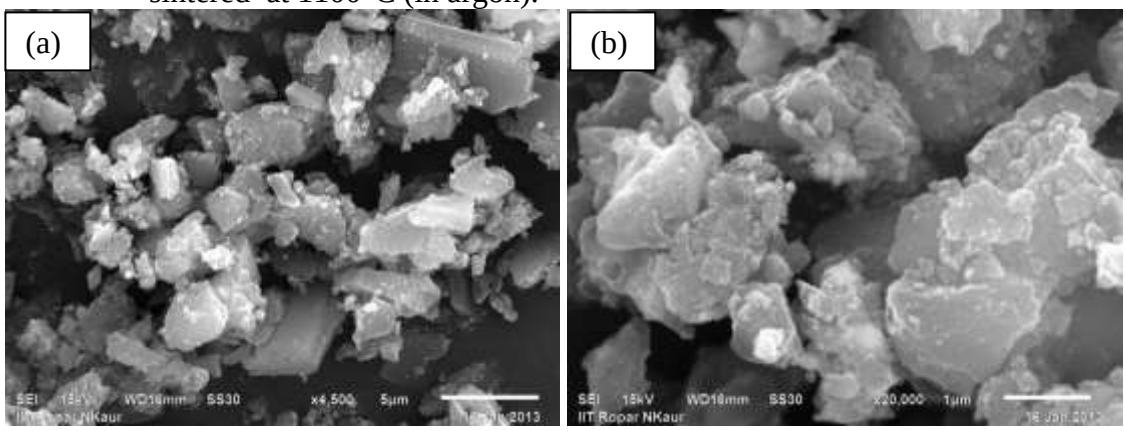

Figure 6.2: SEM of tungsten carbide-cobalt (WC- 10wt.%Co) composite (WTC2) sintered at 1350°C (in argon).

The basic idea behind this work is to check the sintering behavior of the developed the composite at different temperatures. In order to see the growth of nano WC powders with variation in sintering temperature which is a key parameter for good composite, composites were sintered at different temperatures. Fig 6.1 (a & b) shows the top layer

micrograph of tungsten carbide-cobalt (WC-10wt.%Co) composite (WTC1) sintered at 1100°C for 1h (in argon). The structure is highly porous where faceted structure of WC can be seen. The grain growth has occurred but structure is still fine as compared to conventional one [4,5]. Since, the WC samples contained substantial amount of carbon, so proper compacted composite could not be observed. Moreover, carbon could not burn as sintering was done in inert atmosphere. However, agglomerated particles of around 1µm were observed. Similarly loose powders were observed in the sample WTC2 (Fig. 6.2). The particles have grown to higher size (> 1µm) due to increase in sintering temperature at 1350°C. Considering these facts the next samples WTC2 and WTC3 were sintered in air at 1100 and 1350°C as shown in Fig. 6.3 and Fig 6.4. In order to have reducing atmosphere, both ends of the tube were sealed with glass wool and sealed with high temperature tape for avoiding oxidation and also to have partial reducing atmosphere of carbon.

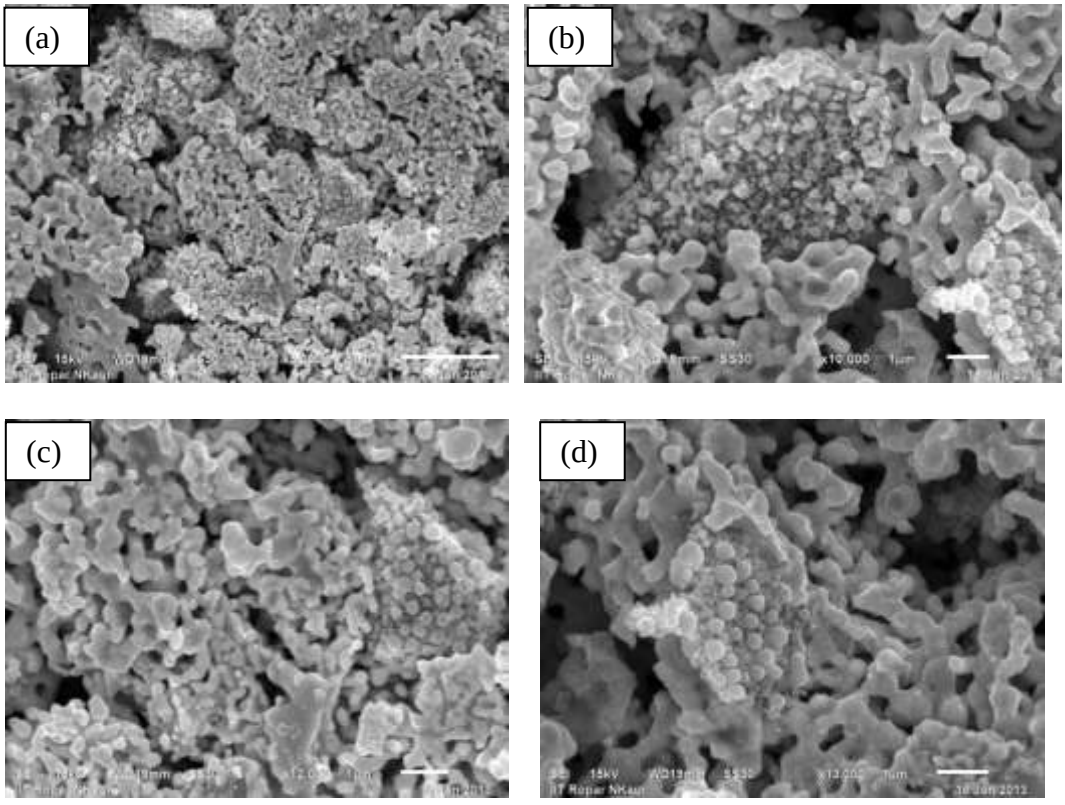

Figure 6.3: SEM micrographs of tungsten carbide (WC- 10Co) composite sintered at 1100°C (in air).

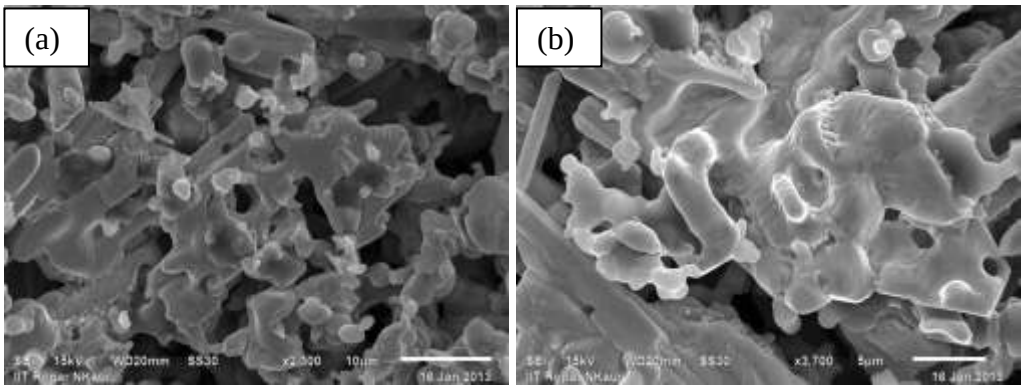

Figure 6.4: SEM micrographs of tungsten carbide Co (WC-10Co) composite sintered at 1350°C (in air).

Sintering in air has facilitated the removal of excess carbon by formation of CO_2. The structure is more homogenous with some amount of porosity. The WC is fully embedded in Co matrix. The size of WC particle is uniform having average size of 0.5µm as shown in Fig. 6.3. However, when the sintering temperature was increased to 1350°C, the grain growth of carbide phases as rod is observed in Fig. 6.4. The structural feature is faceted type. Some packed rod type structure is also observed. At this stage it is not possible to check the crystal structure of grown phases. However, this feasibility study to develop the composite is highly encouraging but requires further investigations.

6.1.1.2 WC-Co composites (WC obtained by solid state reaction method)

The composite developed from WC nanopowders obtained by solid state reaction were also prepared. The optical micrographs of Samples WSS1 to WSS4 are shown in Fig. 6.5. The structure of composite is uniform and has better appearance. Optical micrographs show uniform distribution of WC particles (white one). With the increase in sintering temperature WC grain growth is observed [6-9]. Samples WSS2 and WSS4 were further examined by SEM as shown in Fig. 6.6 and Fig. 6.7.

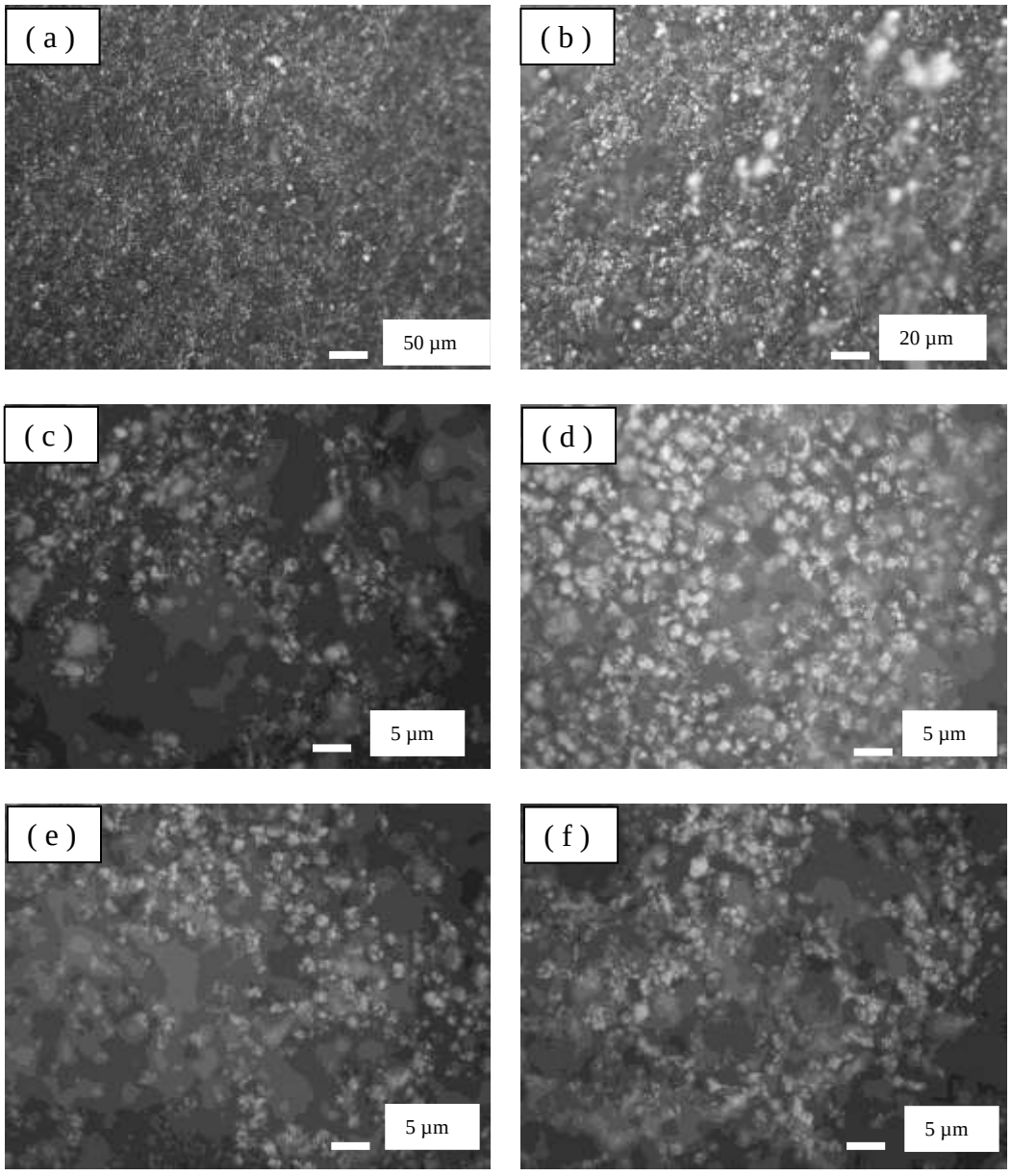

Figure 6.5: Optical micrograph of WC-10% Co composites sintered at (a) 1100°C(200X) WSS1 (b) 1100°C(500X), WSS1 (c) 1100°C (1500X),WSS1 (d) 1200°C(1500X), WSS2 (e) 1300°C(1500X) WSS3 at (f) 1400°C(1500X) WSS4.

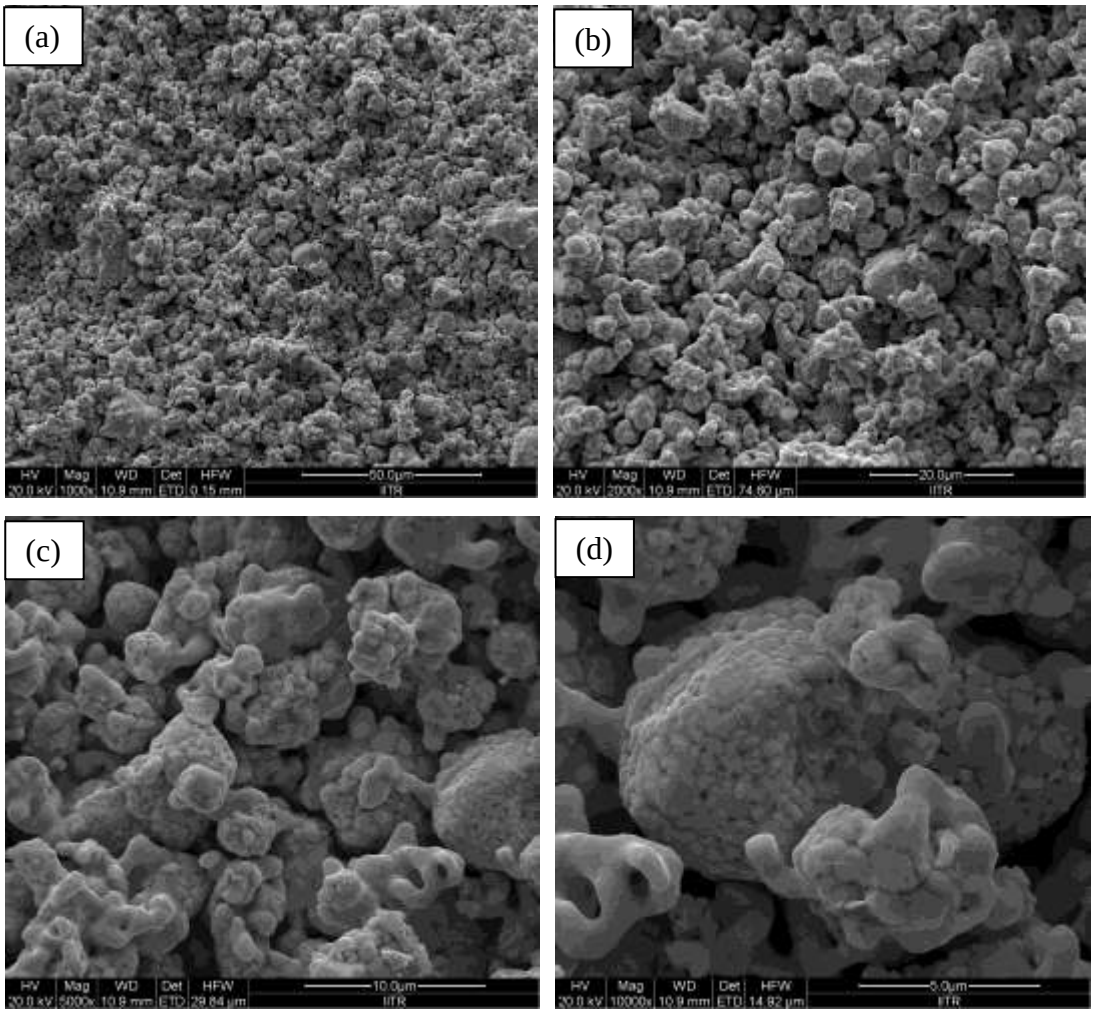

Figure 6.6: SEM of WC-10 % wt Co composite (WSS2) sintered at 1200°C.

Fig. 6.6 shows SEM of WSS2 sample sintered at 1200°C for one h. In the high magnification SEM agglomerated WC particles are seen. Grain growth of WC particles to near 1µm is observed.

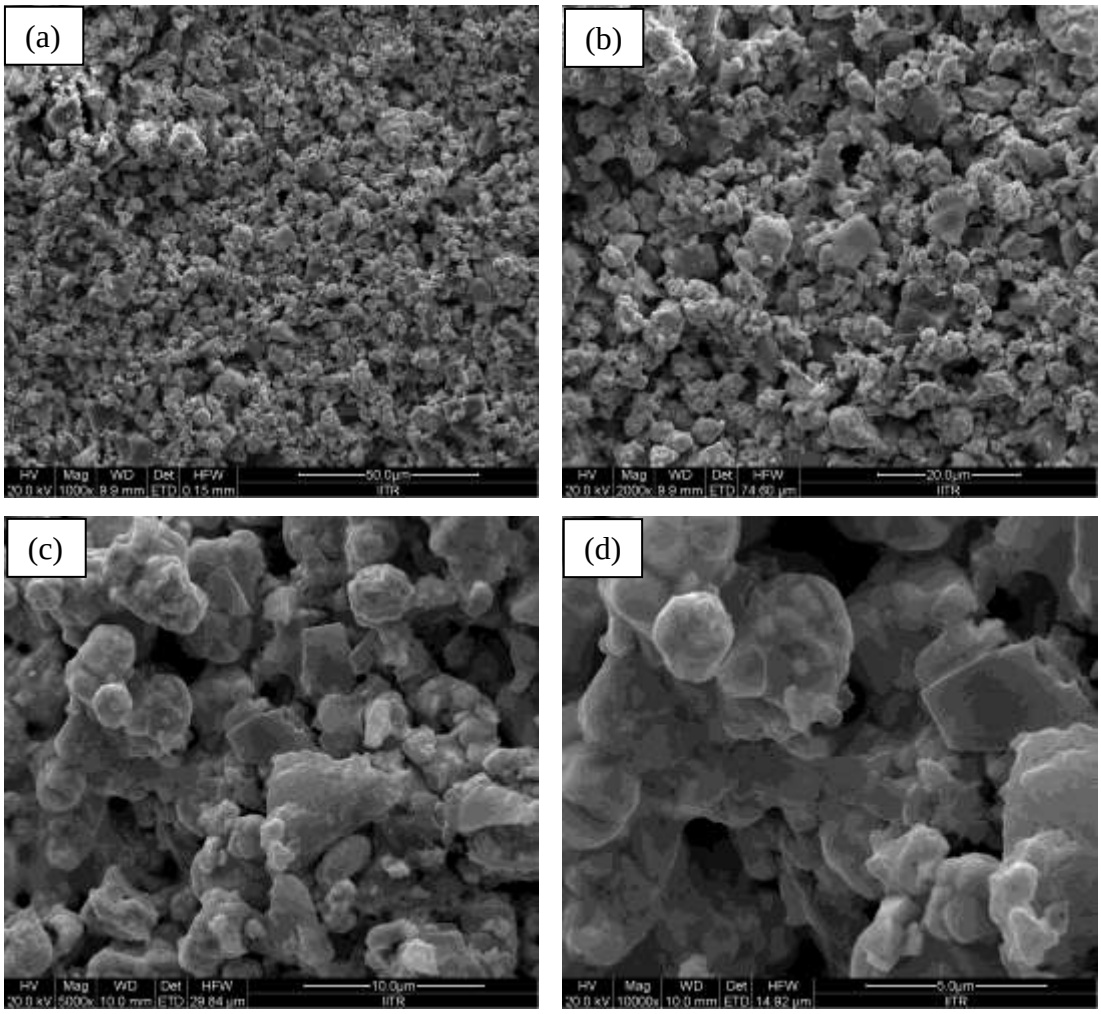

Figure 6.7: SEM of WC-10 % wt Co composite sintered at 1400°C.

Fig. 6.6 shows SEM of WSS4 sample sintered at 1400°C for one h. In sample WSS2 the agglomerated WC particles(<1µm) were observed which have grown further in the range of 5 µm with increase in sintering temperature to 1400°C.

The optical micrographs of WC-15% Co composite (WSS5 to WSS7) are shown in the Fig. 6.8. Uniform distribution of WC particles is observed in the samples. However, growth of WC particles with the increase in sintering temperature is observed.

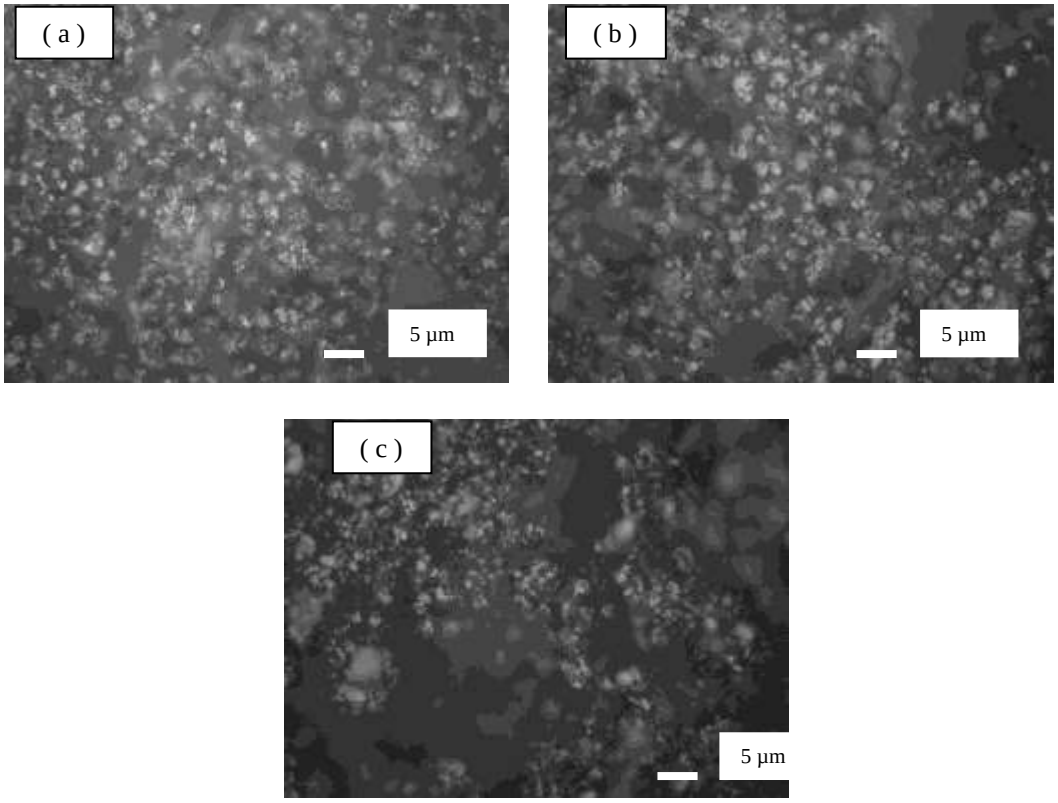

Figure 6.8: Optical micrograph of WC-15% Co composite sintered at (a) 1200°C, WSS5 (b) 1300°C, WSS6 (c) 1400°C,WSS7.

6.1.2 Micro hardness measurement of the composites

In order to study the effect of sintering temperature on the composites containing 10wt% and 15wt% Co binder (WSS1 to WSS7), micro hardness on WC grains were measured. With the increase in sintering temperature micro hardness of both 10wt% and 15wt% Co composites was found to increase as shown in Table 6.2. Though the grain growth with increase in temperature is observed but it also facilitate the proper binding of WC particles with Co matrix. The increase in hardness is due to well compacted grains [10].

Table 6.2 Sample level, their composition, sintering temperature and hardness of the developed WC-Co composite.

Sr. No.	Composition	Sintering Temperature	Vickers Hardness
WSS1	WC-10% Wt. Co	1100°C	HV 1100
WSS2	WC-10% Wt. Co	1200 °C	HV 1250
WSS3	WC-10% Wt. Co	1300 °C	HV 1370
WSS4	WC-10% Wt. Co	1400 °C	HV 1500
WSS5	WC-15% Wt. Co	1200°C	HV 1230
WSS6	WC-15% Wt. Co	1300 °C	HV 1360
WSS7	WC-15% Wt. Co	1400 °C	HV 1460

With increase in binder (Co) content to 15 wt%, the hardness of the composites was relatively lowered as compared to composites with 10 wt% Co. However, hardness of as synthesized composites was well above the conventional grade WC powders (HV 1170) [11].

The above study was a feasibility study. However, it requires further investigations using XRD technique to investigate the phases formed. Moreover, the optimization of reinforcing conditions requires further investigations.

Refernces

[1] Z. Z. Fang, X. Wang, T. Ryu, K. S. Hwang, H.Y. Sohn, Int. J. Ref. Metals Hard Mat., 27 (2009) 288–299.

[2] D.F. Carroll, Int. J. Refract. Metal. Hard Mater., 17(1-3) (1999) 123–132.

[3] Z.Z. Fang, J.W. Eason, Int. J. Refract. Metal Hard Mater., 13(5) (1995) 297–303.

[4] T.S. Srivatsan, R. Woods, M. Petraroli, T.S. Sudarshan, Powder Tech., 122 (2002) 54-60.

[5] E. Soares, L. F. Malheiros, J. Sacramento, M.A. Valente, F.J. Oliveria, J. Am. Cera. Soc., 95(6) (2012) 1822-1831.

[6] L.E. McCandlish, P. Seegopaul, R.K. Sadangi, Adv. Powder Metall. Particulate Mater. (1995)313–317.

[7] R. Porat, S. Berger, A. Rosen, Nanostruct. Mater., 7(4) (1996) 429–436.

[8] X. Wang, Z.Z. Fang, H.Y. Sohn, Int. J. Refract. Metal Hard Mater., 26(3) (2008) 232–241.

[9] Z.J. Shen, H. Peng, J. Liu, M. Nygren, J. Eur. Ceram. Soc. 24(12) (2004) 3447–3452.

[10] Akshay Kumar, K. Singh, O.P. Pandey, Ceramics Int.37 (2011) 1415–1422.

[11] E. Lassner, W.D. Schubert, Tungsten Properties, Chemistry, Technology of the Element, Alloys, and Chemical Compounds. Kluwer Academic/Plenum Publishers, New York, 1999.

Chapter 7

Conclusions and Future Scope

Overview

In this chapter entire work of present study is summarized and concluded. The basic aim of this work is to search for suitable techniques which can facilitate the synthesis of nano WC directly from the ore. The experimental work done on small quantity exhibit feasibility of the process which will be a greater help for commercial production. In this work all the efforts made during experiments was to develop a process which can fulfill the goal of single step synthesis of nano WC involving lesser amounts of chemicals. The work demonstrates that it is possible to synthesize nano WC directly from low grade ore (wolframite) and high grade ore (Scheelite). The study shows the feasibility of producing high purity nano WC by solid state reaction route (1025°C) and also at low temperature at 650°C by thermo chemical route in an autoclave. The impurities in the ore are not harmful in synthesis; rather they help in synthesizing and retaining nano size of WC. Furthermore, removal of impurities is easy and can be done by leaching with dilute acid followed by dilute base washing. For removal of SiO_2 from nano WC sample synthesized from wolframite concentrate, HF leaching was optimized. The as synthesized nano WC samples were used for composite making. These composites show better hardness than conventional grade materials. However, the work requires more experimentation and proper characterization. Since it was a feasibility study, so much emphasis on this work was not given. At the end suggestions for future work in this field is given.

7.1 Conclusions

The aim of the present study was to optimize the conditions for the synthesis of WC nano particles from scheelite concentrate and wolframite ore. For the synthesis two methods were experimented; solid state reaction method and thermo chemical route. In the present study, single phase WC nano particles were synthesized directly from scheelite ore by solid state reaction method at 1025°C. Activated charcoal (carbon source) was used as reducing cum carburizing agent. With the aim to synthesize single phase WC nano particles; two different samples (scheelite and activated charcoal in ratio of excess of stoichiometry of reaction) were milled for 50h, 100h. The scheelite particles in both the milled samples were in the nano size range. The 100h milled sample was reduced to nano size having spheres and capsules types of structure of scheelite. When calcined at 1025°C it got completely converted into WC nano particles. For getting complete conversion several experiments were done by 50h and 100h milled samples at different temperatures. Similarly, 150 h milled samples when calcined have led to formation of nano WC with residual scheelite. From these experiments we found that size of milled powders is very critical for complete conversion to nano WC. It requires homogeneous mixture of nano scheelite particles in non agglomerated state. The impurities were successfully removed from calcined powders by leaching with dilute acid HCl (1:1) followed by dilute base 0.25M NaOH washing.

In this study no intermediate phase like W, W_2C and Ca_3WO_6 were observed in the calcined samples. Only two phases $CaWO_4$ and WC were observed when powders were calcined above 900°C. This behaviour was in contrast to the general solid state reactions which usually proceeds with the formation of intermediate phase followed by final product, whereas in our experiments final phase formed is directly without formation of intermediate product. The probable reason for this variation could be the existence of scheelite particles in nano range and its homogeneous mixing with activated charcoal along with sufficient time duration of heating (4h for each sample). However, it is possible that shorter duration of heating of samples may produce intermediate phase.

These investigations revealed that under optimized conditions single phase nano WC particles can be obtained from scheelite concentrate by solid state reaction method.

Since high temperature synthesis leads to WC grain growth, so to have better control on WC particle size, thermo chemical route was explored. Initial experiments were carried out using Mg as reducing and liquid carbon source (acetone) as carburizing agent at 800°C. The reaction output contained mixed phases only. Single phase nano WC particles were obtained in case of "dry autoclaving" only. The mixture of scheelite, Mg and activated charcoal when heated at 800°C for 20 h led to the formation of nano WC. The impurities and reaction by products like CaO, MgO were removed by dilute acid HCl(1:1) leaching followed by dilute base 0.25 NaOH washing. Further experiments were carried out for optimizing time and temperature. The single phase nano WC was obtained by heating the mixtures at 800°C for 10h or at lowest temperature of 650°C with heating time of 20h. For the above experiments we have used 50 h milled scheelite powders. The interesting feature observed in these experiments is that no intermediate phase like W, W_2C and Ca_3WO_6 were observed in the reaction products as was the case of solid state reaction method. The probable reason for this behavior could be the very small size of active tungsten obtained after reduction of $CaWO_4$, which got carburized completely in short period of holding time even as 10 S. The autogenic pressure helped in disintegeration and carburising process. However, it is possible that during heating some intermediate phase(s) might have formed because the heating rate of the furnace was slow enough (5°C/min) which took nearly 3h to attain 800°C temperature.

By solid state reaction method, nano W_2C and Fe_2W_2C were obtained from the 50h milled mixture of wolframite and activated charcoal calcined at 1100°C in argon atmosphere. The reactions by thermo-chemical route led to direct formation of nano WC. The mixture of wolframite, Mg and activated charcoal was heated at 800°C for 20h in an autoclave. The resultant powders were washed by dilute HCl (1:1). The acid leached powders contained nano WC and SiO_2 impurity. Further, even the very stable impurity SiO_2 was leached out by HF. Furthermore, experiments were conducted at 800, 700 and 650°C with holding time of 4 h. The sample heated at 800°C for 4h, showed complete

reduction. After removal of all the impurities, sample contained single phase nano WC particles of 5 to 7 nm.

Generally ore contains different impurities, and to remove impurities different processes are adopted which make the whole metal extraction process energy intensive and costly. All the experiments from both the ores were conducted without any purification. The impurities present in the ore did not obstruct the synthesis of nanocrystalline WC. Impurities may act as grain growth inhibitor thus facilitating the synthesis of WC nano particles, which are leached out after synthesis. The leaching process of reaction products obtained from scheelite is quite simple and easy. Under optimized conditions most stable impurity SiO_2 can be easily leached out from reaction products of wolframite ore. This technology is reverse of hydrometallurgical practice. Here synthesis is done first and then impurities are removed by simple acid leaching. So, thereby requiring very less amount of acid/base, since only impurities are to be leached out from the product phase and not the entire ore which has to be digested with acid and base in conventional process. Another major advantage is that it will generate lesser effluent (except SiO_2 process) than conventional process.

The feasibility study of as synthesized powders for developing WC-Co composite demonstrate that composite can be made. The sintering behavior of these composites at temperatures 1200, 1300 and 1400°C were studied. Grain growth of WC has occurred with increase in temperature. The hardness of the sintered composites on WC powders was found well above the conventional grade composites. However, this requires a detailed study related to sintering parameters and formed phases.

7.2 Scope for further work

The synthesized WC nanoparticles can be tested for catalytical properties for use in fuel cell to reduce the cost as a substitute for Pt. The sintering kinetics of composite from as synthesized nano WC with grain growth inhibitors can be studied. The leaching kinetics can be studied for impurities removal from scheelite ore. For removal of silica impurity from mixture of WC, C and SiO_2, other processes than usage of HF should be explored. The synthesis of nano structured WC has many challenges and opportunities. The

morphology controlled synthesis of low dimensional tungsten carbide nanostructures (mesoporous WC nano chains, WC nano fibers, WC nano rods and platelets, hollow microspheres, three dimensionally ordered macroporous WC, inverse opal WC nanostrucutres) with high surface area and high redispersibility directly from ores should be explored. Similarly, the work on synthesis of nano structured W, WO_3 and H_2WO_4 from the ores can be explored.